

SYNTHESIS AND OPTIMIZATION OF BORON NITRIDE NANOTUBES FOR  
STABLE AQUEOUS DISPERSIONS

by

DENİZ KÖKEN

Submitted to the Graduate School of Engineering and Natural Sciences

in partial fulfillment of

the requirements for the degree of

Master of Science.

Sabanci University

Fall 2016

SYNTHESIS AND OPTIMIZATION OF BORON NITRIDE NANOTUBES FOR  
STABLE AQUEOUS DISPERSIONS

APPROVED BY:

Asst. Prof. Dr. Fevzi Ç. Cebeci

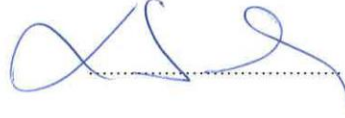
(Thesis Supervisor)



Assoc. Prof. Dr. Selmiye Alkan Gürsel



Asst. Prof. Dr Nuri Solak



DATE OF APPROVAL:

28.12.2016

© Deniz Köken 2016

All Rights Reserved

## ABSTRACT

### SYNTHESIS AND OPTIMIZATION OF BORON NITRIDE NANOTUBES FOR STABLE AQUEOUS DISPERSIONS

DENİZ KÖKEN

M.Sc. THESIS, DECEMBER 2016

Supervisor: Asst. Prof. Dr. Fevzi Çakmak Cebeci

**Keywords:** Boron nitride nanotubes, synthesis, optimization, surface modifications, aqueous dispersion, boron minerals

As structural analogues of carbon nanotubes (CNT), boron nitride nanotubes (BNNT) possesses extraordinary mechanical, electrical, thermal and optical properties. These unique properties, makes them promising materials applications in composite, hydrogen storage, radiation shielding, biomaterials. However, difficulties in high yield BNNT synthesis and obtaining stable dispersions of BNNTs in aqueous media remain as main challenges. This thesis research focuses on the BNNT synthesis and optimization thereof in addition to preparation of stable aqueous dispersions of BNNTs.

High yield synthesis of BNNTs on Si wafers and BNNFs as well as floating BNNT form by modified growth vapor trapping-BOCVD method in conventional tube furnace at 1200 °C were accomplished in this research. Synthesis of BNNTs were optimized in terms of temperature, catalyst ratio, catalyst amount, ammonia flow, reaction time and system parameters which allowed high yield synthesis of good quality BNNTs with vacuum free, low cost, novel growth vapor trapping-BOCVD route. As-synthesized BNNTs were characterized by scanning electron microscopy (SEM), transmission electron microscopy (TEM), Raman spectroscopy, Fourier Transform Infra-Red spectroscopy (FTIR) and electron energy loss spectroscopy (EELS).

Following the successful synthesis of BNNTs, BNNT synthesis from boron minerals were investigated. Boron minerals Ulexite and Etidot-67, gifted from ETİ Maden İşletmeleri,

were used as boron precursors for the synthesis of floating BNNTs in this research. As-synthesized BNNTs were characterized by SEM and RAMAN spectroscopy.

Two modification approaches were utilized for the surface modifications of BNNTs: Covalent functionalization and non-covalent functionalization. In covalent functionalization approach, BNNT's surfaces were hydroxylated by nitric acid treatment and ozone treatment, which reduces the van der Waals forces between nanotubes. Moreover, hydroxyl groups on the surface of BNNTs can be used as starting spots for the further functionalization. In non-covalent functionalization approach, BNNTs were wrapped with ionic surfactants and polymers (b-PEI (branched polyethyleneimine) and poly(allylamine hydrochloride) (PAH) via  $\pi$ - $\pi$  interaction to prevent agglomeration of BNNTs and dispersed in aqueous media. Dispersions of as-functionalized BNNTs characterized by Fourier Transform Infra-Red spectroscopy (FTIR) and dynamic light scattering spectroscopy (DLS).

BNNT thin film production by dip LbL method was investigated. LbL method allows high control over the architecture of thin film in addition to film thickness. BNNT dispersions were used in combination with b-PEI and PSS Poly(styrenesulfonate) for the production of BNNT thin films on glass substrates. Different pH values of as-prepared dispersions were tested in order to achieve 5 bilayers (bilayer) and 10 bilayers thick BNNT thin films by dip LbL method.

Synthesis parameters of BNNTs were successfully optimized and synthesis of BNNTs were achieved. As-synthesized BNNT's surfaces were modified with covalent and non-covalent functionalization methods and stable aqueous dispersions of BNNTs were achieved. We found that, non-covalent functionalization of BNNTs allows BNNTs to be dispersed in aqueous media with good dispersion stability.

## ÖZET

### BOR NİTRÜR NANOTÜPLERİN KARARLI SULU DAĞILIMLARININ HAZIRLANMASI İÇİN SENTEZLENMESİ VE OPTİMİZASYONU

DENİZ KÖKEN

M.Sc TEZ ARALIK, 2016

Danışman: Yrd. Doç. Dr. Fevzi Çakmak Cebeci

**Anahtar Kelimeler:** Bor nitrür nanotüp, sentez, optimizasyon, yüzey işlemleri, sulu dağılım, bor mineralleri

Karbon nanotüplerin (CNT) yapısal benzerleri olan bor nitrür nanotüpler (BNNT), olağanüstü mekanik, elektriksel, ısıl ve optik özelliklere sahiptirler. Bu eşsiz özellikler, BNNT'leri kompozit, hidrojen depolama, radyasyon kalkanı, biyomalzemeler vb. uygulamalarında gelecek vaat eden malzemeler yapmaktadır. Fakat BNNT sentezinin düşük verimi ve BNNT'leri sulu ortamda dağıtmanın zorluğu, BNNT'lerin sahip oldukları potansiyellere ulaşmaları için çözülmesi gerekli problemlerin başında gelmektedir. Bu tez çalışması, BNNT'lerin sentezi ve bu sentezin optimizasyonunun yansira BNNT'lerin sulu ortamda dağıtılmasına odaklanmıştır.

BNNT'lerin silikon (Si) altlıkların ve bor nitrür nanofiber (BNNF) altlıkların üzerinde sentezinin yansira, sabit olmayan BNNT'lerin sentezi bu tez çalışması kapsamında 1200 °C'de büyüme gazı yakalama-bor oksit kimyasal gaz biriktirme (BOCVD) bileşik yöntemi kullanılarak yüksek verimle başarılmıştır. BNNT sentezi sıcaklık, katalizör oranı, katalizör miktarı, amonyak miktarı, reaksiyon zamanı ve sistem parametreleri açısından optimize edilmiştir. Bu optimizasyon iyi kaliteli BNNT'lerin yüksek verim ile vakum kullanılmadan, ucuz ve basit büyüme gazı yakalama-BOCVD metodu ile sentezlenmesine olanak sağlamıştır. Sentezlenen BNNT'ler taramalı elektron mikroskobu (SEM), geçirimli elektron mikroskobu (TEM), RAMAN spektroskopisi, Fourier dönüşümlü kızıl ötesi spektroskopisi (FTIR) ve elektron enerji kaybı spektroskopisi (EELS) yöntemleri ile karakterize edilmiştir.

Başarılı BNNT sentezini takiben, BNNT'lerin bor minerallerinden sentezlenmesi araştırılmıştır. ETİ Maden İşletmeleri tarafından hediye edilen üleksit ve Etidot-67 bor mineralleri, sabit olmayan BNNT sentezi çalışmalarında bor kaynağı olarak kullanılmıştır. Sentezlenen BNNT'ler SEM ve RAMAN spektroskopisi kullanılarak karakterize edilmiştir.

Daha önce de bahsedildiği üzere, BNNT araştırmalarında karşılaşılan ikinci zorluk: Van der Waals kuvveti yüzünden topaklaşan BNNT'lerin sulu ortamda dağıtılmasıdır. BNNT'lerin suda dağıtılabilmesi için, yüzey iyileştirilmesi gerekmektedir ancak BNNT'lerin sahip olduğu yüksek kimyasal dayanıklılık bu işlemi oldukça zor hale getirmektedir. İki farklı iyileştirme yaklaşımı BNNT yüzeyleri için kullanılmıştır: Kovalent fonksiyonlandırma ve kovalent olmayan fonksiyonlandırma. Kovalent fonksiyonlandırma yaklaşımında, BNNT'ler nitrik asit ve ozon işlemlerine maruz bırakılarak hidroksile edilmişlerdir. Bu işlem BNNT'lerin yüzeyinde “-OH” grupları oluşturarak birbirleri arasındaki van der Waals kuvvetinin gücünü azaltmaktadır. Buna ek olarak hidroksile edilmiş BNNT'ler ileri fonksiyonlandırmalar için başlangıç malzemesi olarak kullanılabilirler. Kovalent olmayan fonksiyonlandırma yaklaşımında, BNNT'lerin aglomerasyonunun engellenmesi için (b-PEI (branched polyethyleneimine) ve PAH (Poly[allylamine hydrochloride])) ile BNNT'ler sarılmıştır.  $\pi$ - $\pi$  etkileşimlerinin yardımı ile gerçekleşen sarma işlemi sonucunda BNNT'ler sulu ortamda dağılabilir duruma getirilmiştir.

Katman katman (LbL) kaplama yöntemi kullanılarak BNNT ince film hazırlanması bu tez kapsamında araştırılmıştır. LbL yöntemi ince film mimarisi ve kalınlığı üzerinde yüksek oranda kontrol sağlayan bir yöntem olduğu için seçilmiştir. Hazırlanan sulu BNNT dağıtımları, b-PEI ve PSS polimerleri ile beraber kullanılarak cam altlık üzerinde BNNT ince filmler oluşturulmuştur. Hazırlanan dağıtımların farklı pH değerleri 5 bl (çift katman) ve 10 bl kalınlıkta ince film hazırlanması için daldırma LbL yöntemi ile test edilmiştir.

BNNT sentezi parametreleri bu çalışmada optimize edilmiş ve başarılı BNNT sentezi sağlanmıştır. Sentezlenen BNNT'ler kovalent ve kovalent olmayan fonksiyonlandırma yöntemleri ile yüzey grupları değiştirilmiş ve sulu ortamda kararlı BNNT çözeltileri elde edilmiştir. BNNT'lerin kovalent olmayan fonksiyonlandırılması sonucu, suda dağıtılabildiklerini ve dağıtımın kararlı olduğunu bu çalışma sonucunda tarafımızdan bulunmuştur.

## ACKNOWLEDGEMENTS

First of all, I would like to express my gratitude to Asst. Prof. Dr. Fevzi akmak Cebeci for supervising my master study and related research, for his patience, motivation, wisdom and endless energy.

Along with my advisor, I would like to thank Assoc. Prof. Dr. Selmiye Alkan Grsel and Asst. Prof. Dr. Nuri Solak of my thesis committee for their invaluable comments and suggestions which pushed this thesis to achieve perfection.

My gratitude also goes to Buket Alkan Taş, Cneyt Erdin Taş, Emine Billur Seviniş zubulut and Adnan Taşdemir for their immense help during my research as well as for all the fun we had together for the last 2.5 years.

I thank Omid M. Moradi and Dr. Melike Mercan Yıldızhan for their help with electron microscope characterization I used in this thesis.

Last but not least, I would like to thank my family, for their support through all times, for their unconditional love, for their understanding. I could not even imagine what I would do without them.



## TABLE OF CONTENTS

CHAPTER 1 Introduction .....	17
1.1 Literature Information.....	17
1.2 Previous and Current Synthesis Techniques.....	21
1.2.1 Laser Ablation Method .....	21
1.2.2 Ball-milling Method .....	22
1.2.3 Carbon Substitution Method.....	24
1.2.4 Extended Vapor-Liquid-Solid Method .....	24
1.2.5 Plasma Enhanced Pulsed Laser Deposition (PE-PLD).....	25
1.2.6 Chemical Vapor Deposition Method (CVD).....	26
1.2.7 Boron Oxide Chemical Vapor Deposition.....	27
1.2.8 Growth Vapor Trapping Method .....	28
1.3 Properties of BNNTs .....	29
1.3.9 Mechanical Properties.....	30
1.3.10 Electrical Properties .....	31
1.3.11 Thermal Properties.....	32
1.3.12 Optical Properties .....	33
1.4 Functionalization of BNNTs.....	34
1.4.13 Covalent Functionalization of BNNTs .....	34
1.4.14 Non-Covalent Functionalization of BNNTs.....	36

1.5 Applications of Boron Nitride Nanotubes .....	37
1.5.15 Composites.....	38
1.5.16 Biomedical Applications.....	40
1.5.17 Radiation Shielding.....	41
1.5.18 Hydrogen Storage .....	42
1.6 Motivation.....	44
CHAPTER 2 Experimental Work.....	48
2.1 Materials and equipment.....	48
2.2 Growth Vapor Trapping-BOCVD synthesis of BNNTs.....	49
2.2.1 Nucleation theory of Whisker.....	54
2.2.2 BNNT Synthesis on Silicon Wafers .....	55
2.2.3 Synthesis of floating BNNTs.....	57
2.2.4 BNNT synthesis on BBNF .....	59
2.2.5 BNNT synthesis from various boron minerals .....	61
2.2.6 Purification of Floating BNNTs .....	63
2.3 Surface Modification of BNNTs.....	64
2.3.7 Ozone Treatment of BNNTs.....	65
2.3.8 Nitric Acid Treatment of BNNTs .....	66
2.3.9 Ionic Surfactant Assisted Non-Covalent Functionalization.....	67
2.3.10 Polymer Wrapping of BNNTs .....	68
2.4 BNNT Film Preparation by LbL Method .....	69

2.4.11 Experimental Work for Thin Film Production via LbL Method .....	71
2.5 Characterization .....	73
CHAPTER 3 Optimization of BNNT Synthesis.....	75
3.1 Introduction.....	75
3.2 Optimization of Recipe .....	75
3.2.1 Temperature Optimization.....	76
3.2.2 Catalyst Ratio Optimization.....	79
3.2.3 Ammonia Flow Optimization .....	81
3.2.4 Catalyst Mixture Amount Optimization .....	82
3.2.5 Reaction Time Optimization.....	83
3.3 System Parameter's Optimization .....	84
3.4 Optimized Recipe .....	87
CHAPTER 4 Results and Discussions.....	90
4.1 Materials and Equipments .....	90
4.2 SEM Analysis of as Grown BNNTs .....	90
4.2.1 a. SEM Analysis of BNNTs grown on Si wafers .....	90
4.2.2 b. SEM Analysis of Free-standing BNNTs .....	92
4.2.3 c. SEM analysis of BNNTs synthesized on Fibers .....	94
4.2.4 d. SEM analysis of BNNTs synthesized from boron minerals .....	96
4.3 TEM and EELS analysis of BNNTs .....	97
4.4 Raman and FTIR analysis of BNNTs synthesized on Si wafer .....	100

4.5 Characterization of Functionalized BNNTs. ....	104
4.5.5 FTIR Analysis of Covalent Functionalized BNNTs.....	104
4.5.6 Stability of BNNT Aqueous Solutions Prepared via Non-covalent Functionalization .....	107
CHAPTER 5 Conclusions and Future Work .....	111
5.1 Synthesis of BNNTs .....	111
5.2 Surface Modifications of BNNTs .....	112
5.3 Thin Film Production via LbL method .....	113
5.4 Future Work.....	113
5.4.1 Synthesis .....	114
5.4.2 Surface Modification .....	115
5.4.3 Applications.....	115

## LIST OF FIGURES

Figure 1 a. c-BN Structure, b. h-BN structure, c. graphene structure.....	18
Figure 2 Structural models of BNNT and CNT.....	21
Figure 3 SEM image of BNNT ropes synthesized by the laser ablation method .....	22
Figure 4 TEM image of the as-synthesized BNNTs by ball milling with electron diffraction pattern from the walls of the nanotube.....	23
Figure 5 Schematic of silicon crystal growth by VLS. Same growth mechanism is theorized for BNNT synthesis as well. ....	25
Figure 6 Patterned growth of BNNTs with substrate bias a. -380 mV and b. -450 mV. c. Bundling configurations respectively and d. SEM images of patterned BNNTs on wafer taken from the literature.....	26
Figure 7 a.Schematic of vertical induction furnace used in BOCVD method. b. White coatings of BNNTs on the walls of the reaction chamber. c. As-synthesized product. d. and e. Optical microscope images of as-synthesized BNNTs. ....	27
Figure 8 a.Schematic of the system for the growth vapor trapping method. b. As-synthesized BNNTs on the walls of the alumina boat. ....	29
Figure 9 Force vs displacement curves for the a. Thick and b. Thin BNNTs. Insets shows the morphologies of BNNTs before and after bending taken from the Goldberg et al.'s article. ....	31
Figure 10 Thermal conductivities of as-synthesized BN nanostructure at different temperature gradients.....	33
Figure 11 Schematic of covalent functionalization of BNNTs with stearoyl chloride...	35
Figure 12 Hydroxylation and further functionalization of BNNTs. ....	36
Figure 13 Aqueous BNNT dispersion with the help of ionic surfactant after a. 8 days, b. 11 days, c. 14 days, d. 60 days.....	37
Figure 14 Images of a. PS film b. BNNT/PS composite film c. BNNT/PmPV/PS composite film prepared by solution-evaporation method. ....	39
Figure 15 a. Hydrogen uptake of as-synthesized collapsed and multiwall BNNTs (Gravimetric). b. TGA spectrum of collapsed BNNTs during hydrogen release.....	44
Figure 16 Flow chart of BNNT research done on this thesis work .....	47

Figure 17 a.Schematic of experimental setup, b. tube furnace used for BNNT synthesis, c. Split furnace used for annealing,d. Alumina boats and alumina block.....	53
Figure 18 Flowchart of BNNT synthesis followed by purification .....	54
Figure 19 a. SEM image of as-synthesized BNNTs, b. RAMAN analysis of as-synthesized BNNTs.....	56
Figure 20. a. Catalyst loaded into alumina boat, b. Alumina boat covered by Si wafers, c. BNNTs grown on Si wafers.....	57
Figure 21. a. Catalyst and Si wafer placement on the alumina boat, b. Alumina boat after BNNT synthesis.....	58
Figure 22 SEM image of CNTs synthesized on CNFs. ....	59
Figure 23 a. BNNFs during dipping step, b. BNNFs after reduction step, c. BNNFs loaded alumina boat, d. BNNFs after BNNT growth.....	61
Figure 24 SEM images of BNNTs synthesized from unprocessed colemanite.....	62
Figure 25 Alumina boat a. after preheating. b. Alumina boat covered with Si wafers. c. Alumina boat after synthesis run. ....	63
Figure 26 Flow chart for purification process. a. BNNTs before any purification, b. BNNTs after HCL treatment, c. Purified BNNTs .....	64
Figure 27 a.Flowchart of the chemical modifications, b. Scheme of reaction during covalent functionalization.....	65
Figure 28 a. Ozone air compressor, b. Si wafer after ozone treatment .....	66
Figure 29 BNNT aqueous dispersion with the help of ammonium olate surfactant after tip sonication.....	67
Figure 30 Aqueous dispersion of polymer wrapped BNNTs a. b-PEI, b. PAH.....	68
Figure 31 a. Dip coating equipment used, b. Inside of the dip coater with 6 stages for washing and 2 stages for electrodes.....	71
Figure 32 Si wafers collected after each run.....	78
Figure 33 SEM images of BNNTs synthesized at a. 1200 °C and b. 1300 °C.....	78
Figure 34 SEM images from BNNTs synthesized at a. 1350 °C and b. 1400°C.....	79
Figure 35 SEM images of BNNTs synthesized with a. 2:1:1 (B:MgO:Fe <sub>2</sub> O <sub>3</sub> , w/w), b. 4:1:1 (B:MgO:Fe <sub>2</sub> O <sub>3</sub> w/w) catalyst ratio. ....	80
Figure 36 BN sheets on the Si wafers when the catalyst ratio is 4:1:1 .....	81
Figure 37 Si wafers collected after each run.....	82
Figure 38 Si wafers collected after each run.....	83

Figure 39 SEM images of BNNTs synthesized on Si wafers. a. Surface of the Si wafer, b. Non-coated surface of Si wafer. ....	91
Figure 40 SEM images of a. Floating BNNT cluster on the Si wafer and b. Single BNNT. ....	91
Figure 41 SEM image of catalyst droplet on Si wafer where BNNTs are growing out of. ....	92
Figure 42 SEM images of floating BNNT clusters.....	93
Figure 43 High magnification SEM image of floating BNNTs.....	93
Figure 44 SEM images of floating BNNTs before purification process. a. cluster of floating BNNTs and b. networked structure of floating BNNTs with impurities. ....	94
Figure 45 SEM image of BNNFs after catalyzation.....	95
Figure 46 SEM images of BNNFs after BNNT synthesis. a. Surface of the BNNFs where clusters of BNNTs are visible. b. High magnification image of BNNT cluster with networked structure.....	95
Figure 47 SEM image of BNNFs' surface facing inwards of the alumina boat. ....	96
Figure 48 SEM images of BNNTs synthesized from a. Ulexite and b. Etidot-67.....	97
Figure 49 HRTEM images of single BNNTs. a. Bright core and dark edges are the indicators for the hollow tube structure. b. Dark fringes can be seen on the edges of the nanotube.....	98
Figure 50 Profile analysis of single BNNT. ....	98
Figure 51 Diffraction pattern from the single BNNT. ....	99
Figure 52 EELS data for the as-synthesized BNNTs. ....	99
Figure 53 RAMAN data spectrum from a. BNNTs synthesized on Si wafers, b. free – standing BNNTs .....	100
Figure 54 RAMAN spectra of a. ulexite, b. Etidot-67 .....	101
Figure 55 Vibrations modes of BNNTs. a. TO mode, b. LO mode and c. Radical buckling more .....	102
Figure 56 FTIR analysis of BNNTs on Si wafers.....	103
Figure 57 FTIR spectrum of as-synthesized floating BNNTs. ....	104
Figure 58 FTIR analysis of BNNTs after ozone treatment.....	105
Figure 59 FTIR analysis of BNNTs after nitric acid treatment .....	106
Figure 60 Surfactant assisted dispersion's images from different time intervals.....	109
Figure 61 Images of dispersion with different time intervals. ....	110

Figure 62 Images of BNNT-PAH dispersion from different time intervals. .... 110



## LIST OF TABLES

Table 1 Boron mineral compounds.....	17
Table 2 Comparison between properties of carbon nanotubes and boron nitride nanotubes .....	20
Table 3 Conditions for the LbL thin film production. 5 bL and 10 bL thick films were produced for all conditions. ....	73
Table 4 Experimental design for the optimization.....	76
Table 5 Temperature optimization experiment design .....	77
Table 6 Catalyst ratio optimization experiment design .....	80
Table 7 Ammonia flow optimization experimental design. ....	81
Table 8 Catalyst mixture amount optimization experiment design. ....	83
Table 9 Reaction time optimization experiment design .....	84
Table 10 Optimized recipe with 2:1:1 (B:MgO:Fe <sub>2</sub> O <sub>3</sub> w/w) catalyst mixture ratio, 1 g catalyst mixture.....	89
Table 11 DLS results of the BNNT aqueous dispersions .....	107

## LIST OF SYMBOLS AND ABBREVIATIONS

BNNT: Boron nitride nanotube  
BN: Boron nitride  
c-BN: Cubic boron nitride  
h-BN: Hexagonal boron nitride  
D: Dimension  
CNT: Carbon nanotube  
K: Kelvin  
C: Celsius  
UV: Ultra-violet  
CVD: Chemical vapor deposition  
BOCVD: Boron oxide chemical vapor deposition  
GVT: Growth vapor trapping  
PE-PLD: Plasma enhanced pulsed laser deposition  
COCl: Chloride  
PmPV: Poly[(m-phenylenevinylene)-co-(2,5-dioctoxy-p-phenylenevinylene)]  
PANI: Polyaniline  
b-PEI: branched polyethylenimine  
PAH: Polly(allylamine hydrochloride)  
SPS:  
DI: Distilled  
FTIR: Fourier transform infrared spectroscopy  
SEM: Scanning electron microscopy  
TEM: Transmitting electron microscopy  
DLS: Dynamic light scattering  
P<sub>N</sub>: Partial Pressure  
 $\sigma$ : Surface energy  
 $\alpha$ : Supersaturation ratio  
k: Boltzmann constant  
T: Temperature  
scm: Standart cubic centimeter per minute  
 $\Omega$ : Resistivity  
VLS: Vapor-liquid-solid  
LbL: Layer-by-layer

## CHAPTER 1 Introduction

### 1.1 Literature Information

Boron is an element with the atomic number 5 and molecular weight of 10.81 g/mol (Average molecular weight of 10B and 11B isotopes). Elemental boron produces boron nitride in the presence of nitrogen at 900° C. Main reservoir of boron resides in Turkey having the 53% of the world boron reservoir. Boron can be found in many mineral forms (Table 1 [1]) with a lots of use in the industry starting from glass and ceramic production to research. The main boron compounds can be named as boron carbide, boron nitride, boric acid, borax, sodium perborate and boranes. Qingsongite is the only known natural occurring BN (Boron nitride) mineral. In this work, the main boron compound of interest is the synthetic boron nitride compounds, more precisely among those boron nitride nanotubes (BNNT).

Table 1 Boron mineral compounds

NAME	FORMULA	B <sub>2</sub> O <sub>3</sub> %
Borax	Na <sub>2</sub> B <sub>4</sub> O <sub>7</sub> .10H <sub>2</sub> O	36.6
Tincalconite	Na <sub>2</sub> B <sub>4</sub> O <sub>7</sub> .5H <sub>2</sub> O	47.8
Kernite	Na <sub>2</sub> B <sub>4</sub> O <sub>7</sub> .4H <sub>2</sub> O	51.0
Ulexite	NaCaB <sub>5</sub> O <sub>9</sub> .8H <sub>2</sub> O	43.0
Colemanite	Ca <sub>2</sub> B <sub>6</sub> O <sub>11</sub> .5H <sub>2</sub> O	50.9
Meyerhofferite	Ca <sub>2</sub> B <sub>6</sub> O <sub>11</sub> .7H <sub>2</sub> O	46.7
Inyoite	Ca <sub>2</sub> B <sub>6</sub> O <sub>11</sub> .13H <sub>2</sub> O	37.6
Pandermite	CaB <sub>10</sub> O <sub>19</sub> .7H <sub>2</sub> O	50.0
Kurkakovite	Mg <sub>2</sub> B <sub>6</sub> O <sub>11</sub> .15H <sub>2</sub> O	37.3
Boracite	Mg <sub>3</sub> B <sub>7</sub> O <sub>13</sub> Cl	62.6
Datolite	CaBSiO <sub>4</sub> OH	

Boron nitride structure closely resembles graphite structure since BN possesses same number of electrons as two carbon atoms. Both BN sheet and graphite exhibits  $sp^2$  bonding in their structure. Boron nitride can be found in two different crystal structures: Hexagonal BN (h-BN) structure is found in graphitic sheet form and cubic BN (c-BN) which is harder than diamond (Figure 1). Boron nitride is a widely used boron compound in industry as lubricant [2], cosmetic homogenization agent [3], high temperature applications [4] and many more. BN shows white color, good insulating properties and permanent dipole. [1]

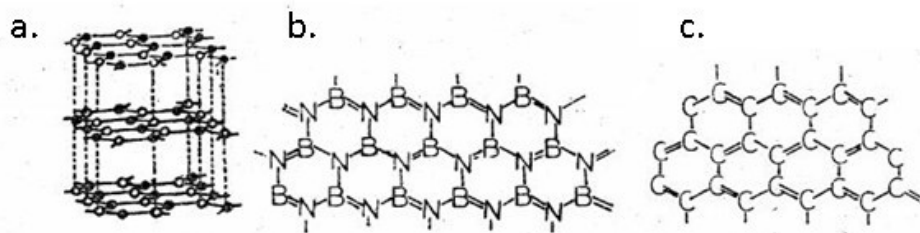


Figure 1 a. c-BN Structure, b. h-BN structure, c. graphene structure

Nanoscience covers the synthesis, characterization, modification and applications of nanomaterials. Nanomaterials are transition materials between molecules and the bulk materials and described as materials with at least one dimension is in the order of nanometer. Nanomaterials can be classified with respect the number of dimensions they have. 0D nanomaterials such as nanoparticles, 1D nanomaterials such as nanotubes, nanorods and nanowires, 2D nanomaterials such as nanofilms, nanolayers, and nanocoatings, 3D nanomaterials as an arrangement of nanosize crystals. Nanomaterials offers significantly different properties of bulk materials in terms of; mechanical strength, surface area, optical properties, structural characteristics, thermal and electronic properties and so on. Nanoscience and nanoengineering focuses on the different properties nanomaterials possess and aims to apply them to different applications.

In recent years, nanomaterials drawn many research groups attention with endless demand for high technology applications. Nanomaterials offers superior properties compared traditional materials that is used in today's industry. Especially, the future of the composites seem to depend on the nanomaterials as filler materials. For example, nanotubes offer superior mechanical, thermal and electronical properties that can

drastically improve the quality and the performance of composites. Addition to being excellent filler materials, nanomaterials also became the driving force behind the technologies such as hydrogen storage, reversible energy, drug delivery *etc.* Nowadays, nanotechnology is already in our daily lives and improving the quality of life [5].

Nanotubes have been attracting lot of research interest since carbon nanotubes (CNTs) have been discovered by Sumio Ijima in 1991 [6-8]. Excellent mechanical and electronical properties CNTs possess, make them a viable material in various applications such as polymer matrix composites [9], biomaterials [10], molecular electronics applications [11], hydrogen storage applications [12] *etc.* Not long after the discovery of CNTs, in 1994 Rubio et al. theorized boron nitride nanotubes (BNNTs) are metastable structures just like CNTs due to the similar structure h-BN shows (like graphene, boron nitrite is also found in  $sp^2$ -and  $sp^3$  bonded hexagonal structures) [13, 14]. Experimental proof came when Chopra et al. synthesized BNNTs by arc-discharge method (modified from arc-discharge synthesis of CNTs) [15]. Boron nanotubes are structural analogues of CNTs with carbon replaced by alternating B and N atoms with almost identical atomic spacing [Figure 2]. BNNTs possesses extraordinary mechanical and structural properties like CNT due to partial ionic bonding of BNNTs, it also exhibits different properties than CNTs. Unlike CNTs which shows metallic or semiconducting properties depending on the chirality and morphology [16], BNNTs are an electrical insulators with 5,5 eV bandgap with no dependence to chirality and morphology meaning they have uniform electronic properties [14]. Furthermore, BNNTs have higher thermal stability and oxidation resistance than CNTs [17]. Boron nitride nanotubes are also excellent filler materials in composite materials due to extraordinary mechanical properties they possess [18]. These excellent properties, create a massive amount of research interest for BNNTs and they are viewed as the successors of CNTs. Researchers are replacing CNT with BNNT in various applications such as hydrogen storage [19], radiation shielding [20] and bio applications [21]. You can find a detailed comparison between CNT and BNNT in (Table 2).

Two main challenges faced in BNNT research are efficient synthesis and the functionalization of BNNTs [22]. Unlike CNTs, BNNTs doesn't have well established synthesis method that can provide large amounts of high quality BNNTs required for the detailed investigation of their applications. Furthermore, high chemical stability of BNNTs makes their functionalization very difficult. Functionalization is required for

19

BNNTs since their natural desire for agglomeration results in poor dispersibility which hinders their ability to be used in composite, biomaterial and thin film applications.

Table 2 Comparison between properties of carbon nanotubes and boron nitride nanotubes

	BNNTs	CNTs
Color	White	Black
Electrical properties	Wide band gap semi-conductors (5,5 eV) [14]	Semiconducting or metallic depending on the number of walls, diameter, chirality[23]
Thermal Properties	~ 1620 W/mK [24] Stable up to 800 °C [25]	~ 3000 W/mK [26] Stable up to 500°C [27]
Mechanical properties	1.18 TPa Young M. [18]	~ 1 TPa Young M. [28]
Optical Properties	Applicable in the deep-UV regime [29]	Applicable in the Infrared to visible region [30]

CNTs have well established and efficient synthesis methods [31-33] whereas BNNTs synthesis is challenging and have low yield. One of the main challenge of the BNNT synthesis is to establish synthesis method which can produce high amounts of BNNT with high quality and efficiency. Some of the challenges encountered during the BNNT synthesis are:

- High temperature requirement
- Uncontrollable growth location
- Low efficiency
- Dangerous chemicals used in the synthesis

In the past decade, many researchers proposed different synthesis methods for the problems encountered in BNNT synthesis and most of the time they are derivatives of well-established CNT synthesis methods. Laser ablation [34, 35], ball-milling [36, 37], arc-discharge [15, 38, 39], carbon substitution from CNT templates [40], CVD (chemical vapor deposition) with borazine precursor [41-43], boron oxide CVD (BOCVD) [44-46], extended vapor-liquid-solid (VLS) method [47], plasma-enhanced pulsed-laser deposition (PE-PLD) [48] and more have been proposed and experimented on. Aside from PE-PLD method, all of the above mentioned techniques requires high temperatures, dangerous chemicals and they have high cost. Patterned growth of BNNTs were achieved by PE-PLD method but the results show, slow growth rate and low quality BNNTs.

CVD method have attracted considerable amount of interest for the synthesis of nanoparticle research. Thermal CVD method is very easy to use, yields high amount of pure product with good quality and easy to scale up in addition to excellent growth control it provides [49]. The discovery of BOCVD (boron oxide chemical vapor deposition) method had a huge impact in BNNT research. BOCVD method granted researchers to integrate thermal CVD with BNNT synthesis which allowed researchers to investigate new properties and applications of BNNTs [50-57]. Growth vapor trapping is a new method employed by the researchers to increase the amount of BNNT synthesized by BOCVD method [29, 58]. This method is also applied in this work with combination with BOCVD method.

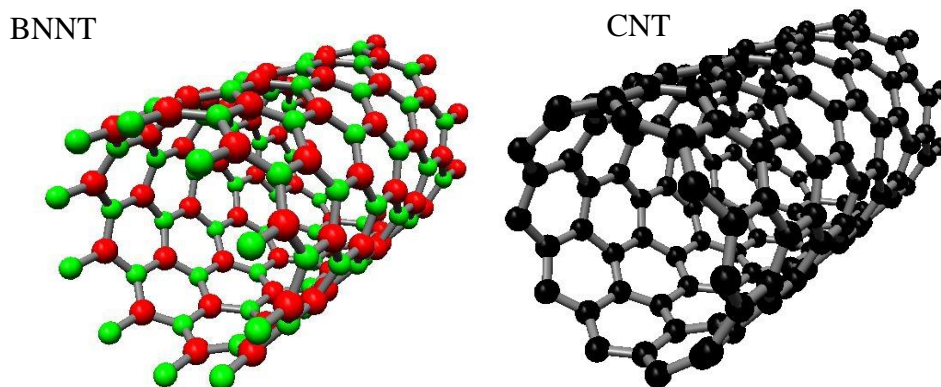


Figure 2 Structural models of BNNT and CNT

## 1.2 Previous and Current Synthesis Techniques

As mentioned above, BNNT synthesis methods are far from perfect and needs further optimization and modifications. Most of the synthesis methods for the BNNTs have been derived from CNT synthesis methods that has been used for over decades now. In this section, various synthesis methods for BNNTs will be briefly explained.

### 1.2.1 Laser Ablation Method

For the investigation of BNNT characteristics, synthesis method capable of producing high quality and high quantity BNNTs were needed. In order to overcome this problem,

Lee et al. [34] proposed a metal-catalyst free BNNT synthesis method which uses CO<sub>2</sub> laser ablation to produce bulk amount of BNNTs. In this synthesis method, catalyst-free, rotating BN target is ablated with the CO<sub>2</sub> laser under nitrogen atmosphere. Ablated material is then carried by the nitrogen flow and filtered, resulting in light beige and dense gray film coating on the filter.

Another way of synthesizing BNNTs by laser ablation method is to use an oven-laser ablation method. In this method the target material is not only h-BN (hexagonal boron nitride) but a mixture of high purity h-BN, nickel nanopowder and cobalt nanopowder. In this method oven is heated up to 1200 °C and target is ablated with a laser. Ablated laser plums then carried by carrier gas such as argon, helium and nitrogen and collected on the water-cooled copper collector. SEM images of the as-synthesized BNNTs can be seen below (Figure 3) [35]. This technique yields BNNTs with 1.8 to 8 nm diameter however purity of the BNNTs are low.

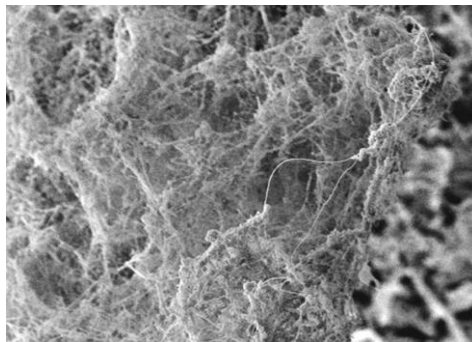


Figure 3 SEM image of BNNT ropes synthesized by the laser ablation method

Laser ablation method is excellent for synthesizing large quantity BNNTs however the cost of the method and low purity are a major disadvantages.

### 1.2.2 Ball-milling Method

Ball-milling synthesis method is a physical solid state process for synthesizing BNNTs with large quantities in low temperatures. Theory behind the technique can be summarized as, mechanical energy is transferred to boron precursor by grinding, fracturing, thermal shock, intimate mixing, *etc.* in order to start structural, morphological and chemical changes. Ball-milling essentially creates metastable disordered BN



nanostructures which with low thermal energy transforms to BNNTs. Due to changes are started with mechanical energy rather than thermal energy, reactions at a low temperature become possible.

Chen et al. [59] used this technique with elemental boron powder as boron precursor and ammonia as nitrogen precursor. They performed ball milling at room temperature using hardened steel balls and stainless steel cell. After the milling process, they annealed powders at  $<1000$  °C under inert gas atmosphere. After annealing they reported BNNTs with diameters between 20-150 nm (Figure 4). Chen et al. further investigated the ball-milling method in their later paper [37] where they reported BNNTs with about 11 nm and with bamboo-like morphologies.

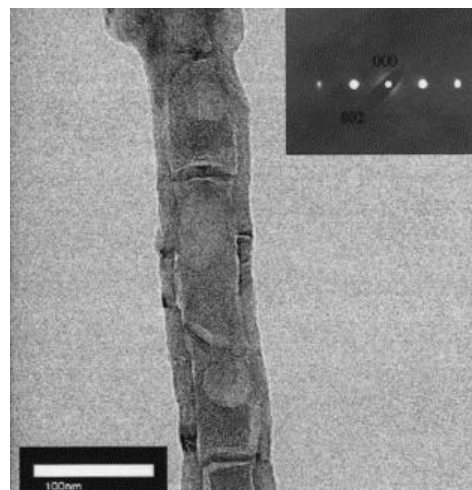


Figure 4 TEM image of the as-synthesized BNNTs by ball milling with electron diffraction pattern from the walls of the nanotube.

Lim et al. [36] used ball-milling method to produce BNNTs for hydrogen storage applications. They used boron-nickel catalyst which is prepared by ball milling and they annealed ball-milled catalyst mixture at  $1025^{\circ}$  C. In contrast to Chen et al., Lim and his group also used hydrogen when annealing catalyst mixture to increase the efficiency of hydrogen uptake. Finally, they reported BNNTs with diameter ranging from 20nm to 250nm with bamboo like morphologies.

### 1.2.3 Carbon Substitution Method

Since structure of CNTs and BNNTs are very similar, researchers suggested to use CNTs as a template to synthesize BNNTs. In this technique carbon atoms present in the CNTs are substituted by boron and nitrogen atoms and it is called carbon substitution method. This method was first employed by Han et. al. [40] where they placed  $B_2O_3$  powder on top of the graphite cubicle and added CNTs onto the  $B_2O_3$  powder. They loaded graphite cubicle into the induction furnace and held them at 1773 K for 30 min. They explain CNT to BNNT conversion with the reaction 1,



CNTs they used was synthesized via CVD route and resulting gray colored powder was further purified by oxidation. This synthesis route later used to synthesize BNNTs from B-C-N tubes [60]. Although this technique results in fine BNNT structures, removing carbon from the final product still remains a challenge. Furthermore, need of induction furnace and high temperature makes this synthesis method unfavorable.

### 1.2.4 Extended Vapor-Liquid-Solid Method

In most of the synthesis methods, boron is supplied from various boron vapors or solid precursors which makes it harder to understand the growth mechanism of BNNTs. In their work, Fu et al. [47] proposed more concise way of producing BNNTs by extended vapor-liquid-solid method. In this method, boron is provided by the iron-boron alloy itself. Fe-B catalyst is nitrated by ammonia at 1100 °C in order to synthesize BNNTs. This method provides BNNTs with diameter around 20 nm and lengths in the order of micrometers. They also proposed a growth mechanism, suggesting that BN species are formed when nitrogen and boron atoms react inside the catalyst droplet and if the BN species inside the droplet reaches to supersaturation, BNNT nucleation begins. This method provides very important insights into growth mechanisms of BNNTs. Similar growth mechanism was also used in the literature for the growth of the Si crystals (Figure 5) [61].

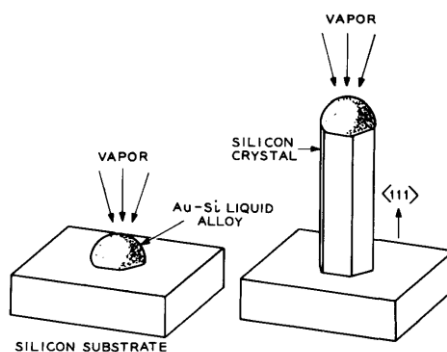


Figure 5 Schematic of silicon crystal growth by VLS. Same growth mechanism is theorized for BNNT synthesis as well.

### 1.2.5 Plasma Enhanced Pulsed Laser Deposition (PE-PLD)

Growing BNNTs on substrates to use in device fabrication have been a challenge since the discovery of BNNTs [62]. Most of the synthesis methods have low production yield and high amount of impurities. Furthermore high temperature requirement for growth also possesses a challenge. Wang et al. [48] proposed a synthesis method for BNNTs which can overcome some of the challenges faced in the synthesis of BNNTs. In summary, they induced negative substrate bias by a nitrogen rf-plasma to supply reaction spots for BNNT growth. Biased substrate with iron coating accelerates both positive ions in the plasma and the BN vapors that result in the bombardment of BN vapors on the substrate surface. When kinetic energy of BN vapor reaches a critical value, total re-sputtering induces BNNT growth on the substrate. Synthesis method requires 600 °C and substrate bias of -360 and -450 V. This method yields high amount of BNNTs with diameter of 20nm that is deposited onto substrate surface. Additionally, iron film on the substrate can also lead to controlled growth of BNNTs (Figure 6) [48].

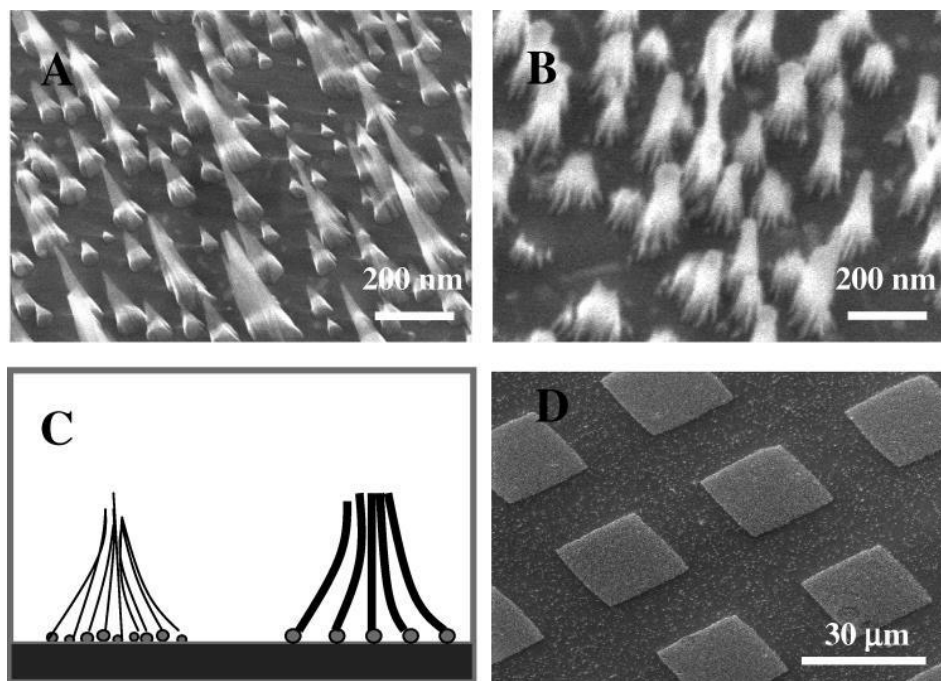


Figure 6 Patterned growth of BNNTs with substrate bias a. -380 mV and b. -450 mV. c. Bundling configurations respectively and d. SEM images of patterned BNNTs on wafer taken from the literature.

### 1.2.6 Chemical Vapor Deposition Method (CVD)

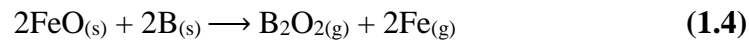
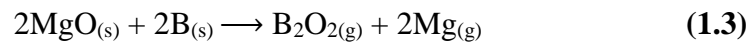
Chemical vapor deposition method has been widely used as CNT and nanowire synthesis method with great success [63-66]. Due to similar structural properties of BNNTs to CNTs, Lourie et al. proposed a new way of synthesizing BNNTs by traditional CVD method which is already used in the synthesis of CNTs [41]. In this method, in situ generated borazine ( $B_3N_3H_6$ ) is used as precursor. Borazine is generated by the reaction 2 given below;



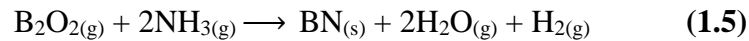
This method synthesizes BNNTs when Co, Ni, NiB and  $Ni_2B$  are used as catalyst. (NiB catalyst gives the best results.) Later on, Kim et al. improved this synthesis method by using nickelocene as a floating catalyst [42]. They reported successful synthesis of double-walled BNNTs with floating nickelocene catalyst in conjunction with borazine. However both nickelocene and borazine are highly dangerous materials which is a big disadvantage of this synthesis method.

### 1.2.7 Boron Oxide Chemical Vapor Deposition

CVD method for synthesizing BNNTs attracted great amount of interest however, dangerous nature of borazine precursor and nickelocene catalyst created a need to find better catalyst and precursor for the CVD process. Discovery of the BOCVD method supplied a solution to this problem [44, 45]. In the BOCVD method B, MgO and FeO powders are used as precursor materials and NH<sub>3</sub> is used as nitrogen source. Boron reacts with MgO and FeO when heated by induction heating to  $\leq 1300^{\circ}\text{C}$  according to reactions 3, 4 given below;



The resulting boron oxide gas reacts with the decomposed ammonia gas and creates BNNTs as the reaction 5 given below;



This method allows BNNTs to be synthesized in vertical induction furnaces with high yield. However, this method requires specially designed vertical induction furnace, high temperature and large temperature gradient, all of which are undesirable demands for the large scale synthesis of BNNTs. Examples of this synthesis method can be found in the literature (Figure 7) [67].

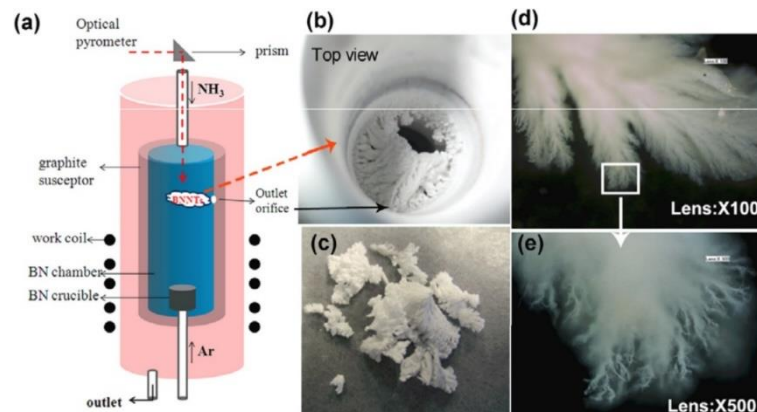


Figure 7 a.Schematic of vertical induction furnace used in BOCVD method. b. White coatings of BNNTs on the walls of the reaction chamber. c. As-synthesized product. d. and e. Optical microscope images of as-synthesized BNNTs.

### 1.2.8 Growth Vapor Trapping Method

There is no doubt that BOCVD method for BNNT synthesis was a big breakthrough. BOCVD system allowed researchers to synthesize high amounts of high quality BNNTs to be used in further research of BNNTs. However, system requires specially designed vertical induction furnace which is not very common in many laboratories. Furthermore, synthesis method also needs high temperatures to achieve efficient BNNT synthesis which in turn makes it impossible to synthesize BNNTs on substrates such as silica. In order to overcome these obstacles Lee et al. proposed a new and simple synthesis route for BNNTs (Figure 7) [58]. This synthesis method takes advantage of nucleation theory of whisker which will be explained greatly in the upcoming parts of this thesis. Additionally, this method makes use of tube furnaces which are very common ovens used in CNT [68] and ZnO [69] nanoparticles.

It can be said that, most essential equipment in growth vapor trapping method is the one-end closed quartz tube with lower outer diameter than of alumina tube of the tube furnace. This quartz tube allows the growth vapor to be trapped and ammonia to diffuse into the alumina boat slower than normal since the close-end of the tube faces off against the ammonia flow which in turn increases the efficiency of the system [58]. BNNT production is achieved by mixing amorphous boron powder, MgO and FeO ( $\text{Fe}_2\text{O}_3$ ) catalyst with a designated ratio and place them into alumina tube which is then placed into the close-end of the quartz tube. Quartz tube is placed into tube furnace in a way that alumina boat's position corresponds to the sweet spot of the furnace. Synthesis takes place at 1200 °C under ammonia atmosphere.

Lee et al. further investigated the growth vapor trapping method with their next paper where they aimed for patterned growth of BNNTs [29]. In order to achieve this goal, they coated silicon wafers with  $\text{Al}_2\text{O}_3$  buffer layer and after that they applied a second coating layer with MgO and third coating layer of Ni or Fe by pulsed laser deposition. The patterned growth of BNNTs were achieved by the same growth vapor trapping technique they used in their previous paper but this time they used coated silicon substrates instead of non-coated silicon substrates.

Growth vapor trapping synthesis method provides high yield, high quality BNNT with controllable growth at low temperatures such as 1200 °C and lower. Some researchers even further modified this method to decrease the temperature parameter and, need of vacuum by using Ar as carrier and sweeping gas [70].

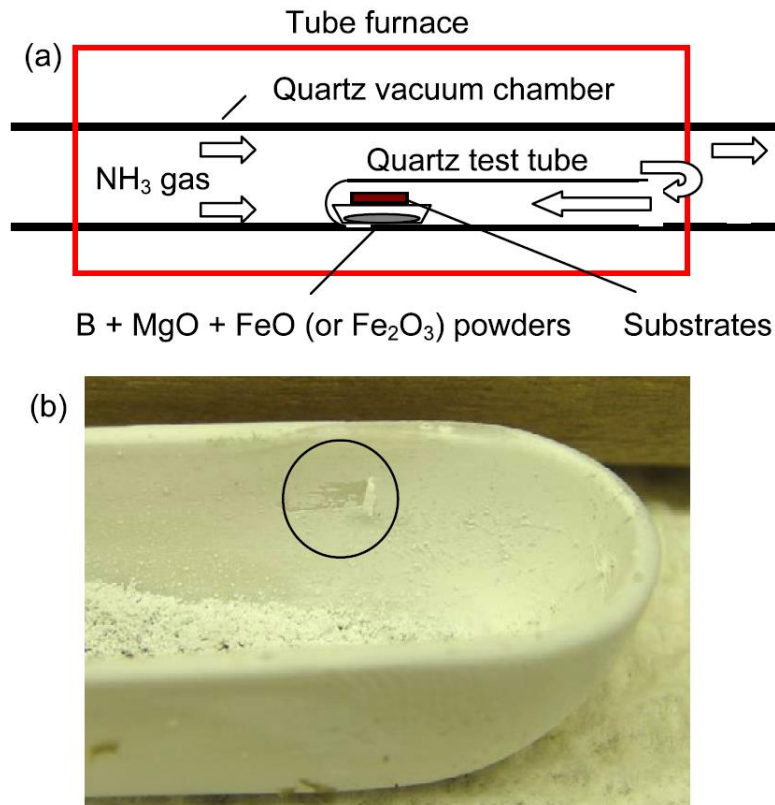


Figure 8 a.Schemtaic of the system for the growth vapor trapping method. b. As-synthesized BNNTs on the walls of the alumina boat.

### 1.3 Properties of BNNTs

Boron nitride nanotubes possesses extraordinary properties just like CNT and even better properties in some cases.

### 1.3.9 Mechanical Properties

Mechanical properties of BNNTs, especially elastic properties they possess have been thoroughly investigated theoretically. Tight binding formalism [71], ab-initio calculations [72, 73], Tersoff-Brenner potential [74] is some of the methods that has been used to calculate elastic modulus of BNNTs. The results in these studies were similar to each other with elastic modulus of BNNT predicted to be at around 0.8 to 0.9 TPa which is slightly smaller value than that of CNTs [71]. However, ab-initio calculations run by Dumitrica et al. showed that, BNNTs' yield defects have higher activation energies than CNT's yield defects, resulting in stronger structure for BNNTs than CNTs at elevated temperatures in contrast to stronger structure of CNTs than BNNTs at low temperatures.

Experimental calculations of BNNTs show different results than each other. Young modulus of BNNTs were reported to be  $1.22 \pm 0.24$  TPa by Chopra et al. [18] which is higher than the theoretically predicted young modulus of BNNTs. However, the group claimed that their nanotubes had high crystalline structure with low defect density and they related sudden increase of young-modulus to fine crystalline structure of as-synthesized BNNTs. Suryavanshi et al. [75] used electric-field-induced resonance method to experimentally calculate young modulus of BNNTs grown by BOCVD method. They reported 722 GPa young modulus value for MWBNNTs which is a closer to theoretical calculations. Like Suryavanshi et al., Goldberg et al. also experimentally calculated young modulus of MWBNNTs grown by BOCVD method but they used more direct method, TEM – AFM piezo driven holder and reported even lower values of 0.5 – 0.6 TPa (Figure 9) [76]. It is obvious from the above literature that, BNNTs grown by BOCVD method exhibits lower young modulus than BNNTs grown by arc-discharge method since they have higher deformation density.



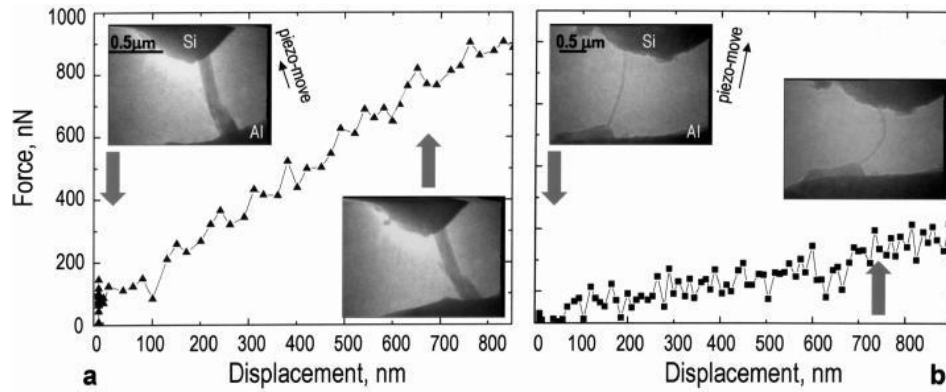


Figure 9 Force vs displacement curves for the a. Thick and b. Thin BNNTs. Insets shows the morphologies of BNNTs before and after bending taken from the Goldberg et al.'s article.

Plastic deformation of BNNTs were also theoretically calculated and results were disappointing [77]. Zhang et al. showed that, although (n, n) BNNTs can withstand plastic deformation as much as CNTs in similar structure whereas (n, 0) BNNTs cannot withstand plastic deformation as well. Bond rotation defects caused by plastic deformation lead to weakening of (n, 0) BNNTs much faster than CNTs or (n, n) BNNTs.

Poisson ratio of BNNTs were also theoretically calculated and found to be 0.16 for BNNTs [74].

### 1.3.10 Electrical Properties

Similar to other boron nitride materials, BNNTs are also wide band gap semiconductors [78] with no dependence to chirality, diameter or number of walls [14]. Because BNNTs possess band gap of 5.5 eV they are considered excellent insulator materials at room temperature [29].

One of the interesting aspect of electrical properties of BNNTs is that, their band gap and electrical properties can be modified by doping. Fluorine doping can decrease their resistivity from  $\sim 300 \Omega \cdot \text{cm}$  to  $0.2 - 0.6 \Omega \cdot \text{cm}$  as reported by Tang et al. [79], or carbon doping can induce well-defined semiconducting electrical properties as shown by the Goldberg et al. [80]. Addition to doping, electrical properties of BNNTs can also be

modified by applying transverse electrical field. Applying transverse electrical field induces giant stark effect which can reduce the band gap of the BNNTs making them more favorable for electrical applications [81].

First signs of piezoelectric behavior of BNNTs were found experimentally by Zettl et al. [82] with their investigation of band gap tuning of BNNTs by bending deformation. This research showed that, insulating characteristic of BNNTs can be altered when tube bending is applied and current can be transported through the tubes with reversible fashion.

Literature shows that, BNNTs are wide band gap insulators without any dependence on the chirality, tube diameter or number of walls. Furthermore, their band can be modified by doping, applying transverse electrical field or deformation to change insulating BNNTs to semiconducting BNNTs [22].

### **1.3.11 Thermal Properties**

BNNTs are electrical insulators with high thermal conductivity [83] with phonons responsible for the conduction of heat [84]. Experimental research on the BNNTs shows, at low temperatures BNNT's thermal conductivity increases with the increase of tube diameter [85]. Thermal conductivity of BNNTs were reported to be ~18 W/mK for pure BNNTs, ~17 W/mK for bamboo-like BNNTs, 46 W/mK for collapsed BNNTs by Tang et al. (Figure 10) [86]. It is suggested that, thermal conductivity of BNNTs are far lower than the CNT's thermal conductivity [26]. However, isotopically enriched BNNTs showed thermal conductivity rivaling CNTs due to isotope effect [87], showing 50% increase of thermal conductivity for isotopically enriched BNNTs.

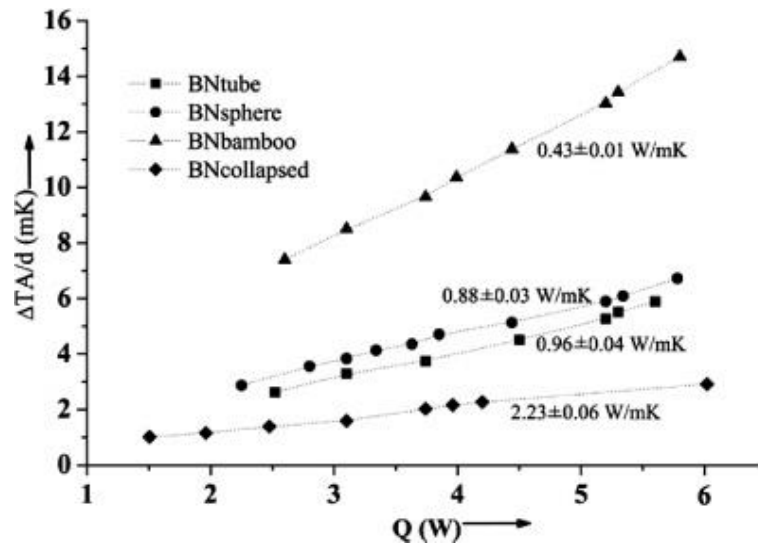


Figure 10 Thermal conductivities of as-synthesized BN nanostructure at different temperature gradients.

Addition to good thermal conductivity, BNNTs also shows good thermal resistance. Unlike CNTs, which shows thermal stability up to 400 °C, BNNTs are stable up to 700 °C in air, and even stable up to 900 °C in air if the BNNTs have small diameters with good crystallinity [88]. As demonstrated with their mechanical properties, thermal stability of BNNTs also depends on the quality of the tube morphology just like CNTs which show higher thermal stability when synthesized via arc-discharge rather than CVD [89]. BNNTs shows thermal stability up to 900 °C if synthesized by the BOCVD method which suggest even higher thermal stability for BNNTs synthesized by arc-discharge method since they have less defects in their structure. Their resistance to oxidation at high temperatures, makes them promising candidates for oxidation resistance polymer composites, or protective film applications.

### 1.3.12 Optical Properties

As pointed out above, BNNTs are promising materials for thin film applications. Due to this possibility, optical properties of the BNNTs must be understood completely. Optical absorption bands for the BNNT were found to be 4.45 eV and 5.5 eV by the Lauret et al. [90]. Cathodoluminescence analysis of BNNTs shows two peaks: strong absorption band at ~320 nm and weak absorption band at ~223 nm [91]. Optical band gap of the BNNTs

changes with their quality: High quality BNNTs experiences optical band gap at ~6.0 eV [29] whereas Lee et al. reported strong optical band gap at ~5.9 eV with two other sub band gaps at 4.75 and 3.7 eV for their growth vapor trapping method synthesized BNNTs [46].

Furthermore, BNNT composites appears to preserve their transparency even after the addition of BNNTs making them viable for numerous applications such as aerospace, automobile and *etc.* [25].

## **1.4 Functionalization of BNNTs**

One of the most challenging aspects of BNNTs is to functionalize them in order to use in applications. High chemical inertness of BNNT structure makes it very hard to chemically functionalize them. Nature of the B-N bond makes it very hard to functionalize BNNTs and like CNTs chemical functionalization of BNNTs highly depends on the defects on the structure. Two main functionalization routes have been proposed for the functionalization of BNNTs: Covalent functionalization and non-covalent functionalization

### **1.4.13 Covalent Functionalization of BNNTs**

Covalent functionalization can be achieved on boron sites (B-site) or nitrogen sites (N-site) of the BNNTs [22]. Covalent functionalization of BNNTs on N-sites mainly relies on the reactions between amino groups of the BNNTs and molecules used for functionalization. First experimental trial for the functionalization of BNNTs on N-sites were reported by Zhi et al. where they linked stearoyl chloride chains to BNNTs (Figure 11) [92]. Reactions between COCl (acyl chloride) groups on the stearoyl chloride and amino groups of the BNNTs allowed long stearoyl chains to attach to the surface of the BNNTs (Figure 11). Resulting functionalized BNNTs were reported to be soluble in organic solvents such as acetone, ethanol, chloroform *etc.* Same group later expanded the N-site functionalization where they functionalized BNNTs with naphthoyl chloride, butyryl chloride and stearoyl chloride [93]. Sainsbury et al. used amine and thiol

functionalized BNNTs as a templates for gold particle assembly [94]. Amine functionalization of BNNTs were achieved by ammonia plasma treatment of BNNTs [95]. This method further increases the amino group concentration on the surfaces of BNNTs to allow more effective functionalization.

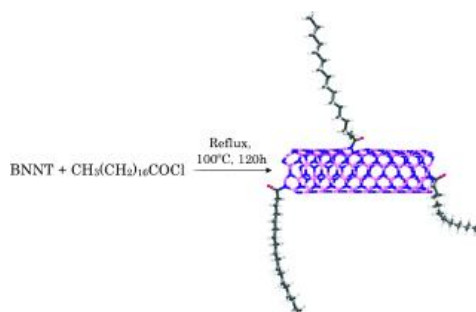


Figure 11 Schematic of covalent functionalization of BNNTs with stearoyl chloride.

B-site functionalization of the BNNTs are also possible. There are two distinct methods for functionalization of BNNTs on B sites and they both involves hydroxyl groups on the surface of the BNNTs on B-sites. Treating BNNTs with  $\text{H}_2\text{O}_2$  was first suggested by Zhi et al. where they reported successful hydroxylation of BNNTs after treatment with hydrogen peroxide [96]. They reported hydroxylated BNNTs showed good solubility in water, and suggested that, attached hydroxyl groups can be used for further functionalization. Later, Huang et al. used BNNTs hydroxylated by hydrogen peroxide for further functionalization with POSS (Polyhedral Oligomeric Silsesquioxane) [97]. Resulting BNNTs were further used for the production of epoxy composites. Another way for hydroxylation of BNNTs were proposed by Ciofani et al. (Figure 12) [98] where they used nitric acid treatment instead of hydrogen peroxide treatment to hydroxylate the surfaces of BNNTs (Figure 11). They reported water soluble hydroxylated BNNTs and they used the hydroxylated BNNTs for further functionalization with APTES ((3-Aminopropyl)triethoxysilane)). Overall, B-site functionalization is favored for the functionalization of BNNTs since hydroxylated BNNTs are dispersible in aqueous media and can be used as starting materials for further functionalization.

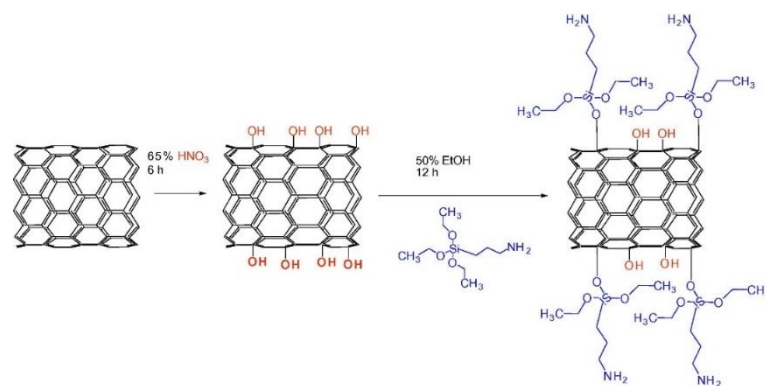


Figure 12 Hydroxylation and further functionalization of BNNTs.

#### 1.4.14 Non-Covalent Functionalization of BNNTs.

BNNTs can interact with materials via  $\pi$ - $\pi$  stacking. This advantage of BNNTs over CNTs, allow polymer wrapping of the BNNTs. Non-functionalized BNNTs are not soluble in aqueous media and this hinders their ability to be used in applications. Wrapping BNNTs with polymers can be a one way to solve them in aqueous media. BNNTs interact with the polymer chains due to  $\pi$ - $\pi$  interaction and this interaction results in the wrapping of BNNTs with the polymer. Polymer wrapped BNNTs then can be dispersed in aqueous media. First example of this non-covalent functionalization was achieved by wrapping BNNTs with PmPV (Poly[(m-phenylenevinylene)-co-(2, 5-dioctoxy-p-phenylenevinylene)] [99]. BNNTs wrapped with PmPV showed good solubility in water and they preserved their unique properties since the functionalization is achieved by non-covalent interactions and no chemical reactions were present during the functionalization. Following the success of the polymer wrapping with PmPV, researchers tried different polymers to wrap BNNTs to achieve aqueous dispersion. Ciofani et al. wrapped BNNTs with glycol-chitosan in order to disperse BNNTs in water and reported concentrated dispersions of BNNTs in aqueous media [100]. Same group later wrapped BNNTs with PEI and again reported successful dispersion of BNNTs in aqueous media [101]. Wrapping of BNNTs with poly-Lysine also resulted in the dispersion of BNNTs in aqueous media [102]. To summarize, polymer wrapping of BNNTs appears to be very promising route for dispersing them in aqueous media. Addition to dispersing them in aqueous media, polymer wrapped BNNTs can also be used

in the production of polymer composites since they have a good interface interactions with the polymers due to  $\pi$ - $\pi$  stacking.

Apart from polymer wrapping, surfactants can also be used for the non-covalent functionalization of BNNTs. Yu et al. reported successful dispersion of BNNT with the help of ionic surfactant ammonium oleate (Figure 13) [103]. Their work showed that, due to non-covalent interactions between the ionic surfactant and the BNNT, BNNTs can be dispersed in aqueous media without losing their intrinsic properties.

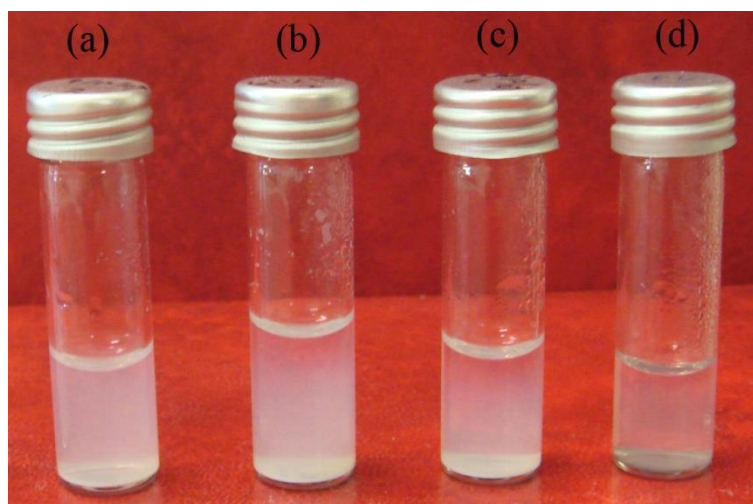


Figure 13 Aqueous BNNT dispersion with the help of ionic surfactant after a. 8 days, b. 11 days, c. 14 days, d. 60 days.

In summary, non-covalent functionalization of BNNTs appears to be promising route for dispersion of BNNTs in aqueous media. Aqueous dispersions of BNNTs enables researchers to investigate toxicity of BNNTs for biomedical applications as well as allowing production of polymer composites. In our work, we used non-covalent functionalization methods in order to disperse BNNTs in aqueous media.

### 1.5 Applications of Boron Nitride Nanotubes

Nanotechnology and nanoscience has opened up new and promising fields of research for the last decades. Extraordinary properties of nanomaterials such as nanotubes, nanoparticles, nanowhiskers, nanoplates, etc. opened up a way to modify and enhance the traditional materials. Composites with nano fillers [104], nano circuits for optical

applications [105], nano coatings for corrosion resistance materials [106], Li-ion batteries with nano electrodes [107], drug delivery systems with nano materials [108], radiation shielding nano composites [109] and such showed the world potential of nanomaterials.

Especially, discovery of CNT and their excellent properties attracted tremendous research interest in many science and technology fields [9-12, 110-120]. Functionalization [121], dispersion [122] and biological risk assessment and CNT composites [123] have been investigated by many research groups and still being researched today. Since BNNTs also possess similar structural properties as CNTs and sometimes even better properties, excessive effort has been put onto BNNT research. In this section, we will discuss the current state of BNNT research in various applications such as composites, biomaterial, radiation shielding, hydrogen storing.

### **1.5.15 Composites**

Composite materials are widely used in various industries such as, aerospace, biology, construction, automotive, military etc. Composite materials offer properties like lightweight, high mechanical strength and durability, corrosion resistance, low cost/performance ratio and much more. Excellent properties presented by composites increases their demand from the technology. Nanotechnology offers new and advanced filler materials for composite materials. Nanotubes are the very promising nano fillers that has been offered by nanotechnology since its first proposal by Ajayan et al. [124] by using carbon nanotubes as fillers materials in polymer matrix. Nanotube-polymer composites offers better electrical, optical and mechanical properties then that of polymers.

BNNTs offers electrical, mechanical and optical properties that are similar or greater than CNTs thus they attracted lot of interest by research groups all over the world as a composite material. First ever BNNT nanocomposite was reported by Zhi et al. [125] where the group used solution mixing method to achieve self-organized BNNT-PANI (Polyaniline) composite films. They showed that there is a strong interaction between BNNTs and PANI and also stated that PANI became more ordered when paired with BNNTs in nanocomposite structure. Researchers also produced BNNT nanocomposites



with different polymers, Zhi et al. [50] reported BNNT/polystyrene composites prepared by sonication assisted solution-evaporation method and they showed 7% to %20 increase in elastic modulus of the polymer when BNNT is added (Figure 14). Ravichandran et al. [126] fabricated BNNT/Saran (co-polymer of vinylidene chloride and acrylonitrile) composites for photovoltaic packaging applications which showed desired transparency in visible region and also good thermal stability and barrier properties (which are very important parameters for photovoltaic packaging applications.). Lahiri et al. [127] synthesized PLC-BNNT composite films as an biodegradable material which shows 1370% increase in elastic modulus and 109% increase in tensile strength of starting polymer without any biocompatibility issues. Due to their high mechanical properties and the fact that they are thermal insulators, BNNT composites shows promising future.

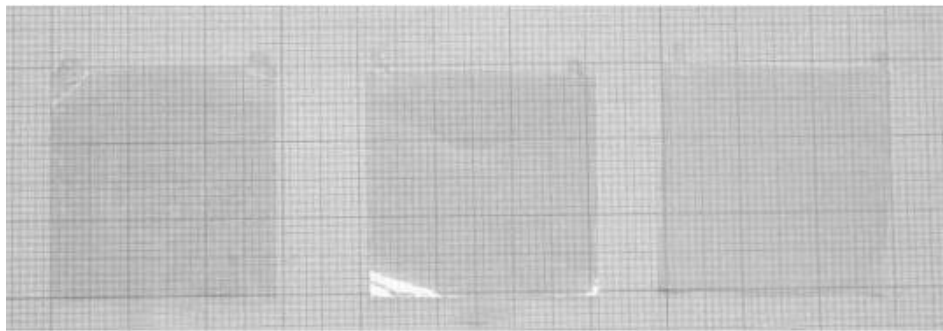


Figure 14 Images of a. PS film b. BNNT/PS composite film c. BNNT/PmPV/PS composite film prepared by solution-evaporation method.

BNNT reinforced glass composites are another topic of research in this subject. The main aim of BNNT/glass composites is to increase strength and fracture toughness of glass. Choi et al. fabricated BNNT – SOFC seal glass via hot pressing in order to achieve these goals [128]. They reported 90% improvement in the strength of the glass and 35% increase in fracture toughness in the composite compared to unreinforced glass. However, they also observed decrease in density, elastic modulus and Vickers microhardness. One interesting result they reported was, the rule of mixture was not applicable to the glass-BNNT composite.

BNNTs are also investigated as ceramic composite filler materials. Since BNNTs have high oxidation resistance, they can be used in ceramic composites. Huang et al. [129] produced first BNNT-ceramic composites by adding BNNTs to engineering composites. They report that addition of BNNT makes it easier for  $Al_2O_3$  and  $Si_3N_4$  to be molded

without altering any other properties they possess. Lahiri et al. [130] proposed BNNT reinforce hydroxyapatite composite where they achieved 120% increase in elastic modulus, 129% increase in hardness and 86% increase in fracture toughness. Other BNNT – ceramic composites includes BNNT reinforced SiO<sub>2</sub> [131] and BNNT-alumina composites [132].

BNNT composites shows great future as they enhance the properties of the matrix materials greatly. BNNTs ability to interact with polymers via  $\pi$ - $\pi$  interactions, remain optic transparent with glass matrix and high oxidation resistance to temperature makes them great reinforce materials for polymer, glass and ceramic matrixes respectively.

### **1.5.16 Biomedical Applications**

Stable structure, chemical inertness, bandgap without any dependence to helicity, diameter or chirality, tunable bandgap and adsorption only at deep-UV makes BNNTs perfect candidates for biomedical applications. Applications may range from diagnostic, therapeutic applications to cancer therapy.

As explained above, BNNTs shows good interactions with polymers, ceramics and glass. Furthermore, due to  $\pi$ - $\pi$  stacking interactions between BNNT side-walls and single-stranded DNA allows BNNT to interact with DNA. This can led to aqueous dispersions of BNNT which are biocompatible and non-toxic to biological tissues. Literature also shows that, there is strong interaction between proteins and BNNT [133]. Using the interactions between BNNT and proteins, researchers achieved immobilization of proteins on BNNTs which allows BNNTs to be used as biomaterials or biosensors [134].

Use of BNNTs in biomedical applications requires toxicity investigations. Chen et al. [135] investigated the toxicity of BNNTs and found that they are not cytotoxic and can be applied to therapeutic or diagnostic applications. Their findings further supported by Ciofani et al. 's [100] findings with MTT assay, reporting cytocompatible polymer wrapped BNNTs. Lately, study published by Çulha et al. also showed that surface functionalized BNNTs are non-toxic on HDF cells whereas they are toxic to cancer cells

such as A549 cancer cells. Furthermore carbohydrate modification further increases their cytocompatibility and their ability to disperse [136].

Addition to what is mentioned above, BNNT can be used in cancer research in different way. Boron's isotope  $^{10}\text{B}$  possesses very high neutron capture cross-section, using this information researchers invented BNCT (boron neutron capture theory) where sufficient amounts of  $^{10}\text{B}$  atoms targets cancer cells and radiation therapy is applied.  $^{10}\text{B}$  atoms absorbs the incoming low-energy thermal neutron and produces  $^4\text{He}$  ( $\alpha$ ) and  $^7\text{Li}$  linear recoiling particles that have very short penetration range [137]. Ciofani et al. [138] proposed using BNNTs as an effective boron atom carriers due to their high boron content, cytocompatibility [100] and chemical inertness. They reported high uptake of boron content on glioblastoma multiforme cells and nearly no uptake on normal human fibroblast. This results shows a promising future for the BNNTs in BNCT.

### 1.5.17 Radiation Shielding

Radiation damage is one of the main problems encountered in aerospace industry. Materials used in radiation shielding application should have properties such as;

- Low atomic number
- Lightweight
- Low volume
- High mechanical strength
- High thermal stability
- Low flammability
- High neutron absorption cross section
- High neutron-scattering cross section.

BNNTs satisfy all the needs for the radiation shielding materials. Furthermore,  $^{10}\text{B}$  atoms (isotope of B atoms) are very effective neutron absorbers since they have almost 3800 barn neutron-capture cross section [139].

There are three different types of use for BNNTs as radiation shielding materials. First, they can be used as hydrogen carrier and storage materials. Hydrogen is the most effective radiation shielding material known. However due to their inability to be processed prevents them from being used directly in radiation shielding applications. Researchers

suggested that since BNNTs show good hydrogen storage abilities as it will be mentioned later in this thesis too, they are good candidates for hydrogen-containing nanostructures for radiation shielding [140].

Another way of integrating BNNTs to radiation shielding applications to use their polymer composites as radiation shielding material. High hydrogen content polymers are widely used in radiation shielding applications however, their low mechanical strength creates a problem. Since BNNTs have high mechanical strength it's logical to think that they can be used to enhance mechanical properties of polymers in addition to increase their shielding capacities. Harrison et al. [141] investigated BN particles as a filler material for improving mechanical strength of polyethylene, a material that is widely used in radiation shielding applications. They showed that addition of BN particles improved the mechanical properties of polyethylene. This opens up possibility of BNNTs as filler materials since they have even better mechanical and shielding properties than BN particles.

Lastly, it has been suggested that, BNNTs with isotopically enriched  $^{10}\text{B}$  atoms can be synthesized using traditional CVD synthesis method and since they have great radiation shielding properties they can be used as radiation shielding materials on their own [139]. Sauti et al. patented boron nitride and boron nitride nanotubes as an effective radiation shielding material [25]. They patented both polymer-BNNT composites and free-standing BNNT films as effective radiation shielding material and even theorized space equipment can be fabricated using BNNT-polymer composites since the composite do not lose transparency when exposed to radiation.

### **1.5.18 Hydrogen Storage**

BNNTs' electrical properties which are independent of helicity, diameter and number of walls, and dipolar nature of the BN bonds creates a great advantage in their hydrogen storage abilities. Addition to that, as mentioned before, BNNTs shows great oxidation resistance, chemical inertness, high mechanical strength, thermal insulation, thermal and chemical stability which also makes them very viable options for hydrogen storage systems.

Pseudopotential density functional method calculations performed by Jhi et al. [142] showed there are 3 possible binding sites viable for hydrogen on BNNTs with high binding energy of 60 meV which is higher than their graphite counterparts. Following the various other theoretical calculations [143, 144], experimental studies were carried out to test the theories.

First experiments were carried out using h-BN particles. Wang et al. [145] reported when h-BN particles milled in hydrogen atmosphere hydrogen concentration reaches up to 2.6 wt% and theorized from their findings that (de-)hydriding process depends on the electronic structure rather than the defective nanostructure itself. After the reporting of the Wang et al. first investigation was done on BNNTs by Ma et al. [146]. They reported hydrogen uptake up to 1.8 – 2.6 wt% and highlighted the increase in hydrogen uptake compared to CNTs. Tang et al. [147] further modified the BNNT morphologies by heat treating them in the presence of platinum and the post treatment resulted in the collapsed BNNTs which showed increased hydrogen uptake as they give 4.2 wt.% hydrogen absorption. (Figure 15).

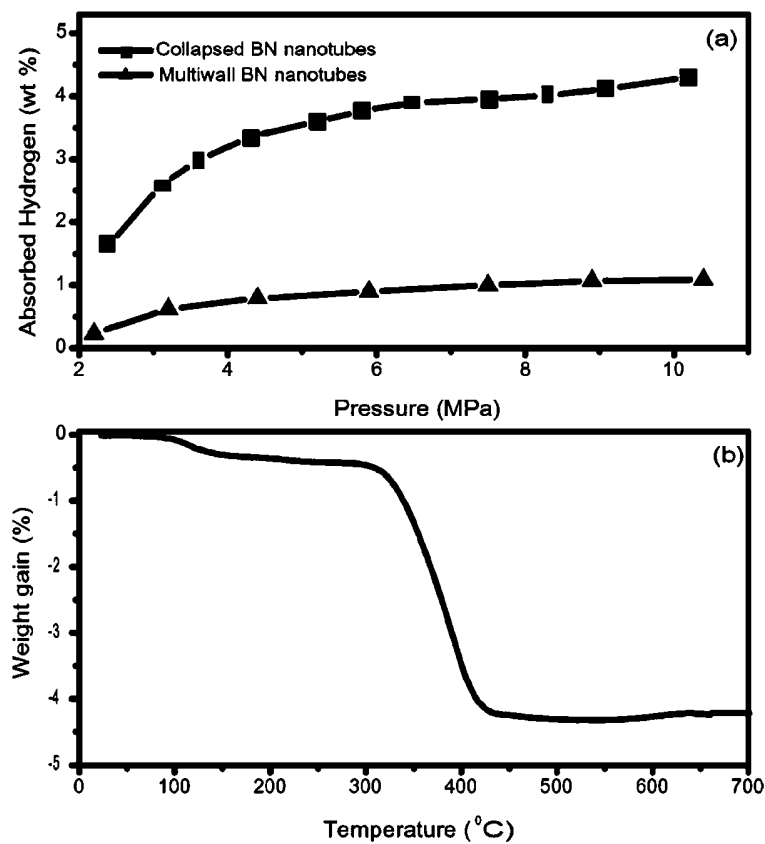


Figure 15 a. Hydrogen uptake of as-synthesized collapsed and multiwall BNNTs (Gravimetric). b. TGA spectrum of collapsed BNNTs during hydrogen release.

BNNT are very promising candidates for the hydrogen storage systems as they have good cycle life, high hydrogen uptake and thermal and chemical stability. However, for BNNTs to be considered commercial hydrogen storage material the hydrogen uptakes should increase to the levels of 6%.

## 1.6 Motivation

BNNT research have a very promising and important future ahead of it just like CNTs. As explained in the section 1.5, possible composite, hydrogen storage, radiation shielding and biomedical applications of BNNTs shows appealing results for the future of the BNNT research. However, two main challenges exist in the BNNT research: high yield synthesis of BNNTs and chemical modification of surfaces of boron nitride nanotubes.

Reliable, efficient and high yield synthesis of good quality BNNTs has been a considerable problem in the BNNT research [22]. In this thesis research, growth vapor trapping-BOCVD was optimized and used for the high yield synthesis of good quality BNNTs. Optimization studies were performed for the synthesis method, in terms of temperature, catalyst ratio, ammonia flow, catalyst amount and reaction time for high yield synthesis. Optimized recipe was further used for the synthesis of floating BNNTs, BNNTs on BNNFs and the BNNT synthesis from boron minerals. Moreover, optimization of the synthesis also allowed us to expand our knowledge about the growth mechanism of BNNTs.

Chemical modification of BNNTs is the next step for the BNNT research however high chemical inertness of the BNNTs [148] and agglomeration behavior of BNNTs in aqueous media makes it very problematic to chemically modify BNNTs. In this thesis work, we prepared aqueous dispersions of BNNTs, using covalent and non-covalent functionalization methods. Nitric acid [98] and ozone treatment was performed in order to hydroxylate as-synthesized BNNTs. Hydroxylation of BNNTs creates hydroxyl groups on the B sites of the BNNTs thus prevents nanotubes from agglomerating during the dispersion. Another advantage of hydroxylated BNNTs is, hydroxyl groups on the surface

can be used as a starting site for the further functionalization. In contrast to covalent functionalization methods, non-covalent functionalization methods for BNNTs do not alter the surface chemistry of the nanotubes since driving force behind the functionalization is  $\pi$ - $\pi$  non-covalent interactions [99]. In this work, polymer wrapping and surfactant assisted non-covalent functionalization methods were utilized in order to prepare stable aqueous dispersions of BNNTs. First, b-PEI was used as wrapping polymer to as-synthesized BNNTs in a similar fashion to what have been reported in the literature [101], followed by PAH wrapping of the as-synthesized BNNTs. In addition to polymer wrapping of BNNTs, ionic surfactant was also used for the dispersion of BNNTs in aqueous media in this thesis work in a similar procedure reported in the literature [103].

Finally, different boron minerals were tested as a boron source in the BNNT synthesis by growth vapor trapping-BOCVD method since they are cheaper and environmentally friendly compared to amorphous boron commonly used in the BNNT synthesis. To author's knowledge, there is only one reported research for the synthesis of BNNTs from boron minerals, where Kalay et al. [149] synthesized BNNTs from unprocessed colemanite. In this thesis work, investigation of boron minerals for BNNT synthesis were further expanded to include Ulexite and Etidot-67 boron minerals. These minerals have higher  $B_2O_2$  content in their structure which is an advantage for the synthesis of BNNTs by growth vapor trapping BOCVD method since growth vapors are produced by the reaction between ammonia and  $B_2O_2$ .

This thesis can be divided into 4 main topics (Figure 16); synthesis of BNNTs and optimization of CVD synthesis method, investigation of alternative boron sources for BNNT synthesis, functionalization and dispersion of BNNTs in aqueous media, and utilization of LbL technique to achieve free-standing BNNT thin films.

In chapter 2, experimental work done on this research will be discussed. Mainly, synthesis of BNNTs on Si wafers, free-standing BNNT synthesis, synthesis of BNNTs on BNNFs and synthesis of BNNTs from boron minerals will be detailed for the synthesis part of this thesis work. Following the synthesis of BNNT, we will discuss the surface modifications of the BNNTs aimed at dispersing them in aqueous media. Functionalization of BNNTs can be divided into two different routes: Non-covalent and covalent functionalization of BNNTs. In non-covalent functionalization of BNNTs,

polymer wrapping and ionic surfactant methods were used and later as-functionalized BNNTs were dispersed in aqueous media. In covalent functionalization of BNNTs, Nitric acid treatment and ozone treatment was used for the hydroxylation of BNNTs. Finally, our first investigation for the BNNT thin film production via LbL method will be presented in the chapter 2. In this work, as-prepared dispersions of BNNTs were used in LbL method to produce BNNT thin films on the glass micro-slide substrates.

In chapter 3, optimization of BNNT synthesis will be presented. Growth vapor trapping-BOCVD method allows synthesis of BNNTs on Si wafers as well as floating BNNTs with good efficiency and quality in commonly used horizontal tube furnaces at relatively low temperatures of 1200 °C. Optimization of the synthesis method can enhance the quantity and the quality of the synthesized BNNTs. Furthermore, each CVD system possess its unique characteristics and because of that, great effort was put into optimization of our BNNT synthesis method's parameters such as temperature, catalyst ratio, ammonia flow, catalyst amount, reaction time and other system variables which directly effects the above mentioned properties of BNNT synthesis.

Chapter 4 focuses on the interpretation of data we collected from the research of the BNNTs and their aqueous dispersions. SEM (scanning electron microscope), TEM (transmitting electron microscope), RAMAN spectroscopy, FTIR (Fourier transform infrared) spectroscopy and EELS (electron energy loss spectroscopy) characterization techniques were utilized for the characterization of the as-grown BNNTs. SEM and TEM analysis were used for the morphological characterization of BNNTs addition to RAMAN, FTIR and EELS spectroscopy for the investigation of chemical composition of as-synthesized BNNTs. FTIR and DLS analysis methods were utilized for the characterization of the functionalized BNNTs. FTIR analysis were performed in order to investigate bonds in the functionalized BNNT's structure and DLS analyses were performed to investigate stability of aqueous dispersions of BNNT with the help of the ionic surfactant and polymer wrapping.

Chapter 5, summarizes the overall conclusions of the research performed during the thesis work and proposes future work for the BNNTs.



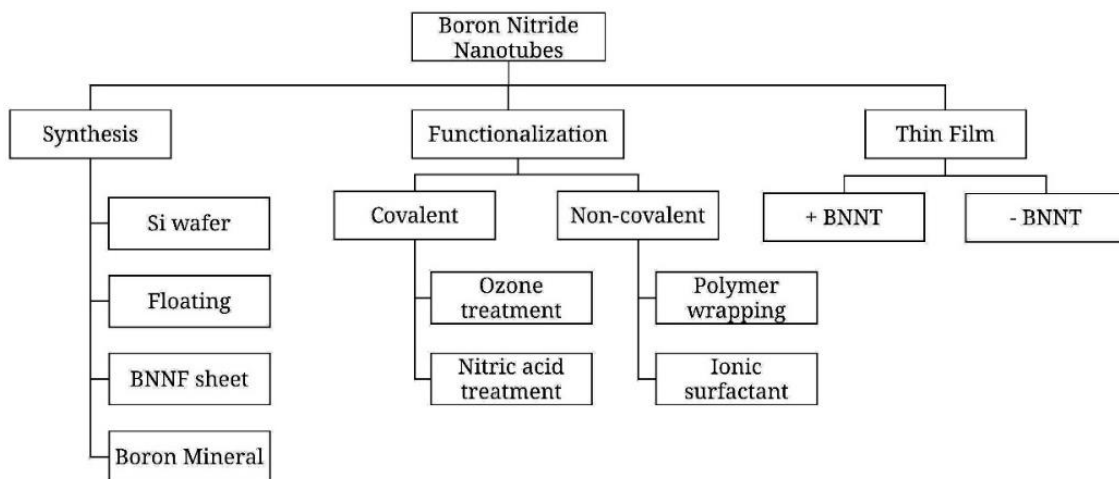


Figure 16 Flow chart of BNNT research done on this thesis work

## CHAPTER 2 Experimental Work

### 2.1 Materials and equipment

For the synthesis, hydroxylation, dispersion and BNNT thin film production of BNNTs, below equipment were used:

PFT 15/50/450 Protherm tube furnace, TFF 55035C-1 Thermo Fisher Scientific split furnace, 0-1 slpm Alicat flowmeter, 0-500 sccm Alicat flowmeter with corrosive gas resistance, 0-500 sccm Aalborg flowmeter with hydrogen gas calibration, 0-5 slpm Aalborg flowmeter with argon gas calibration, 2" diameter, 1 meter long alumina tube, 36mm inner diameter, 1 meter long one-end closed quartz test tube, 1" diameter, 500mm long quartz tube, alumina boats with various sizes, quartz substrate holder, 6" silicon wafer, Honeywell ammonia sensor, United ultrasonic bath, Qsonica tip sonicator, micro/solid sonicator tips, A2Z ozone generator, Ozone Systems Inc., Harric plasma, PDS-002 (230V) plasma cleaner

For the synthesis, hydroxylation, dispersion and thin film production of BNNTs, below chemicals were used:

Hydrogen peroxide solution, 34.5-36.5%, Sigma Aldrich, iron (III) oxide powder, < 5 $\mu$ m,  $\geq$ 99%, Sigma Aldrich, boron,  $\geq$ 99%, amorphous powder, magnesium oxide,  $\geq$ 99% trace metals basis, -325 mesh, polyethylenimine-branched (bPEI) MW ~ 25000, poly(allyamine hydrochloride MW ~ 58000, Poly(styrenesulfonate) MW ~ 70000, hydrochloric acid, puriss,  $\geq$ 37%, nitric acid,  $\geq$ 65%, BNNF, provided by Ayşemin Top and her group at İTÜ. |Boron minerals kindly provided by ETI Mine Works General Management (Turkey), anhydrous Borax – Na<sub>2</sub>B<sub>4</sub>O<sub>7</sub>, Etibor-68, Etidot-67, Na<sub>2</sub>B<sub>8</sub>O<sub>13</sub>.4H<sub>2</sub>O, ground colemanite, -45 micron, ground ulexite, -45 micron.

## 2.2 Growth Vapor Trapping-BOCVD synthesis of BNNTs

BNNTs were synthesized on Si wafers, BNNFs (boron nitride nanofiber) and as floating BNNT from amorphous boron powders with MgO and Fe<sub>2</sub>O<sub>3</sub> as catalyst. Additionally, various boron minerals as possible precursor for floating BNNTs were investigated. Growth vapor trapping-BOCVD method has been utilized for all the synthesis trials with necessary modifications. One of the objectives is to synthesize floating BNNTs and disperse them in aqueous media. Synthesis of BNNTs with low cost, high yield and quality is the first step to achieve this goal. As-used growth vapor trapping-BOCVD synthesis method offers desired synthesis possibility and also allows investigation of BNNT synthesis with new boron precursor materials and onto various substrates. Most crucial step of this experimental work is to synthesize floating BNNTs since our aim is to disperse them in aqueous media to further use future applications.

As mentioned in introduction chapter, BOCVD method requires temperatures higher than 1300 °C. This high temperature requirement makes BOCVD method very expensive and presents a huge disadvantage in future large-scale synthesis of BNNTs since it increases both time and energy needed for BNNT synthesis. Additionally, BOCVD method is only possible with special vertical induction furnaces.

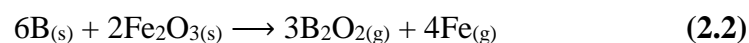
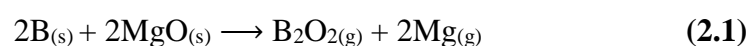
Combining growth vapor trapping method for BNNT synthesis with BOCVD method, offers low temperature, high yield, and high quality BNNT synthesis in frequently used tube furnaces [58]. In this work, modifications to growth vapor trapping-BOCVD method described in the literature were performed to suit our purposes.

First, vacuum was removed from the synthesis. Vacuum allows BNNT synthesis at relatively low temperatures with high quality and yield but it also increases the overall cost of the BNNT synthesis by 18% [70]. Furthermore, although it is relatively easy to achieve vacuum atmosphere in small-scale synthesis, it is a challenge in the large-scale synthesis of BNNTs. In our BNNT synthesis, vacuum atmosphere was replaced with inert Ar gas atmosphere. Argon flow worked as a both carrier for growth vapors and false vacuum generator. Apart from the reaction step of the synthesis, Ar gas flow was always present during BNNT synthesis.

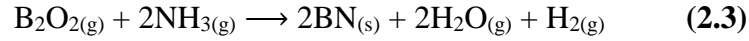
Second, 36 mm inner diameter, 450 mm long one-end closed quartz tube was used in our BNNT synthesis in order to trap growth vapors. There are several examples of one-end closed quartz tube usage in the literature [29, 58, 62]. As explained by the whiskers theory of nucleation, increasing partial pressures of growth vapors increases the nucleation probability of whiskers. One-end closed quartz test tube traps the growth vapors so that increase in partial pressures of growth vapors is acquired. Addition to trapping, one-end closed quartz tube also prevents ammonia flow to sweep away growth vapors away from the alumina boat. Quartz test tube is placed in a way that, open-end of the test tube faces the outlet of the furnace. This allows ammonia flow to enter quartz test tube in-directly thus reducing the flux of the ammonia gas.

Synthesis starts with the purging of the system by Ar gas. Inert Ar gas is flowed through the tube furnace in order to get rid of moisture and air. Following the purging, precursors are heated to 1100 °C under constant Ar flow and ammonia is introduced. Under ammonia/Ar mixture flow precursors are heated to 1200 °C reaction temperature and held there for 60 min under ammonia flow. After the reaction ends, ammonia flow is stopped and replaced by Ar flow until furnace temperature cools down to room temperature. At room temperature, samples are collected by simple mechanical extraction and they are stored at room temperature without the presence of moisture. Ammonia flow is introduced before the reaction temperature because of two reasons: First, boron-catalyst reactions start before 1200 °C and by introducing ammonia flow earlier than reaction temperature, no waste of as-produced B<sub>2</sub>O<sub>2</sub> vapors are ensured. Second, starting ammonia flow earlier than the desired growth temperature increases the reaction efficiency since reaction chamber is completely filled with ammonia. Except for the synthesis of BNNTs from various boron minerals all other synthesis routes follows the same growth recipe. Details of the recipe will be explained in the optimization chapter.

MgO (Magnesium oxide) and Fe<sub>2</sub>O<sub>3</sub> (Iron (III) oxide) were used as catalysts in BNNT synthesis except for BNNT synthesis from various boron minerals. After 1100 °C, boron powder starts reacting with catalysts according to reactions 2.1, 2.2 given below,



In-situ generated B<sub>2</sub>O<sub>2</sub> vapor acts as a boron precursor for BNNT synthesis and reacts with the ammonia where the reaction 2.3 given below produces BN species which are growth vapors,



Although, the main aspects of the growth mechanisms of BNNTs is still unknown, we support the theory proposed by Lee et al [58]. In summary, during the growth step of the reaction, catalyst vapors are generated as a result of boron-catalyst reactions and condenses onto the surface and creates droplets. When BN species' partial pressure reaches a certain point they began diffusing into the droplets and droplets became saturated. After supersaturation of BN species is achieved inside the catalyst droplet, nucleation of BNNTs begin. Our data also supports this theory since floating BNNT synthesis is only possible when the VLS synthesis mechanism is present.

In order to achieve high efficiency during the boron-catalyst reaction, homogeneous dispersion of the powders are crucial. To ensure that, catalyst powders were vortex mixed until such homogeneity is achieved. Homogenous dispersion also grants even growth in every positions of the alumina boat which is essential to BNNT growth on Si wafers.

On the other hand, in order to control the synthesis locations of floating BNNTs and BNNTs on BNNFs, alumina boat was loaded only partially with catalyst mixture to have empty spaces on the surface of the alumina boat. This provides two advantages; first, control over the synthesis locations for the high portion of BNNTs. This control is crucial for the BNNT synthesis on BNNFs in order to achieve synthesis of BNNTs mainly on the BNNFs. Furthermore, this allowed BNNTs to grow near the catalyst mixture in contrast to on top of them. Catalyst mixture was loaded into alumina boats in a way that, catalyst mixture filled portion of the alumina boat was positioned just next to close-end of the quartz tube. Due to this positioning, when ammonia gas entered the alumina boat, it carried B<sub>2</sub>O<sub>2</sub> and catalyst vapors over the catalyst mixture hence floating BNNT's nucleation started next to catalyst mixture rather than on top of it, preventing contamination by left-over catalyst and other impurities.

Different size alumina boats were used for each synthesis route. For BNNT synthesis on Si wafers smaller alumina boat was used for achieving smaller surface area of the alumina

boat and ensured main portion of the BNNTs were synthesized on the Si wafers. For floating BNNT synthesis bigger size boat was used in order to increase surface area of the alumina boat and ensure main portion of BNNTs were synthesized on the alumina boat's surfaces. For the synthesis of BNNTs on BNNFs, size of the boat was further reduced by using alumina blocks to increase amount of BNNTs on BNNFs rather than on the walls of alumina boat.

To investigate synthesis mechanisms behind the BNNT synthesis, BNNTs were synthesized on Si wafers. Si wafers have well defined surfaces with low roughness. They are easy to acquire and cheap compared to other wafers. Furthermore, they are partially stable up to 1100 °C making them suitable for our work. After the initial work was finished, Si wafers were continued to be used to cover our alumina boat to further trap growth vapors. Si wafers were placed diagonally as oppose to parallel since it ensures higher reduction of the volume and more efficient trapping of the growth vapors.

As our growth mechanism theory suggest, BNNTs need catalyst droplets in order to start nucleation. BNNFs were catalyzed by dipping them inside a catalyst solution. BNNFs absorbed both Mg and Fe catalysts from the solution creating catalyst coatings on the surfaces of the BNNFs. Later, to reduce Fe ions and oxidize Mg ions BNNFs were annealed, resulting in active catalyst coating on the surfaces of the BNNFs. Catalyst coating on the BNNFs are needed to create catalyst droplets where BN and catalyst vapor species diffuses into and starts nucleation of BNNTs.

For the synthesis of BNNTs from various minerals, commonly used boron minerals in industry were used as precursor materials. Ulexite, borax, colemanite and Etidot 67 were gifts from Eti Mine Works General Management (Turkey) and used without further processing. Boron mineral and catalysts were mixed inside DI water to ensure homogeneous mixing of the catalyst and boron minerals. Furthermore, mixing them in water, results in higher catalyst content on the surface of the boat which increases the efficiency [149]. Unlike BNNT synthesis by using borazine [42, 43], boron minerals are safe to use, safe to store and most importantly they are environmental friendly. Borazine is highly flammable, corrosive to human skin and upon decomposition produces toxic fume. Using borazine as precursor for BNNT synthesis is very risky say the least. In contrast to borazine, boron minerals are heavily used in the industry for multiple

applications, can be stored in normal conditions and do not decompose to produce toxic fumes. They are inexpensive and easy to acquire. Turkey is the leading producer of boron minerals for industrial use. All these advantages of boron minerals motivated us to investigate them as a boron precursor for BNNT synthesis. If successful, they can be promising candidates for the large-scale synthesis of BNNTs.

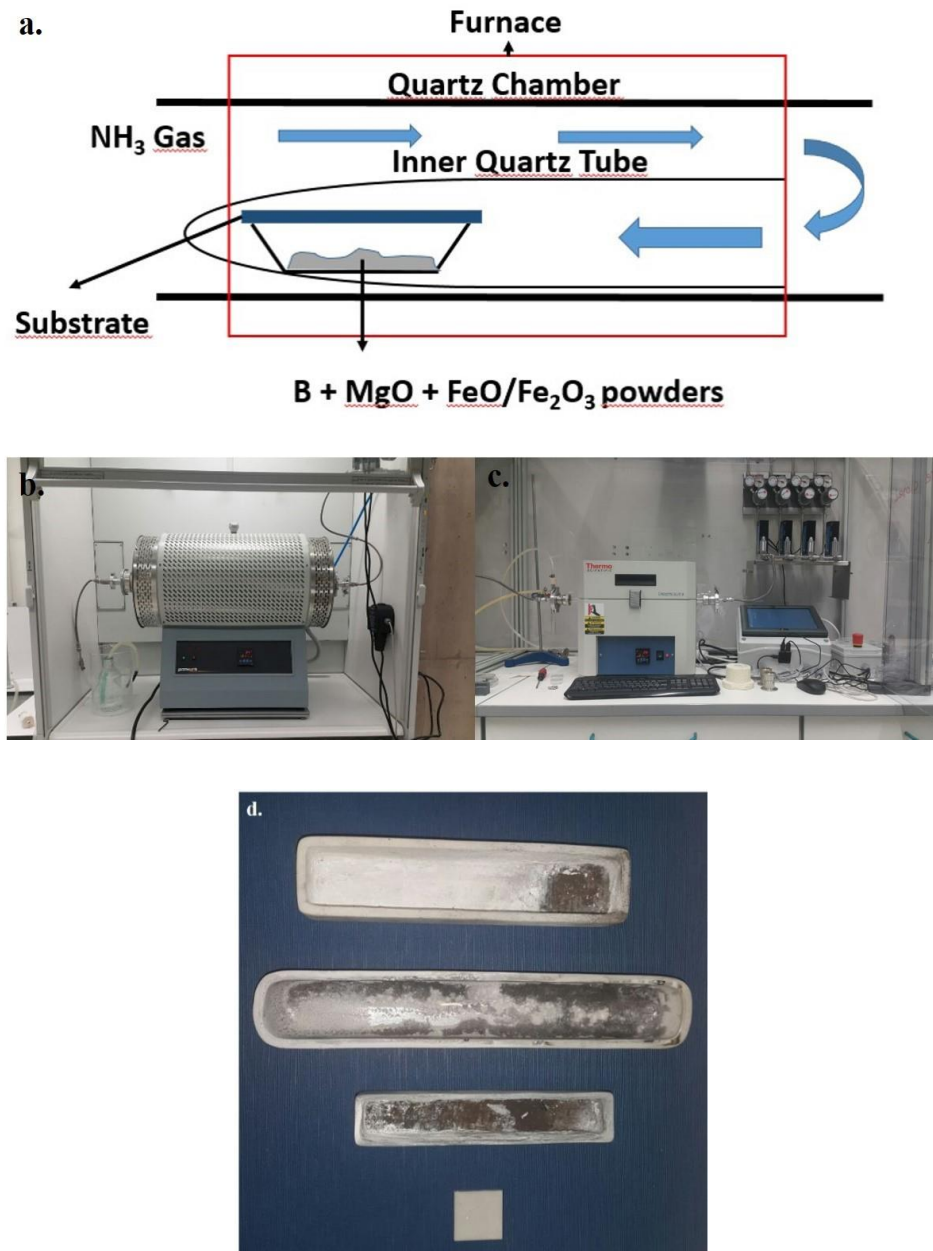


Figure 17 a. Schematic of experimental setup, b. tube furnace used for BNNT synthesis, c. Split furnace used for annealing, d. Alumina boats and alumina block

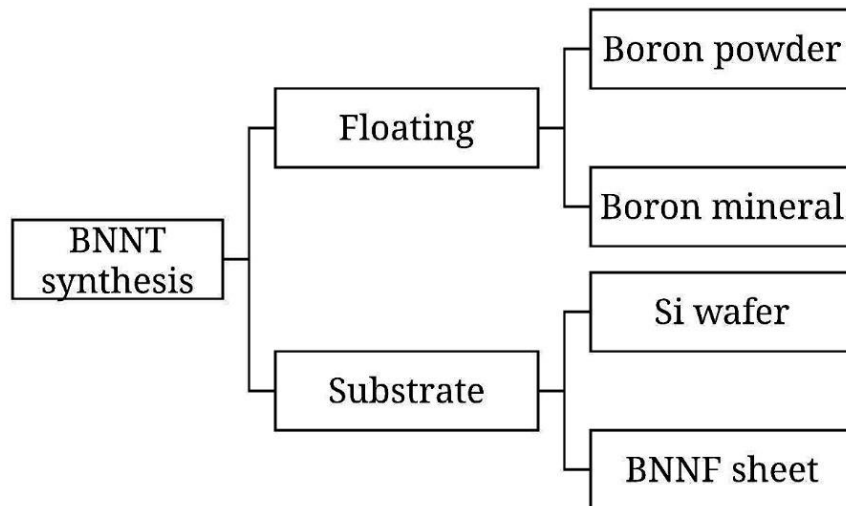


Figure 18 Flowchart of BNNT synthesis followed by purification

### 2.2.1 Nucleation theory of Whisker

BOCVD-growth vapor trapping BNNT synthesis method uses theory of nucleation as the fundamental starting point. Researchers suggested a link between nucleation of nanotubes and crystal growth.[58, 150, 151] This theory suggest that probability of nucleation depends on the equation 2.4 given below;

$$P_N = B \exp\left(-\frac{\pi\sigma^2}{k^2T^2 \ln \alpha}\right) \quad (2.4)$$

In this equation  $P_N$  shows the whiskers nucleation probability,  $B$  is a constant,  $\sigma$  corresponds to surface energy of the whisker grown,  $k$  is the Boltzmann constant,  $\alpha$  is  $p/p_0$ , ( $p$  is the partial pressure of growth vapors,  $p_0$  is the partial pressure of the condensed phase at the equilibrium) supersaturation ratio and  $T$  is the temperature.

This equation explains three important properties of the nanotube formation. First,  $P_N$  is proportional to  $\exp\left(\frac{1}{T^2}\right)$  and indicate when the growth temperature increases, probability of nanotube nucleation also increases. This can explain high BNNT yield in high temperature synthesis. Second, surface energy of the catalyst also effects the probability of nucleation for nanotubes. In BNNT synthesis,  $\sigma$  refers to surface energy of the metal



catalyst used (MgO and Fe<sub>2</sub>O<sub>3</sub> in our case). Effectiveness of MgO and Fe<sub>2</sub>O<sub>3</sub> catalyst can be linked to their surface energy. Lastly but most importantly, theory of nucleation states that supersaturation  $\alpha$  and  $P_N$  is also directly proportional to each other. Supersaturation is directly dependent of the partial pressures of the growth vapors. As the partial pressures of the growth vapors increases, supersaturation also increases resulting in higher probability of nucleation. In growth vapor trapping-BOCVD method, using both one end-closed quartz test tube and Si wafers to cover alumina boat, traps growth vapors thus increasing their partial pressures. Increased partial pressure of growth vapors increases the supersaturation which in turn increases the probability of nucleation. Increasing the supersaturation might also be used to decrease temperature of growth. As explained before, high temperature results in higher nucleation probability however, keeping every other parameter constant and selecting relatively low temperature with high supersaturation can also result in high probability of nucleation as stated in the equation. Of course, temperature also effects partial pressures of the growth vapors since it directly effects the forming of the said growth vapors, however it can be suggested that, with constant growth temperature and constant surface energy, increasing the partial pressures of the growth vapors increases the probability of nucleation of nanotubes.

### **2.2.2 BNNT Synthesis on Silicon Wafers**

Synthesis of floating BNNTs with high efficiency and quality, requires full understanding of synthesis mechanism of BNNTs as well as assertion of the thermal CVD system's characteristics. For this purposes, BNNTs were synthesized on Si wafers. Well-defined surface of the Si wafers eliminates the effect of surface on the synthesis of BNNTs. Moreover, low cost and temperature resistance of Si wafers allowed us to use them in great number of synthesis in a short time with low cost. During the synthesis of floating BNNTs, Si wafers are also used for the trapping of the growth vapors so observing the synthesis of the BNNTs on Si wafers is a great importance to us.

Optimization of the BNNT synthesis were performed during the synthesis of BNNTs on Si wafers for the reasons explained above. Examples of the synthesized BNNTs by growth vapor trapping-BOCVD method can be seen below (Figure 19). We expect as-

synthesized BNNT on Si wafers to have similar characteristics as reported on the literature (Figure 19) [58].

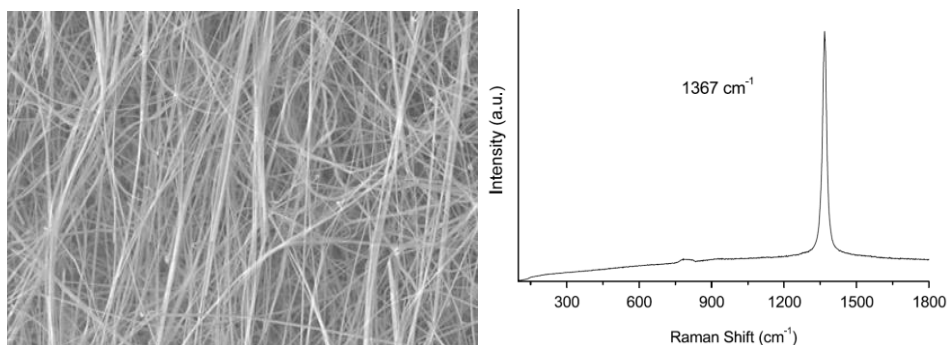


Figure 19 a. SEM image of as-synthesized BNNTs, b. RAMAN analysis of as-synthesized BNNTs.

In order to synthesize BNNTs on Si wafers, 1 g of catalyst mixture was prepared by vortex mixing B, MgO, and Fe<sub>2</sub>O<sub>3</sub> powders with the weight ratio of 2:1:1 (w/w). Prepared catalyst mixture was then loaded into alumina boat and spread evenly among the surface of the alumina boat. Pre-cleaned Si wafers placed on top of the alumina boat diagonally, with no gap allowed between them. Following the preparation of alumina boat, alumina boat is placed near the close-end of the quartz test tube. Quartz tube was then placed into the tube furnace reaction chamber such a way that alumina boats position corresponds to sweet spot of the tube furnace. Furthermore, open-end of the quartz test tube faced the outlet of the reaction chamber.

BNNT growth synthesis started with the purging of the reaction chamber. 1000 sccm Ar gas was flowed for 5 to 10 minutes to sweep oxygen and moisture from the reaction chamber. Following the purging, catalyst mixture is heated to 1100 °C in a constant 300 sccm Ar flow with +5 °C/min heating rate. At 1100 °C ammonia was first introduced to the system. Argon flow was reduced to 100 sccm and 100 sccm ammonia flow were started. With the same heating rate as before, furnace was heated to 1200 °C where it was held for 60 minutes with only 200 sccm ammonia flow present.

Ammonia flow was stopped when the reaction at 1200 °C ended and replaced with 200 sccm Ar flow until room temperature. After the completion of the reaction, furnace was allowed to cool down to 1000 °C with -2.5 °C/min cooling rate and further cooled down to 500 °C with -5 °C/min cooling rate. From that point on, natural cooling of the furnace

was allowed until room temperature where the quartz test tube was then collected and alumina boat was extracted. Thick, white BNNT coatings were observed on the Si wafer surfaces (side which faces the catalyst mixture), alumina boats inner walls and even on the inner wall of the quartz test tube. Overall, growth reaction lasted 12 to 18 hours.

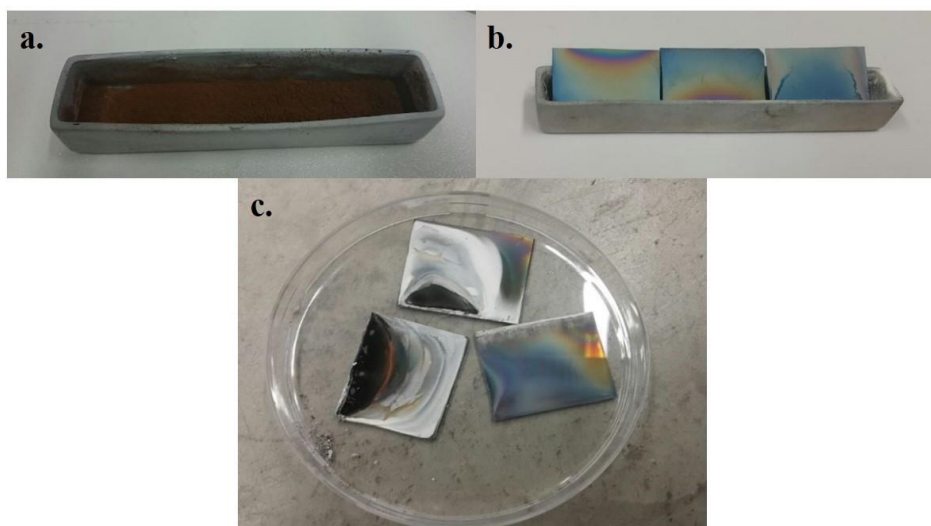


Figure 20. a. Catalyst loaded into alumina boat, b. Alumina boat covered by Si wafers, c. BNNTs grown on Si wafers

### 2.2.3 Synthesis of floating BNNTs

Exploring exciting and extraordinary applications of BNNTs in various applications such as nanocomposites, drug delivery and thin film requires dispersions of the BNNTs. However, as mentioned before, strong interactions between nanotubes causes agglomeration of BNNTs, preventing them from fully dispersing [152] thus synthesis of floating BNNTs with low diameters and high quality in large amounts can enhance the investigation of BNNT dispersions. Low diameter and high quality BNNTs are preferred so that intrinsic properties of the BNNTs can be preserved after the dispersing them in aqueous media and synthesizing high amounts of the BNNTs allows detailed research for the dispersion of BNNTs. Aim of this work is to achieve floating BNNT synthesis which results in low diameter, high quality, high yield, high purity BNNTs. Success of floating BNNT synthesis, allowed further research to disperse them in aqueous media which is desperately needed for the exploration of possible applications for BNNTs.

In the literature, floating BNNTs are usually collected from the walls of the alumina boat [58, 148, 153]. On the other hand, floating BNNTs synthesized in this thesis research were collected near the catalyst mixture on the bottom of the alumina boat ensuring good purity of the as-synthesized BNNTs. In this synthesis our goal is to synthesize high quality, good purity and high yield floating BNNTs by growth vapor trapping-BNNT method.

Floating BNNT synthesis via GVT-BOCVD method is very similar to technique used in BNNT synthesis on Si wafers which is explained in detail above. However, some key modifications have been made to produce floating BNNTs.

Catalyst mixture was prepared same as before: B, MgO, and Fe<sub>2</sub>O<sub>3</sub> powders were vortex mixed until homogeneous mixture was achieved and loaded into alumina boat. In contrast to spread evenly, in this synthesis catalyst mixture was placed in a way that only part of the alumina boat was covered with catalyst mixture. Pre-cleaned wafers were then placed on top of the alumina boat diagonally and alumina boat was inserted into the quartz test tube. Important parameter here is to make sure part of the alumina boat where the catalyst mixture was placed positioned near the close-end of the quartz test tube. Quartz tube was then placed in a similar fashion as BNNT synthesis on Si wafers.

Heating, reaction and cooling steps of the synthesis was exactly same as BNNT synthesis on Si wafers. After the furnace was cooled down to room temperature, the alumina boat was extracted. Floating BNNTs was collected from the walls of the alumina boat by simple mechanical extraction. White coatings on the Si wafers were observed with decreasing thickness as they got further from the catalyst mixture

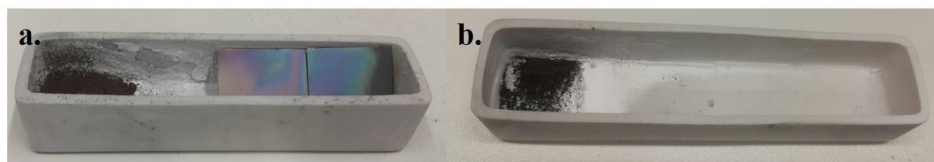


Figure 21. a. Catalyst and Si wafer placement on the alumina boat, b. Alumina boat after BNNT synthesis

#### 2.2.4 BNNT synthesis on BNNF

One of the main challenges for the composite materials is interface problems between filler and matrix material. Good interactions between the filler material and matrix can result in better interlaminar shear strength, delamination resistance, fatigue, corrosion resistance and increases the enhancement of matrix by the filler material greatly [154]. In theory, synthesis of nanotubes on nanofibers can increase the interface surface area and improve the interactions between nanotubes and nanofibers. Hou et al. showed that synthesis of CNTs on CNF (Carbon nanofiber) are possible with the proper catalyzation of the CNFs (Figure 22) [155]. This research inspired us to synthesize BNNTs on BNNFs to create nanocomposite architecture with better interface interactions than the novel composites. Catalyzation of BNNFs with Mg and Fe were performed in order to create nucleation sites for the BNNTs on the BNNF surfaces. Synthesis method highly resembles the floating BNNT synthesis with minor alterations.

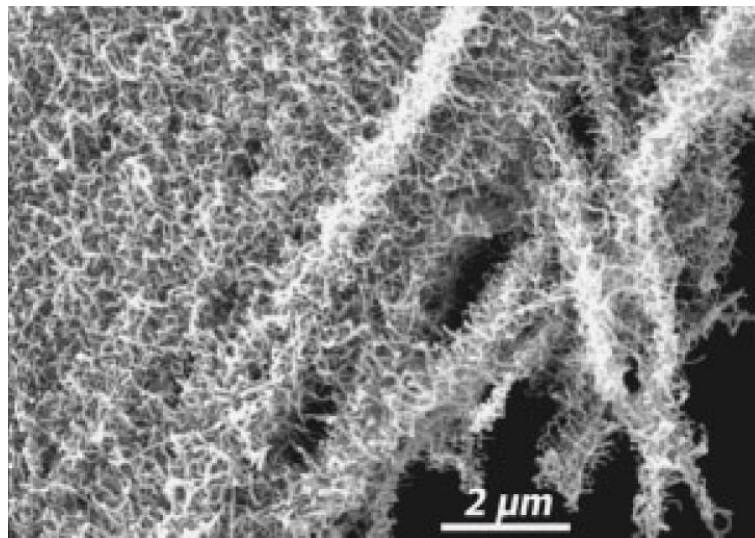


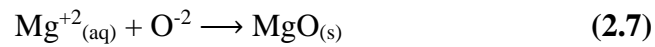
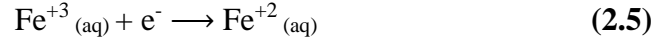
Figure 22 SEM image of CNTs synthesized on CNFs.

BNNT synthesis on BNNFs (as substrates) involves three steps, (1) catalyzing, (2) reduction and (3) BNNT growth.

In the first step, 0.375 g of  $\text{Fe}(\text{acac})_3$  (Iron (III) acetylacetonate) and 0.375 g  $\text{Mg}(\text{acac})_2$  (Magnesium acetylacetonate dehydrate) were mixed in 20 mL of ethanol in order to prepare  $\text{Fe}(\text{acac})_3$  (2.5% w/w) +  $\text{Mg}(\text{acac})_2$  (2.5% w/w) solution. BNNFs were then

dipped into the prepared solutions for 15 minutes at room temperature. Dipped BNNFs were dried at vacuum oven for 1 hour at 60 °C to get rid of any ethanol residues.

After drying dipped BNNFs, they were placed into a split furnace for reduction of Fe<sup>+3</sup> and oxidation of Mg ions in accordance half reactions 2.5, 2.6 and 2.7 given below:



BNNFs were reduced in split furnace. First, BNNFs were heated to 250 °C under air atmosphere with the heating rate of +10 °C/min and kept there for 60 minutes for annealing of the BNNFs. Second, argon flow was introduced to the system with 200 sccm and the system was heated to 500 °C with +5 °C/min heating rate. When the 500 °C is reached, hydrogen flow is added to argon flow with the 150 sccm argon flow and 50 sccm hydrogen flow. Iron particles in the BNNFs were allowed to reduce for 4 hours under the hydrogen flow at 500 °C. At the last step, system was allowed to cool down to room temperature and BNNFs with slight color change and smaller size were collected.

Last step of this study is the BNNT synthesis on BNNFs. In this step, like floating BNNT synthesis, B, MgO and Fe<sub>2</sub>O<sub>3</sub> powders were vortex mixed until homogenous mixture is achieved and catalyst mixture were placed into alumina boat in a way that only part of the alumina boat is covered with catalyst mixture. BNNFs were then placed next to catalyst mixture, boat was covered with Si wafers diagonally and alumina boat was loaded into quartz test tube such a way that catalyst mixture position corresponds to sweet spot of the furnace.

Heating, reaction and cooling steps of the synthesis were exactly same as BNNT synthesis on Si wafers. When the furnace reached room temperature, boat was removed from the furnace and BNNFs with white coatings on them were collected from the alumina boat. White coatings with less amounts were observed on the walls of the alumina boat and on the Si wafers than what was observed during the floating BNNT synthesis.

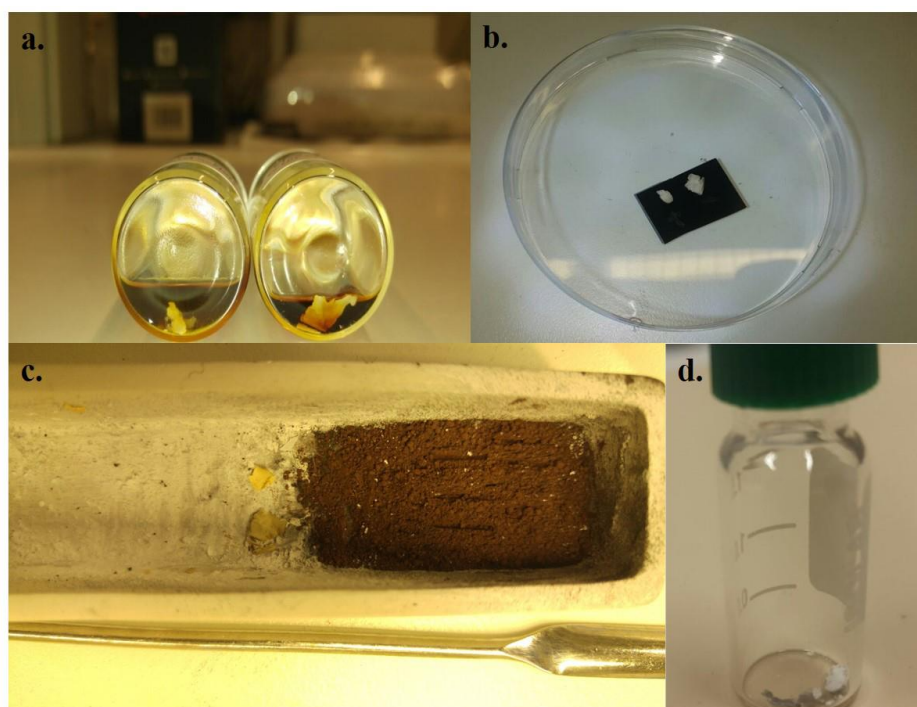


Figure 23 a. BNNFs during dipping step, b. BNNFs after reduction step, c. BNNFs loaded alumina boat, d. BNNFs after BNNT growth

### 2.2.5 BNNT synthesis from various boron minerals

In contrast to previously used boron precursors in BNNT synthesis like borazine [42, 43] and boron powder [20, 41, 153], boron minerals offers safer, cheaper, and more environmentally friendly alternative as boron precursor in BNNT synthesis. Ulexite, colemanite and Etidot-67 are commercially used boron minerals in various applications by the industry with the price nearly five thousand times lower than the boron powder. In addition to lower cost, boron minerals have no immediate danger to human health, they do not decompose and produce toxic fumes unlike borazine, they are chemically stable meaning they could easily store as opposed to boron powder which oxidizes very quickly if exposed to air. In our research, we aimed for the synthesis of BNNTs with growth vapor trapping-BOCVD method by using boron minerals which can result in the low cost and safe synthesis route for the synthesis of BNNTs. BNNT synthesis from unprocessed colemanite were reported by Kalay et al. in the literature which inspired us to investigate other boron minerals for the BNNT synthesis (Figure 24) [149].

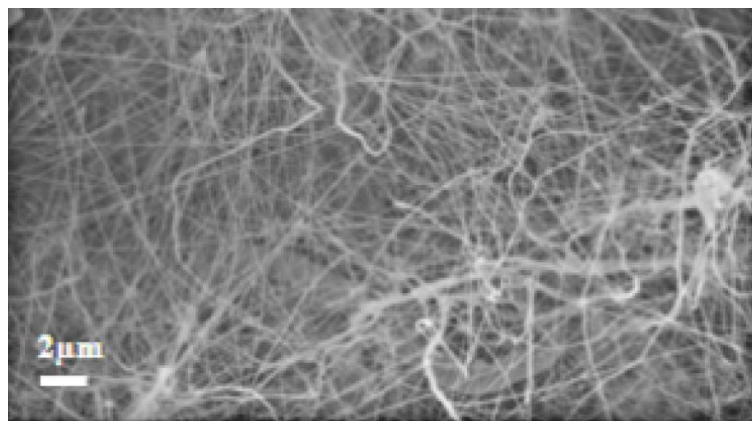


Figure 24 SEM images of BNNTs synthesized from unprocessed colemanite.

In order to synthesize floating BNNTs from various boron minerals, 4 g of ulexite/Etidot-67 and 0.322 g  $\text{Fe}_2\text{O}_3$  were added into 8 mL of DI water and vortex mixed until homogeneous dispersion of the precursors were achieved. Obtained dispersion loaded into alumina boat and heated to 180 °C in oven for 30 min in order to evaporate water. Following the pre-heating, alumina boat was covered with pre-cleaned Si wafers by placing them diagonally. Si wafers covered boat was then placed into quartz test tube near the close-end of the test tube. Quartz tube was loaded into tube furnace such a way that alumina boat's position corresponds to sweet spot of our furnace.

The furnace was first purged by flowing 1000 sccm Ar followed by heating of the precursor to 1100 °C in 214 minutes with heating rate of +8 °C/min under constant 200 sccm Ar flow. At 1100 °C, ammonia was first introduced to system with 100 sccm flow rate. Heating was continued until 1280 °C with +8 °C/min heating rate under 100 sccm Ar flow and 100 sccm ammonia flow. At 1280 °C, reaction started and temperature was held constant with only 100 sccm ammonia flow present for 120 minutes. Later, system was cooled down to 500 °C with -5 °C/min cooling rate followed by natural cooling until room temperature. White materials were collected from the walls of the alumina boat and stored at room temperature.





Figure 25 Alumina boat a. after preheating. b. Alumina boat covered with Si wafers. c. Alumina boat after synthesis run.

### 2.2.6 Purification of Floating BNNTs

High technology applications of BNNTs requires highly pure BNNTs to fully incorporate extraordinary properties of BNNTs. Addition to that, impurities in the final product greatly reduces the dispersibility of the BNNTs since the impurities causes heterogeneous charge distribution on the dispersion. Catalyst residues, BN particles and boron oxide layers on the surfaces of the nanotubes after synthesis, greatly reduces the purity of the final product [156]. Number of purification routes have been proposed for the purification of BNNTs: strong acid oxidation [54], chemical leaching followed by hot water washing [156] or polymer wrapping[51]. In this research, strong acid oxidation for the purification of the BNNTs were selected because of the ease of application and the high efficiency of the purification process. Aim for this purification process is to achieve high purity in as-synthesized floating BNNT which will later be dispersed in aqueous media.

Purification process consisted of two steps. First, crude BNNTs were added to 4M HCl acid solution with final concentration of 1 mg/ml. As-prepared solution was then stirred for 1 hour at room temperature to break large BNNT clusters. After BNNTs were dispersed, dispersion was further stirred for 4 hours at 50 °C, and washed with DI water three times at 16,900 rpm for 60 minutes. In the second step, washed BNNTs were added to 1M HNO<sub>3</sub> acid solution with concentration of 1mg/ml (BNNT: HNO<sub>3</sub>) and sonicated for 6 hours at room temperature. Sonicated solution was washed one time with ethanol and 3 times with DI water at 16900 rpm for 60 minutes and 30 minutes respectively. Precipitated BNNTs were then dried at vacuum oven at 80 °C overnight. BNNTs color changed from white-gray to white after purification (Figure 25. c).

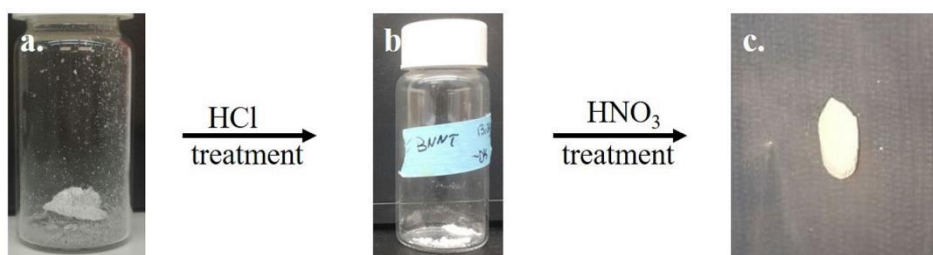


Figure 26 Flow chart for purification process. a. BNNTs before any purification, b. BNNTs after HCL treatment, c. Purified BNNTs

### 2.3 Surface Modification of BNNTs

After the successful synthesis of floating BNNTs, our focus was directed at the surface modifications of BNNTs. Although BNNTs possess extraordinary properties, difficulty to disperse them in water hinders their ability to be used in composite applications. BNNTs exhibits strong van der Waals forces when dispersed in water which causes agglomeration and accumulation in clusters. In this work, our aim is to prepare stable aqueous dispersions of as-synthesized BNNTs which can be further used in various applications. In order to achieve homogeneously dispersed, high quality dispersion of BNNTs with satisfying BNNT uptake in aqueous media, covalent and non-covalent functionalization methods were utilized which helps with the prevention of agglomeration of BNNTs in aqueous media.

In covalent functionalization methods, the main goal is to attach hydroxyl groups to the B sites on the surface of BNNTs. This goal is achieved by hydroxylation of the BNNTs with strong oxidizing agents such as nitric acid and ozone. Oxidizing agents, activates the B atoms on the surfaces of BNNTs and creates hydroxyl groups on the surface (Figure 27. b). Creating hydroxyl groups on the surface of BNNTs have two advantages; First, hydroxyl groups on the surface can be used to further modify BNNTs. Unlike BN structure, hydroxyl groups are chemically active and allows additional groups to bond with them. Few examples of this were discussed in introduction chapter. Second, hydroxyl groups can help with the dispersion of BNNTs in aqueous media by preventing them from agglomerating and bundling which is one of the main challenges of dispersing BNNTs in aqueous media. Some degree of oxidizing is expected on BNNTs during purification process however, 1M of  $\text{HNO}_3$  is used during purification and its oxidizing

effect can be neglected. In this thesis research, concentrated  $\text{HNO}_3$  treatment and ozone treatment were used in order to achieve covalent functionalization of BNNTs which later can help to disperse them in water.

In non-covalent functionalization methods, main goal is to use achieve aqueous dispersions of BNNTs with the help of materials which can interact with BNNTs via  $\pi$ - $\pi$  interactions. In contrast to covalent method, non-covalent functionalization provides more effective dispersion of BNNTs since non-covalent modification density is higher than covalent functionalization density because  $\pi$ - $\pi$  interactions are driven by the thermodynamic laws and require no additional energy like covalent functionalization.  $\pi$ - $\pi$  interactions occurs between nanotube surface and the backbone of the polymer (polymer wrapping) or surface of the surfactant. Detailed explanations were given in the section 1.3. In this work, aqueous dispersions of BNNTs with the help of ionic surfactant and polymer wrapping were prepared.

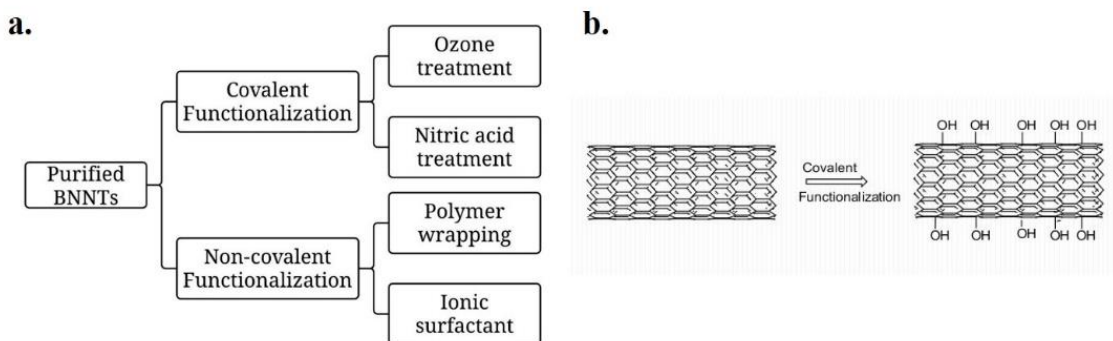


Figure 27 a.Flowchart of the chemical modifications, b. Scheme of reaction during covalent functionalization

### 2.3.7 Ozone Treatment of BNNTs

In this covalent functionalization method, Ozone's high oxidation ability was utilized for the hydroxylation of the BNNTs. To author's knowledge, no prior results were reported for the hydroxylation of BNNTs with ozone treatment in the literature. Novelty of this hydroxylation method allows hydroxylation of high amounts BNNTs at room temperature without the use of highly dangerous acids. Furthermore, this method allows hydroxylation of BNNTs synthesized on Si wafers without damaging the Si wafer.

BNNTs synthesized on Si wafers were placed on the chamber of ozone air compressor unit and ozone was flowed through the chamber for 48 hours at room temperature with 3 L/min flow rate. After 48 h Si wafers with color change were collected from the chamber and stored at moisture-free atmosphere for further characterization.

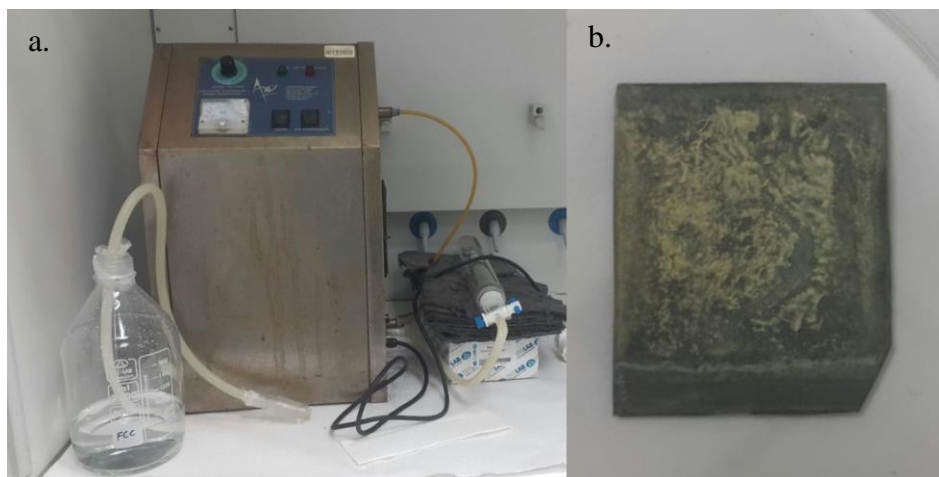
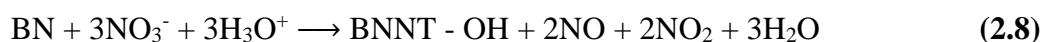


Figure 28 a. Ozone air compressor, b. Si wafer after ozone treatment

### 2.3.8 Nitric Acid Treatment of BNNTs

In this covalent functionalization method, nitric acid was used as an oxidizing agent. 10mL of 68% w/w HNO<sub>3</sub> was added to 10 mg of purified, as-synthesized floating BNNTs and stirred for 3 hours in order to break up large clusters of BNNTs. Resulting mixture was sonicated for 6 h in bath sonication at room temperature in order to achieve full dispersion of BNNTs. After sonication, BNNTs were washed with ethanol one time for 60 min at 16900 rpm at room temperature in order to get rid of HNO<sub>3</sub> residue and washed with DI water three times at 16900 rpm at room temperature. BNNTs were then dried in vacuum oven at 60 °C overnight and stored in moisture-free environment. During the sonication below reaction 2.8 occurs and hydroxylates the surface of BNNTs.



### 2.3.9 Ionic Surfactant Assisted Non-Covalent Functionalization

Surfactants used in the dispersion of BNNTs with the help of ionic surfactants were prepared by mixing 1 mL of oleic acid with 1 mL of ammonia hydroxide in 50 mL DI water. Solution was stirred at room temperature until ammonium olate surfactant started to produce.

After allowing solution to stabilize after stirring, 1 g of viscous ammonium olate surfactant solution was added to 150 mL of DI water to dilute surfactant solution. BNNT dispersion was achieved by adding 8.4 mg of floating BNNTs to 2 mL of the diluted ammonium olate surfactant solution. In order to achieve good interaction between BNNT and ionic surfactant, dispersion was bath sonicated for three hours at room temperature with 20 W output power until milky color was observed.

48 mL of DI water was further added to BNNT-water dispersion to achieve 0.084 g/L final concentration and solution was tip sonicated for 2 hours in order to break big clusters of BNNT and agglomerated nature of grown BNNTs. Following tip sonication, final dispersion was left to stabilize for 24 hours so large clusters and excess surfactant dropped down to the bottom of the container. Stabilized dispersion after 24 hours was transferred to new container and used for further applications.



Figure 29 BNNT aqueous dispersion with the help of ammonium olate surfactant after tip sonication

### 2.3.10 Polymer Wrapping of BNNTs

In order to wrap BNNTs with polymer, 4 mL of PEI (50% DI water) was added to 2 mg of purified floating BNNTs and stirred for 6 hours at 70 °C. Achieved dispersion then sonicated for 12 hours in bath sonicator with output power of 20 W. After the sonication of the solution, 6 mL of DI water was added and resulting solution was stirred overnight at room temperature to ensure homogenous dispersion of the PEI wrapped BNNTs. Tip sonication for 1 hours was utilized to ensure breaking of the large BNNT clusters and agglomerates. After tip sonication dispersion was left to stabilize for 24 hours in order to allow catalyst impurities and large BNNT clusters to drop down to the bottom of the container and remaining dispersion was transferred to new container. 40 mL of DI water was further added to polymer-BNNT dispersion to achieve 0,02 g/L final concentration and stored at room temperature for further use.

Polymer wrapping of BNNTs were repeated with another polymer for the second time. 1 mg of poly(allylamine hydrochloride) (PAH) was added to 10mL of DI water and stirred until solution became transparent. Following, 1 mg of purified floating BNNTs were added to solution and stirred at 50 °C for 4 hours in order to break large clusters of BNNT. Solution was then sonicated for 12 hours in bath sonicator with output power of 20 W. Resulting dispersion was further diluted by adding 40 mL of DI water resulting in 0.02 g/L concentration. Tip sonication for 1 hours was utilized to ensure breaking of large BNNT clusters and agglomerates. After tip sonication, dispersion was left to stabilize for 24 hours in order to allow catalyst impurities and large BNNT clusters to drop down to the bottom of the container and remaining dispersion was transferred to a new container.

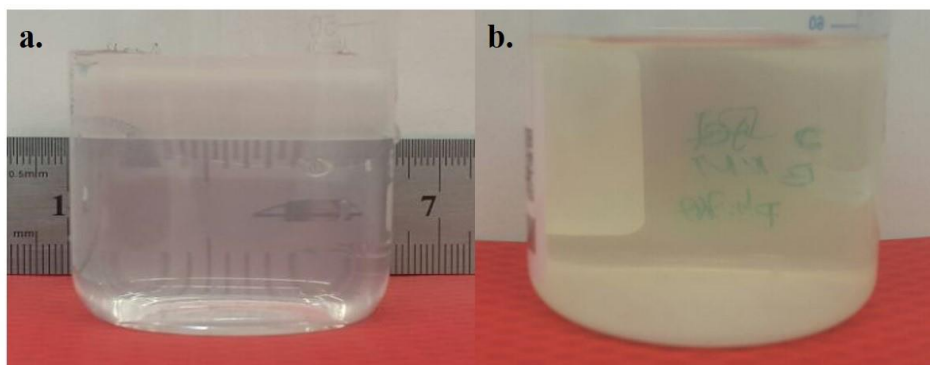


Figure 30 Aqueous dispersion of polymer wrapped BNNTs a. b-PEI, b. PAH

## 2.4 BNNT Film Preparation by LbL Method

After the discovery of BNNTs, researchers suggested that BNNTs can be good filler materials for polymer matrix composites due to their high mechanical properties, high structural stability at high temperatures and inertness, high band gap (5.5 eV), high thermal conductivity and desirable optical properties. Unfortunately, difficulties in dispersing BNNTs in various solvents and challenges encountered during synthesis of BNNTs (low yield, low quality, high impurity content) hindered the research towards polymer-BNNT composites. BOCVD method followed by growth vapor trapping method of synthesizing BNNTs allowed high amount synthesis of BNNTs with high quality. Advancements in production methods allowed researchers to start working on polymer-BNNT composites.

Polymer wrapping have been suggested as an efficient way of dispersing BNNTs in aqueous media. Researchers used PmPV [99], G-Chitosan [100], PEI [101] and other polymers to disperse BNNTs and showed that BNNTs can interact with polymers strongly via  $\pi$ - $\pi$  interactions between the backbone of the polymer and the surface of the tube. In our work, we also utilized this interaction to prepare aqueous dispersion of BNNTs with the help of polymer wrapping. Addition to polymer-wrapping covalent functionalization of BNNTs also provides dispersions of BNNTs in various solvents. [92, 95, 157].

One of the first examples of BNNT-polymer composite was BNNT/PS (polystyrene) composite [50] where researchers prepared BNNT-PS films by simple solution evaporation method and showed increased mechanical properties. Following this work many other composite materials was produced [52, 96] with different composite preparation techniques and showed improved mechanical and optical properties of polymers. However, none of this techniques offers high content of BNNTs inside the polymer and they do not offer precise control over BNNT content or polymer architecture.

One of the techniques that can be used for forming polymer-BNNT composites as thin films is LbL technique. LbL technique was first proposed over 25 years ago [158, 159] and depends on the absorption of cationic and anionic inorganic or organic particles organize their selves alternately. In general, thin films are created on the substrates (glass, SiO<sub>2</sub> wafers etc.) by introducing substrates into positively or negatively charged polymers or nanomaterials in an alternating cycle, allowing absorption of the species. Cycle can be repeated until desired bilayer number. Thickness of the thin films, growth rate of the layers and nanoparticle concentration inside the thin film depends on the chemistry used, charge density of the particles, molecular weight of the species, temperature, deposition time, pH values of dispersions, concentration of dispersions and the number of bilayers [160]. This technique allowed researchers to efficiently modify thin films and incorporate nearly unlimited functional groups into the thin film structure. Furthermore, the basic absorption principle behind the LbL process success is also very cheap and easily accessible. LbL process allows combining of desired physical properties of macromolecules (polymers) with extraordinary mechanical, optical, thermal and electronic properties of nanomaterials. CNT thin films produced by LbL is reported in the literature [161-163] suggesting LbL technique can be utilized for BNNTs as well.

In this work we proposed using LbL method to produce BNNT thin films. LbL method offers number of advantages to BNNT thin film. First of all, LbL method allows one to control the thickness of BNNT thin films by control over number of bilayers. Increasing number of bilayers results in higher thickness content on the BNNT thin film which can increase properties of the thin film. Thickness control can also be achieved by changing number of bilayers, dipping duration and pH levels of electrode dispersions. Additionally, LbL method also provides designing BNNT thin films with various architectures such as bilayer of polymer-BNNT followed by buffer layer followed by BNNT film or differently charged BNNT bilayers coated on top of each other, or one can choose last layer to be negatively charged electrode or positively charged electrode achieve BNNT thin film surfaces with desired charge, depending on the charge of the last layer. LbL method also allows BNNT thin film coatings on top of complex geometries as well as large surfaces.

Oxygen plasma treatment was applied to micro slides in order to charge their surface negatively. However, only plasma treated micro slides doesn't have enough charge density on their surface to support LbL of BNNTs. For BNNTs to have strong interactions



with the surface of the substrate, we coated micro-slides with adhesive layers. Last layer of adhesive film was chosen as negative since our system starts with positive electrode. Adhesive layer provides high charge density on the surfaces of glass substrates which increases the strength of interaction between the BNNTs and substrate surface.

During the preparation of BNNT thin films, as-prepared BNNT aqueous dispersions was used as BNNT layer's source. SPS (poly(styrenesulfonate)) and b-PEI aqueous dispersions was utilized to produce polymer layers. Glass micro slides with adhesive layer coating was used as substrates because they have smooth and well-defined surfaces in addition to their low cost. The primary aim is to create polymer-BNNT bilayers and stack them on top of each other in order to acquire polymer-BNNT composite thin films on glass substrates. BNNT aqueous dispersions prepared by different methods and different pH levels of said dispersions was tested to obtain BNNT thin films.

Dip coating LbL method was used to obtain BNNT films since this method allows relatively short times to produce composite films and with well-defined parameters. For each different BNNT aqueous dispersions 5 and 10 cycles of dip coating were conducted which creates 5 bilayer and 10 bilayer thick thin films respectively. Used dip coating equipment can be seen below (Figure 31).

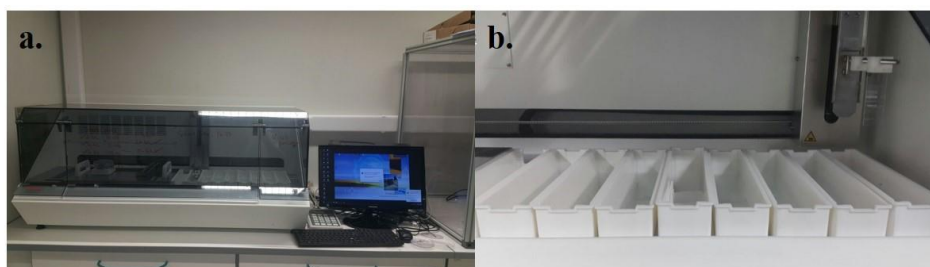


Figure 31 a. Dip coating equipment used, b. Inside of the dip coater with 6 stages for washing and 2 stages for electrodes

#### 2.4.11 Experimental Work for Thin Film Production via LbL Method

BNNT thin film production consist of three steps: (1) Preparation of substrates and dispersions, (2) adhesive layer formation on the substrates, and lastly (3) thin film formation on the substrates. In this work, we used glass micro-slides as substrates, (b-

PEI/SPS)<sub>5</sub> layer as adhesive layer, b-PEI (1 g/L pH: 4) as positively charged counter solution and SPS (1 g/L pH: 4) as negatively charged counter solution. For the investigation of thin film formation, dip LbL method was used since it is one of the easy and fast LbL methods.

As-prepared BNNT dispersion with the help of ionic surfactant was used as negatively charged dispersion with 2 different concentration values of ionic surfactant: 1:1 (BNNT : surfactant w/w) and 2:1 (BNNT : surfactant w/w) with pH values of 7.5 and 8.5.

As-prepared BNNT dispersions with polymer wrapping was used as positively charged dispersion with different pH values: b-PEI – BNNT dispersion with pH: 7.5 and pH: 8.5 and PAH – BNNT dispersion with pH: 4 and pH: 5.

General LbL procedure is as follows: First glass micro-slides were cleaned with micro-90 glass cleaning solution for 15 minutes and DI water for another 15 minutes in ultrasonic cleaner followed by oxygen plasma cleaning for 2 minutes. After cleaning process, substrates were coated with b-PEI and SPS layers forming 5 bilayer adhesive layer on the substrates by the following cycle: Substrates are dipped in positively charged solution for 10 mins and washed with DI water in three steps: 2 minutes dipping, 1 minute dipping and 1 minute dipping in DI water. Following the first cleaning steps, substrates are dipped in negatively charged solution for 10 minutes followed by the same washing steps with 2 minutes, 1 minutes and 1 minutes dipping in DI water. This step is repeated 5 times to achieve 5 bilayer adhesive layer on the substrate surface. Lastly, adhesive layer coated substrates were used in LbL of BNNT-polymer films. BNNT-surfactant dispersion was used as negatively charged dispersion and b-PEI was used as counter positively charged solution. Cycle described above was repeated 5 times and 10 times in order to create 5 bilayer and 10 bilayer thin films on the substrates with each aqueous dispersion and glass substrates were collected subsequently. BNNT-polymer wrap dispersions were used as positively charged dispersions and SPS solution was used as negatively charged counter solution. Cycle was again repeated 5 times and 10 times followed by the collection of substrates. Recipes of the LbL processes is shown at Table 3.

Table 3 Conditions for the LbL thin film production. 5 bL and 10 bL thick films were produced for all conditions.

«+» charged dispersion	«-» charged dispersion
b-PEI pH: 4	2:1 BNNT-surfactant pH: 7,5
b-PEI pH: 4	2:1 BNNT-surfactant pH: 8,5
b-PEI pH: 4	1:1 BNNT-surfactant pH: 7,5
b-PEI pH: 4	1:1 BNNT-surfactant pH: 8,5
b-PEI/BNNT pH: 7,5	SPS pH: 4
b-PEI/BNNT pH: 8,5	SPS pH: 4
PAH/BNNT pH: 4,5	SPS pH: 4
PAH/BNNT pH: 5,5	SPS pH: 4

## 2.5 Characterization

Experimental section of this thesis work can be divided into three different parts; (1) synthesis of BNNTs, (2) surface modification and dispersion of BNNTs and (3) LbL thin film production of BNNTs.

In the first part, floating BNNTs, BNNTs on Si wafers and BNNFs were successfully synthesized. Additionally, boron minerals were used as boron precursor for the synthesis of floating BNNTs for the first time for the Ulexit and Etidot-67. Growth vapor trapping-BOCVD method were chosen for the synthesis of BNNTs without vacuum and at relatively low temperature of 1200 °C. MgO and FeO powders were used as catalyst with boron powders as boron source and ammonia as nitrogen source for the synthesis of BNNTs. Vacuum was replaced with Ar atmosphere which reduced the cost of the BNNT synthesis. Control of synthesis locations were possible due to unique positioning of catalyst mixture into the alumina boat which allowed floating BNNT synthesis as well as BNNTs on BNNFs synthesis with success. All as-synthesized BNNTs were collected and store in moisture free environment for characterization. Only floating BNNTs were purified before the characterization.

In second part, successful surface modifications of BNNTs and dispersion of BNNTs on aqueous media were achieved. Both covalent and non-covalent functionalization methods were utilized on BNNTs in order to (1) create hydroxyl groups on their surfaces to prevent

agglomeration (2) disperse them in water without chemical modifications. For covalent functionalization of BNNTs: ozone treatment was used on BNNTs synthesized on Si wafers, and nitric acid treatment on floating BNNTs. After both treatment, samples were collected for further characterization. For non-covalent functionalization of BNNTs: Ionic surfactant and polymer wrapping were used in order to disperse BNNTs in aqueous media without any chemical modifications. Resulting products were further characterized with FTIR and DLS.

Last part of our research was the trial of LbL method for the production of the BNNT thin films. Different conditions for the dispersions were tested in order to produce thin BNNT films on glass micro-slides. General architecture was bilayer of polymer <sup>(+)</sup>/BNNT-surfactant <sup>(-)</sup> over adhesive layer and bilayer of BNNT dispersion <sup>(+)</sup>/polymer <sup>(-)</sup> over adhesive layer.

As synthesized BNNTs were characterized with SEM and TEM electron microscopes for the morphological investigation and composition analysis. RAMAN and FTIR analyses were also performed in order to determine bonds inside the as-synthesized BNNTs.

FTIR analysis were performed for all hydroxylated BNNTs prepared by covalent functionalization for the investigation of hydroxyl groups. Non-covalent functionalized BNNTs were dispersed in aqueous media and DLS Zeta potential analysis were performed for the aqueous BNNT dispersions for the determination of stability. BNNT dispersions were left to stabilize for 24 hours and overserved for precipitation of BNNTs.

## CHAPTER 3 Optimization of BNNT Synthesis

### 3.1 Introduction

Since growth vapor trapping-BOCVD method allows BNNT synthesis on tube furnace with relatively low temperatures, it is a promising candidate for the synthesis of BNNTs. Moreover, tube furnace system is very suitable for our purposes because it allows simple and novel route for the synthesis of BNNTs in addition to experience our group has with the synthesis methods with tube furnaces. However, every CVD synthesis method differs from each other due to furnace, laboratory conditions and even sometimes depending on the researcher. Optimization of the synthesis system can increase the yield of the synthesis and the quality of the product. Furthermore, optimization of the system can decrease the cost and the duration of the synthesis.

### 3.2 Optimization of Recipe

Temperature and the catalyst ratio parameters directly effects the quality of the BNNTs synthesized [153]. To synthesize good quality BNNTs, temperature and catalyst ratio values for our synthesis were optimized. Ammonia flow, catalyst amount and the reaction time parameters effects the yield of the BNNT synthesis as well as cost of the synthesis so optimization of these parameters were performed for our synthesis system as well. Additionally, there are some small parameters that effects the BNNT synthesis that must be determined such as sweet spot, grade of chemicals, direction of the quartz test tube used, positioning of quartz substrates and the different oxides of catalyst. These parameters were optimized before finding the optimum values for 5 main parameters mentioned above. Table 4 gives the experimental design for the optimization process.

Table 4 Experimental design for the optimization

Temperature	Catalyst Ratio	NH <sub>3</sub> Amount	Catalyst Amount	Reaction Time
°C	(w/w)	sccm	g	h
1200	1:1:1	50	0.5	0.5
1250	2:1:1	100	1	1
1300	4:1:1	150	1.5	1.5
1350		200	2	2
1400		250		5

### 3.2.1 Temperature Optimization

Temperature optimization of BNNT synthesis was chosen as first step of optimization since its effect on the quality of BNNTs are substantial compared to other parameters. Temperature value of the BNNT synthesis effects in a four different ways: (1) nucleation probability of nanotubes, (2) quality of the synthesized nanotubes, (3) cost of the BNNT synthesis and finally (4) overall BNNT synthesis time.

First, as the nucleation theory of whiskers suggest, temperature of the synthesis greatly effects the probability of nucleation. If surface energy of the nanotube ( $\sigma$ ) and supersaturation ratio ( $\alpha$ ) are constant, probability of whisker nucleation increases with the increasing temperature. Two conclusions can be drawn from this theory regarding the temperature: (1) As the temperature of synthesis increase, the yield of the synthesis also increases and (2) there is a minimum temperature requirement for the nucleation of whiskers if the other parameters to be kept constant. Temperature optimization of the synthesis aimed for the determination of minimum required temperature.

Second, Pakdel et al. [153] showed that, quality of the BNNTs also changes with the temperature. Their theory is, temperature directly effects the amount of BN growth vapor generated and causes agglomeration of catalyst powders which in turn creates differences in the final BNNT product such as increasing tube diameter, loss of homogeneity and the loss of purity. Homogenous growth of BNNTs in the sense of diameter with good purity was the aim for the temperature optimization. Moreover, preservation of tube morphology were also considered.

Third, increase in the temperature raises the cost of the BNNT synthesis due to high energy consumption of tube furnace. Although this effect can be neglected during the small-scale synthesis of the BNNTs, when large-scale synthesis of BNNTs considered, it creates a big problem. In order to proclaim BNNTs as viable materials for future applications and the commercialization of BNNTs their cost of production should be decreased as much as possible.

Finally, reaction time for the synthesis of BNNTs directly gets effected by the synthesis temperature. For example, heating the furnace up to 1400 °C takes 274 minutes and takes 180 minutes to cool down to 500 °C where natural cooling can start however, heating the furnace up to 1200 °C takes about 234 minutes and takes 140 minutes to cool down to 500 °C where natural cooling can start. This means 80 minutes longer time for the synthesis of the BNNTs at 1400 °C. As illustrated, determination of the optimum temperature value holds a great importance for the overall time consumption of BNNT synthesis.

During the synthesis, ammonia flow was fixed at 200 sccm, reaction time was fixed at 1 h, catalyst ratio was fixed to 2:1:1 (w/w) and catalyst amount was fixed to 1 g. Si wafers were placed diagonally and the quartz test tube was positioned in an opposite direction of the reaction flow. Table 5 shows the recipes followed during temperature optimization.

Table 5 Temperature optimization experiment design

No	Temperature °C	B:MgO:Fe <sub>2</sub> O <sub>3</sub> (w/w)	NH <sub>3</sub> Amount sccm	Reaction Time hour	Catalyst Amount g
1	1200	2:1:1	200	1	1
2	1250	2:1:1	200	1	1
3	1300	2:1:1	200	1	1
4	1350	2:1:1	200	1	1
5	1400	2:1:1	200	1	1

Figure 32 shows the Si wafers after each synthesis run. As can be seen from the images, BNNT synthesis were present at 1200 °C since white coatings are visible on the wafer surfaces. The main portion of the BNNTs were located on the edges of the Si wafers as predicted since partial pressure of growth vapor is higher on the edges of the Si wafer.



However, after the 1300 °C, Si wafers began to decompose and lost their structural integrity so usage of Si wafers after this temperature value is impractical. The wafers on the image are the ones taken from the sweet spot position of the alumina boat and they were later used as SEM samples.

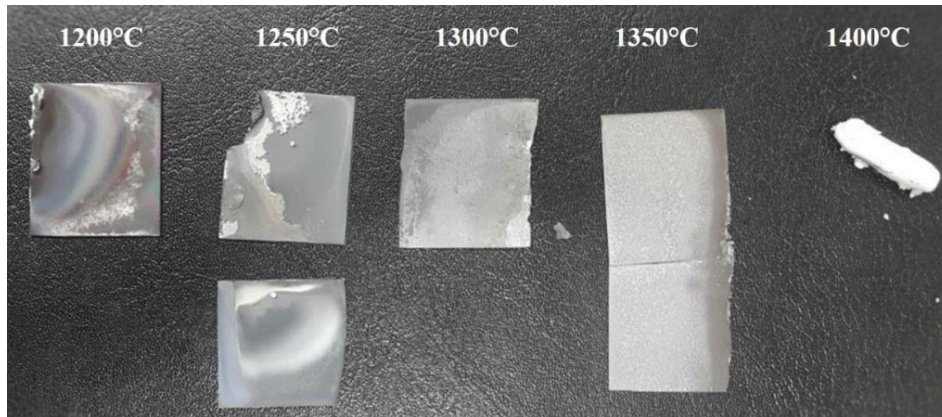


Figure 32 Si wafers collected after each run

Figure 33. a shows the BNNTs synthesized on 1200 °C. Average diameter of nanotubes is 280 nm and homogenous coating of the BNNTs are visible on the Si wafer surface. They have a tube morphology and they are not agglomerated, with lengths in the order of  $\mu\text{m}$ . Figure 33. b is from the BNNTs grown on 1300 °C. The diameter homogeneity is completely disappeared and nanotube diameters increased to  $\sim 350$  nm along with the large nanotubes with the diameters exceeding  $2 \mu\text{m}$ .

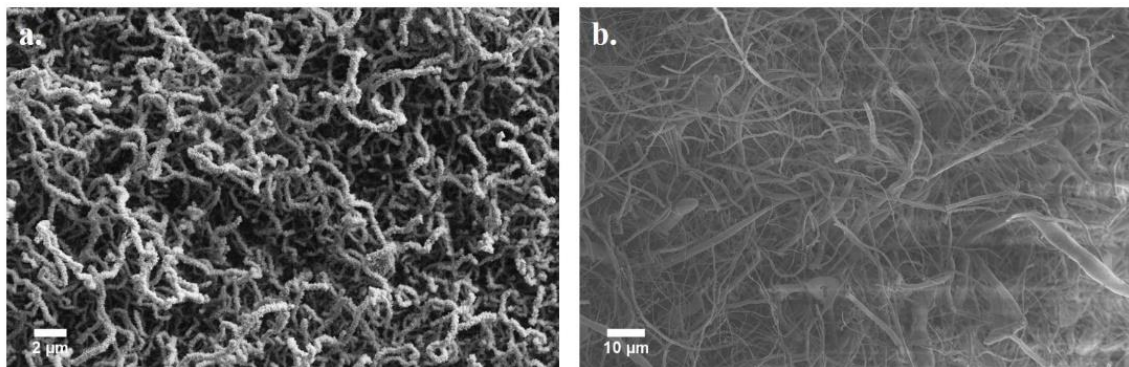


Figure 33 SEM images of BNNTs synthesized at a. 1200 °C and b. 1300 °C

Further increase of the temperature results in the complete loss of homogeneity. Figure 34. a was taken from the BNNTs synthesized on 1350 °C, where large diameter, tube-like morphologies with diameters up to  $1 \mu\text{m}$  can be seen to be dominant thorough out the



wafer surface. Small amounts of low diameter BNNTs are also visible in the image but their numbers are low compared to other structures. Addition to loss of homogeneity, structures observed on the SEM image do not resemble nanotube structure since the tubes have filled inner cores and very short lengths. Walls of the tubes are also coated with the unidentified particles which can be catalyst droplets or undesired BN products. When the temperature was increased to 1400 °C, diameter of the tubes increases to a point where it is more logical to call them microtubes rather than nanotubes. Figure 34. b shows single microtube structure. Diameter of the tube is close to 6 $\mu$ m with catalyst impurities covering the surface of the tube. Overall images points 1200 °C for the optimum temperature value for the BNNT synthesis, as it shows homogeneously distributed nanotubes with low diameters.

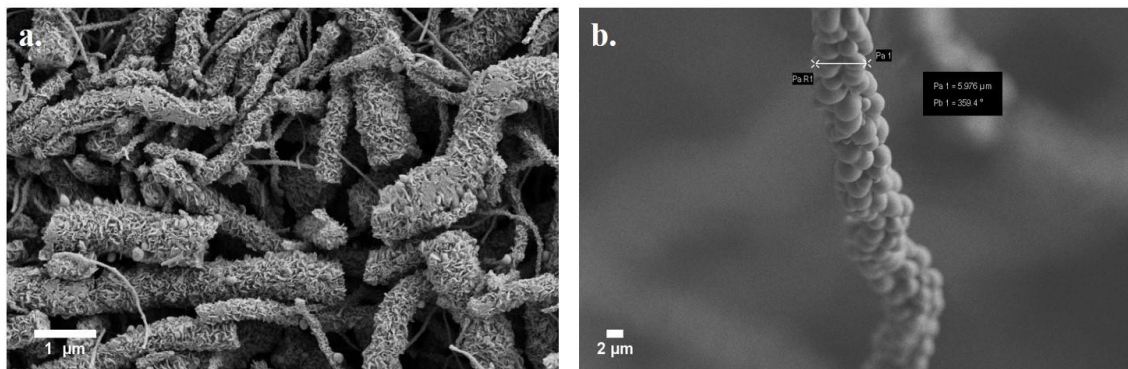


Figure 34 SEM images from BNNTs synthesized at a. 1350 °C and b. 1400°C

### 3.2.2 Catalyst Ratio Optimization

Optimization of the catalyst ratio for the good quality BNNT synthesis were performed. Goal of this optimization work is to find optimal catalyst ratio amount in the catalyst mixture so that good quality of BNNTs can be synthesized. During the synthesis, temperature was fixed at 1200 °C, reaction time was fixed at 1 h, ammonia flow rate was fixed at 200 sccm and catalyst mixture amount was fixed at 1 g with the varying catalyst mixture ratios. Three different catalyst ratios were tested, showed on the table 6 below;

Table 6 Catalyst ratio optimization experiment design

No	Temperature °C	B:MgO:Fe <sub>2</sub> O <sub>3</sub> (w/w)	NH <sub>3</sub> Amount sccm	Reaction Time hour	Catalyst Amount g
1	1200	1:1:1	200	1	1
2	1200	2:1:1	200	1	1
3	1200	4:1:1	200	1	1

After each synthesis, wafers were collected for the SEM analysis. BNNT synthesis with 1:1:1 weight ratio was unsuccessful. However, BNNT synthesis with 2:1:1 (Figure 35. a) and 4:1:1 (Figure 35. b) catalyst ratios were successful. Our findings are the opposite of what has been reported in the literature [153]. As can be seen from images, when the B weight ratio of catalyst increases, the tube's diameters also increases and they start to orientate in a flower-like structure. Figure 35. a shows tubes with average diameter 280 nm for 2:1:1 weight ratio whereas as the B weight ratio of catalyst increases, the diameter of the tubes increases to >500 nm and flower-like bundles of BNNTs are observed (Figure 35. b).

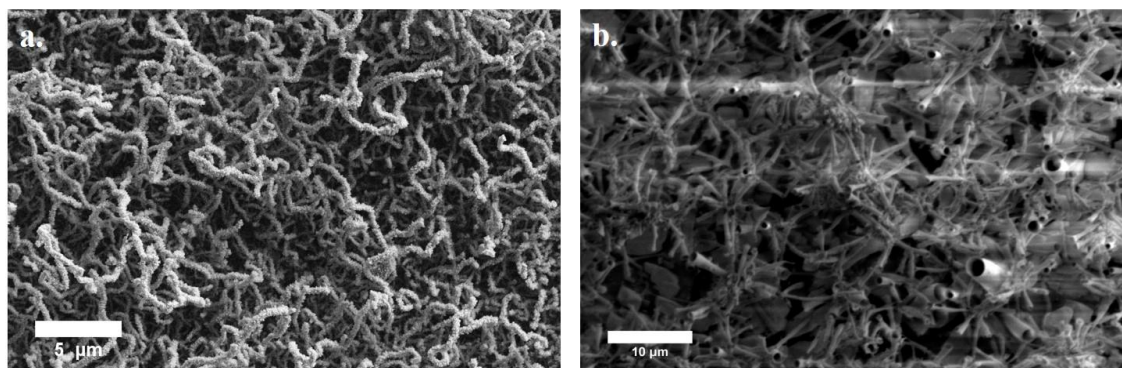


Figure 35 SEM images of BNNTs synthesized with a. 2:1:1 (B:MgO:Fe<sub>2</sub>O<sub>3</sub>, w/w), b. 4:1:1 (B:MgO:Fe<sub>2</sub>O<sub>3</sub> w/w) catalyst ratio.

Furthermore, SEM analysis showed that only some parts of the Si wafer is covered with the BNNTs when the catalyst ratio was selected 4:1:1 and more interestingly some microsheets were synthesized during the synthesis of BNNTs (Figure 36). Optimum value for the catalyst ratio was determined to be 2:1:1 because nanotubes exhibit lower tube diameter with no flower like bundling.

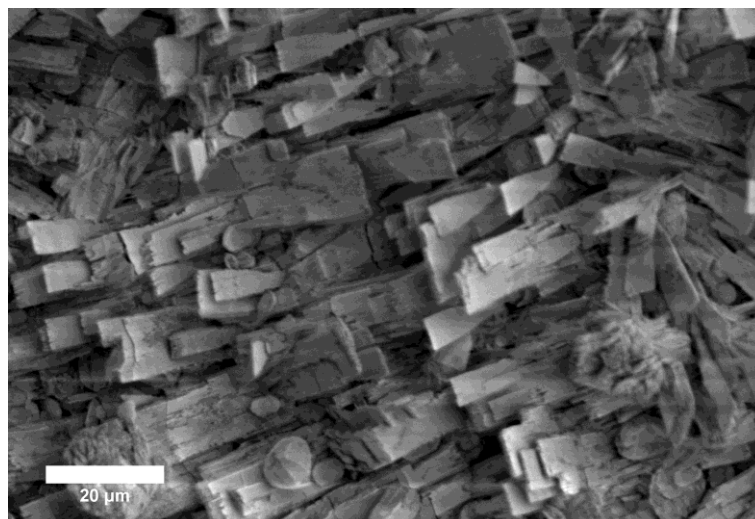


Figure 36 BN sheets on the Si wafers when the catalyst ratio is 4:1:1

### 3.2.3 Ammonia Flow Optimization

Determination of optimum ammonia flow for the BNNT synthesis was aimed during ammonia flow optimization which can be interpreted as minimum amount required for the synthesis of BNNT with good yield. During the optimization, temperature was fixed at 1200 °C, reaction time was fixed at 1 h, catalyst mixture amount was fixed at 1 g with the catalyst ratio constant at 2:1:1 (w/w) and Si wafers were placed diagonally. Like before, one-end closed quartz test tube placed in the opposite direction of the gas flow. Ammonia flows ranging from 50 sccm to 250 sccm were tested. Table 7 provided below gives the parameters used during the ammonia flow optimization.

Table 7 Ammonia flow optimization experimental design.

No	Temperature °C	B:MgO:Fe <sub>2</sub> O <sub>3</sub> (w/w)	NH <sub>3</sub> Amount sccm	Reaction Time hour	Catalyst Amount g
1	1200	2:1:1	50	1	1
2	1200	2:1:1	100	1	1
3	1200	2:1:1	150	1	1
4	1200	2:1:1	200	1	1
5	1200	2:1:1	250	1	1

Wafer images taken after each synthesis run is given below (Figure 37). As can be seen from the wafer images: until 150 sccm of ammonia flow, the yield of BNNT synthesis is low. After 200 sccm, amount of white coatings on the Si wafers increases to meaningful amount. However, further increase of the ammonia amount results in no yield change for the BNNT synthesis. 200 sccm ammonia flow was selected to be optimum value for the synthesis of BNNTs.

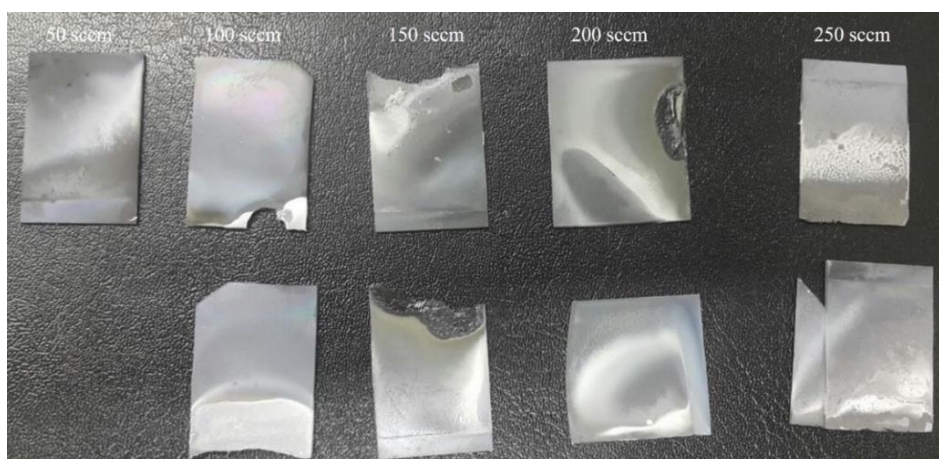


Figure 37 Si wafers collected after each run

### 3.2.4 Catalyst Mixture Amount Optimization

The goal of this optimization process is to find minimum catalyst mixture amount for the successful BNT synthesis. Volume of the boat is considered to be limiting parameter for the amount of catalyst that can be used in synthesis. Two separate things were considered during optimization, (1) amount of catalyst used during the synthesis run and (2) the amount of BNNT synthesized on the Si wafers in contrast to BNNTs synthesized on the walls of the quartz tube. During the synthesis, ammonia amount was fixed at 200 sccm, reaction time was fixed at 1 h, catalyst ratio was fixed to 2:1:1 (w/w) and temperature was fixed to 1200 °C. Si wafers were placed diagonally and the quartz test tube was positioned in an opposite direction of the reaction flow. Table 8 gives the optimization parameters during the experiments.



Table 8 Catalyst mixture amount optimization experiment design.

No	Temperature °C	B:MgO:Fe <sub>2</sub> O <sub>3</sub> (w/w)	NH <sub>3</sub> Amount sccm	Reaction Time hour	Catalyst Amount g
1	1200	2:1:1	200	1	0.5
2	1200	2:1:1	200	1	1
3	1200	2:1:1	200	1	1.5
4	1200	2:1:1	200	1	2

Si wafer images after the synthesis shows that (Figure 38), BNNT synthesis starts after 1 g of catalyst mixture is used. Increasing the amount of catalyst mixture doesn't increase the observed BNNT amount until 2 g of catalyst mixture is used. However, BNNT synthesis is observed on the quartz test tube's surfaces rather than the Si wafer's surface with 2 g of catalyst. Although Figure 38 shows higher yield for the BNNT synthesis with 2 g of catalyst mixture, efficiency of the system decreases since high portion of catalyst mixture is wasted and doesn't react with the boron. Additionally, most of the BNNTs synthesized are collected from the walls of the quartz test tube rather than the surfaces of the Si wafers when catalyst amount increased.

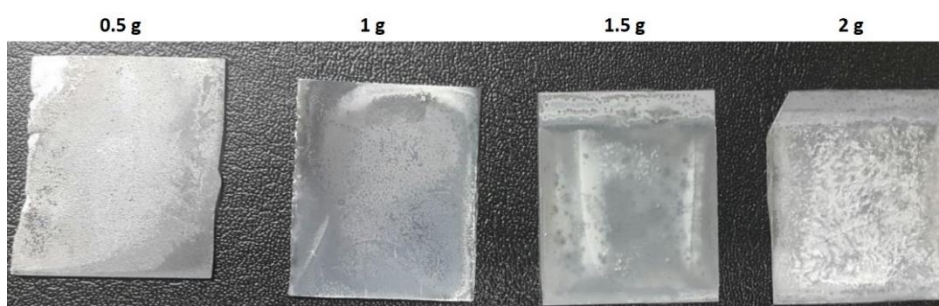


Figure 38 Si wafers collected after each run

### 3.2.5 Reaction Time Optimization

Reaction time of the synthesis corresponds to not overall reaction time but the time furnace stays under the determined synthesis temperature. Goal of optimization is to find minimum required time for the synthesis of the BNNTs with good yield. For this purpose, during the synthesis, temperature was fixed at 1200 °C, ammonia flow was fixed at 200 sccm, catalyst ratio was fixed to 2:1:1 (w/w) and catalyst amount was fixed to 1 g. Si

wafers were placed diagonally and the quartz test tube was positioned in an opposite direction of the reaction flow. Table 9 shows experiment parameters for the reaction time optimization.

Table 9 Reaction time optimization experiment design

No	Temperature °C	B:MgO:Fe <sub>2</sub> O <sub>3</sub> (w/w)	NH <sub>3</sub> Amount sccm	Reaction Time hour	Catalyst Amount g
1	1200	2:1:1	200	0.5	1
2	1200	2:1:1	200	1	1
3	1200	2:1:1	200	1.5	1
4	1200	2:1:1	200	2	1
5	1200	2:1:1	200	2.5	1

Our results showed that, 1 h is the minimum reaction time required for the synthesis of the BNNTs. Reaction times higher than this value creates no observable difference in the yield of the synthesis. Furthermore, after 1.5 h of reaction time, buffer solution, used for the trapping of excess ammonia, decayed and loses its ability to trap ammonia gas. This situation points out that, after 1 h of reaction time, most of the ammonia flowed into the furnace, comes out from the outlet without reacting since B<sub>2</sub>O<sub>2</sub> generation is not present after 1 h. Unfortunately, synthesis of BNNTs with 5 h reaction time was not conducted since ammonia gas detector started to shut down whole system after 3 hours due to high ammonia concentration in the hood. Ammonia sensor starts to read ammonia presence in the hood after 1 hour of synthesis and reading increases with the passing time. When the reaction time gets to 3 hours, the ammonia concentration inside the hood reaches 15ppm which is the safety limit for ammonia and the ammonia sensor shut downs all the systems. This situation suggest that excess ammonia is being flown out of the outlet and no BN generation reaction is taking place inside the reaction chamber after 1 hours.

### 3.3 System Parameter's Optimization

In this optimization step, we investigated the effect of system parameters on the synthesis of BNNTs. Effect of quartz test tube, direction of the quartz test tube, processing catalyst powders before use, position of the wafers, placement of the wafers, introduction

temperature of ammonia flow, effect of catalyst powder milling, size of the alumina boat and size of the quartz test tube was investigated and optimized for the BNNT synthesis.

First, BNNT synthesis without one end closed quartz test tube was tested. As explained before, quartz test tube increases the partial pressures of growth vapors so that nucleation probability of nanotube increases. In order to fully prove the necessity of quartz test tube, BNNT synthesis without it was performed which showed very low yield of BNNT synthesis and also the big portion of BNNTs were on the outer walls of the alumina boat as expected since there is no trapping of the growth gases inside the alumina boat.

Direction of the quartz tube essentially means, where the open end of the quartz tube is facing. In the literature, quartz tube is always placed in a way that open end of the tube faces outlet of the furnace. In order to investigate the effect of the direction of quartz tube, quartz test tube was placed in a way that open end of it faced the inlet of the furnace. After the synthesis, very low yield of BNNT growth was observed on the close end of the quartz tube which is undesirable. Our theory is, ammonia flow sweeps the growth vapors to the close end of the quartz tube so little nucleation is observed on the walls of the alumina boat. Ammonia gas can't sweep the growth vapors when the quartz tube is placed in the opposite direction since the flow rate of ammonia is reduced when entering the quartz tube.

Processing catalyst powders before synthesis essentially means ball milling them individually in order to decrease their particle size. Ball milling process were applied to the catalyst powders individually and resulting powders were used for the synthesis. No increase on the yield was observed when the processed catalyst mixture was used suggesting at 1200 °C, reactions happens efficiently without the requirement of low particle size.

Position of wafers relates to sweet spot of the furnace. As explained in the experimental section, every furnace have its sweet spot where the temperature is constant and at the desired level all the times. Due to this, highest yield is expected for the BNNTs on the wafer which's position corresponds to sweet spot of the furnace. Observations showed that, 2<sup>nd</sup> Si wafer always has the highest yield, suggesting the sweet spot of the furnace corresponds to position of 2<sup>nd</sup> Si wafer. This result were further used during the synthesis

of floating BNNT by placing the catalyst mixture on the sweet spot of the furnace to increase reaction efficiency of catalyst mixture.

Placement of the wafers is one of the most important parameters of system optimization. In one of our synthesis, Si wafers placed on top of the alumina boat fell during the loading of the alumina boat and placement of the Si wafers become diagonal. After the synthesis we realized that, we achieved the highest yield of BNNT synthesis during this flawed run. After that, Si wafers were placed diagonally on the alumina wafers for the all synthesis route because, placing Si wafers diagonally decreases the overall volume of the reaction and thus increases the partial pressures of the growth vapors during the reaction. This can lead to increased probability of nucleation as explained in 2.2.

As explained before, ammonia gas is introduced into the system before the reaction temperature is reached in order to increase efficiency. Two different temperatures for introduction of ammonia gas, namely 1000 °C and 1100 °C were tested. When yields of the syntheses were compared, no change was observed. This shows that, B<sub>2</sub>O<sub>2</sub> vapor starts producing after 1000 °C and introducing ammonia before to reaction temperature of 1200 °C increases the efficiency of the BNNT synthesis.

Size of the alumina boat for the different synthesis routes were also investigated. Our findings showed that, larger boat results in better free-standing BNNT whereas smaller boat is more suitable for the synthesis of BNNTs on Si wafers or BNNFs. Smaller boat allows growth vapors to mainly condense and start the growth on the wafers whereas bigger boat means bigger portion of BNNT nucleation starts on the walls of the alumina boat rather than on the Si wafers.

Effect of length of the quartz test tube was also investigated. Two different size quartz test tubes with 35 cm and 45 cm length were used during the synthesis. It was observed that, there is virtually no difference in results when different quartz test tubes are used, suggesting length of the quartz test tube doesn't affect the BNNT synthesis.



### 3.4 Optimized Recipe

Optimization of BNNT synthesis in terms of temperature, catalyst ratio, catalyst mixture amount, ammonia flow, reaction time parameters as well as system variables were conducted. Set of experiments were performed for each parameter mentioned above and optimum value for this parameters were selected for the final recipe.

For the optimum temperature value, we have selected 1200 °C. As the temperature increases, diameter of the nanotubes also increases and the homogenous diameter distribution disappears. Furthermore, after 1300 °C as-synthesized products cannot be referred to as nanotubes since their diameters exceeds nanometers to  $\mu\text{m}$  and they lose their tube morphology. Catalyst residues also start to deposit on the walls of the nanotubes when temperature is increased from 1300 °C. 1200 °C was observed to be the lowest reaction temperature where the BNNT growth is present. 1200 °C is the selected optimum temperature for our final optimized recipe because best quality and high yield were achieved at this temperature. Furthermore, 1200 °C is the most cost and time efficient temperature value for the BNNT synthesis.

2:1:1 (B : MgO : Fe<sub>2</sub>O<sub>3</sub>, w/w) catalyst ratio was selected to be optimum catalyst ratio. As the boron content of the catalyst mixture increases, diameter of the nanotubes also increases and they began to cluster in flower-like structures. When the boron content of the catalyst mixture decreases, no BNNT synthesis is observed. Additionally, SEM images showed BN sheets on the surfaces of Si wafers when the catalyst ratio is selected 4:1:1 (B : MgO : Fe<sub>2</sub>O<sub>3</sub>, w/w) whereas only nanotubes are present when the catalyst ratio is selected 2:1:1 (B:MgO:Fe<sub>2</sub>O<sub>3</sub>, w/w).

Optimum catalyst mixture amount was determined to be 1 g. Before 1 g of catalyst mixture, yield of the BNNTs is low. However, our findings showed that increasing the catalyst mixture amount without increasing the surface area of the alumina boat doesn't increase the yield of the synthesis. Due to this result, we selected minimum amount of catalyst mixture where BNNT yield is high as our optimum catalyst mixture amount value which is 1 g.

Optimum ammonia gas flow for the synthesis of BNNTs were selected to be 200 sccm. Observations from the wafers after BNNT synthesis shows that, amount of BNNT synthesized increases until 200 sccm and stays the same when the ammonia flow is increased to 250 sccm. Due to this result, 200 sccm of ammonia flow during the BNNT synthesis reaction was used in our final recipe of BNNT synthesis. Our findings suggest that, if critical amount of ammonia is reached inside the reaction chamber, increasing the ammonia amount doesn't affect the amount of growth vapor generated during the reaction between  $B_2O_2$  and ammonia. Ammonia flow higher than 200 sccm flows out of the reaction zone without interacting with  $B_2O_2$  vapors and doesn't affect the final yield of the reaction.

Reaction time for the optimum recipe was selected to be 1 h. If the reaction time is lower than the 1 h, yield of the BNNTs decreases to a point where no growth is observable. On the other hand, increasing reaction time to 1.5 h or higher doesn't affect the yield of the BNNT synthesis. Moreover, increasing the reaction time result in more excess ammonia gas flowing out of exhaust which is apparent since the stability of the buffer solution disappears after 1.5 h and the concentration of ammonia gas inside the hood starts to increase. When the reaction time was selected 1 h, buffer preserves its stability.

In our optimized synthesis, quartz tube was used since experiments showed that, no growth of BNNTs is present when quartz tube is not used. Vortex mixing of catalyst powders were preferred to achieve homogenous mixture which results in better yield, as oppose to no mixing. Ball-mill mixing catalyst mixture results in no observable change and it adds another time consuming step to the overall synthesis as well as causes loss of catalyst powders. Using nano-sized catalyst have no real effect on the efficiency of the synthesis as observed other than increased cost of the synthesis, however at lower temperatures they can be useful. Starting ammonia flow at 1000 °C is found to be useless since same amount of BNNT growth is observed when the ammonia was first introduced at 1100 °C. Heating rate of the synthesis was selected as +5 °C/min since higher heating rate results in loss of quartz tube which we unfortunately experienced several times.

Final recipe for the BNNT synthesis is given below (Table 10) with all optimum parameters. Same recipe was used in all BNNT synthesis runs except for the synthesis of BNNTs from boron minerals.

Table 10 Optimized recipe with 2:1:1 (B:MgO:Fe<sub>2</sub>O<sub>3</sub> w/w) catalyst mixture ratio, 1 g catalyst mixture.

	Time	Temperature	NH <sub>3</sub> Flow	Ar Flow	Step
No	Min	°C	sccm	Sccm	
1	5	30	-	1000	Purge
2	214	1100	-	300	Heating
3	20	1200	200	100	NH <sub>3</sub> introduction
4	60	1200	200	-	Reaction
5	40	1000	-	200	Cooling I
6	100	500	-	200	Cooling II
7	600+	30	-	150	Natural Cooling

## CHAPTER 4 Results and Discussions

### 4.1 Materials and Equipments

Jeolden JEM-200CFEG UHR-TEM CS corrected equipped with Garanti Quantum GIF, Thermo Scientific iS10 FTIR with ATR accessory, Renishaw inVia Reflex Raman Microscopy and Spectrometer (532 nm laser unite), JEOL JEM 4601 MultiBeam FIB-SEM system (equipped with EDS and RAITH Elphy Quantum FIB/SEM Nanolithography Systems), Zeiss LEO Supra 35VP FESEM, Cressington Sputter Coater, 108 auto.

### 4.2 SEM Analysis of as Grown BNNTs

#### 4.2.1 a. SEM Analysis of BNNTs grown on Si wafers

Morphologies of the synthesized BNNTs on Si wafers were analyzed by scanning electron microscopy. BNNT coatings were not extracted from Si wafers during sample preparation and since BNNTs are semiconductors with high band-gap on top of an insulator Si wafer, they were coated with carbon before SEM analysis to prevent charging on the samples. Carbon contamination from this coating can be observed in Figure 39. a.

As-synthesized BNNTs have average diameter of 280 nm with lengths in the order of  $\mu\text{m}$  and BNNT coating is homogeneous across the Si wafer surface with a network structure (Figure 39. a). SEM image were also taken from the surface of the Si wafer where no white coating was observable to eye (Figure 39. b). Along with impurities which are assumed to be BN particles and catalyst impurities, some resemblance of BNNT growth is also present in the image suggesting that, growth of BNNTs are highly dependent of the growth conditions and the sweet spot of the furnace must be determined to achieve high quality BNNTs.

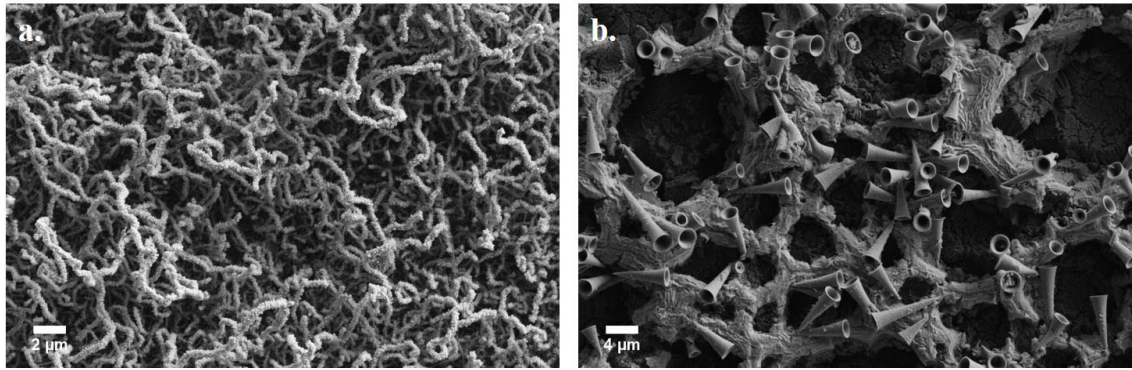


Figure 39 SEM images of BNNTs synthesized on Si wafers. a. Surface of the Si wafer, b. Non-coated surface of Si wafer.

Big clusters of floating BNNTs is also synthesized during the BNNT synthesis on Si wafers with 50  $\mu\text{m}$  diameter in size (Figure 40. a). Bamboo-like structure of the BNNTs can be seen from the SEM image of the single nanotube (Figure 40. b). Figure 40. b also shows that, as-synthesized BNNTs have hollow, tube like morphologies which is consistent with nanotubes. As-synthesized BNNTs have no catalyst particle present on the tips or on the walls, suggesting clean BNNT synthesis on Si wafers (Figure 40. b).

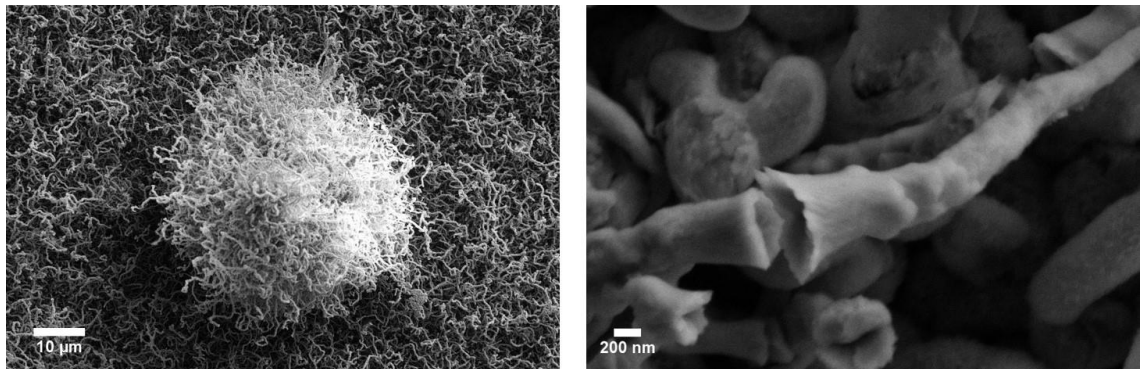


Figure 40 SEM images of a. Floating BNNT cluster on the Si wafer and b. Single BNNT.

SEM image of the BNNTs growing out of catalyst droplet (Figure 41) further solidifies that BNNT's growth is governed by VLS mechanism and supersaturation of catalyst droplets with growth vapors (BN vapors) starts the nucleation from the catalyst droplet.

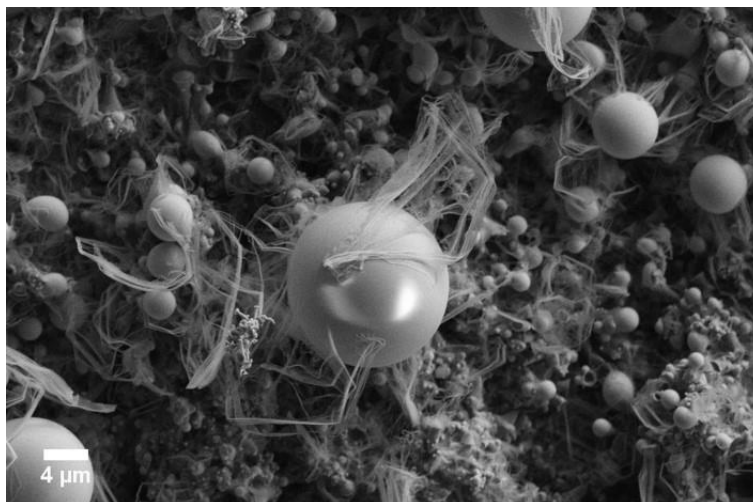


Figure 41 SEM image of catalyst droplet on Si wafer where BNNTs are growing out of. SEM images of the BNNTs synthesized on Si wafers shows, tube morphology of the as-synthesized product, homogeneous diameter distribution with  $\sim 200\text{-}300$  nm and lengths in the order of  $\mu\text{m}$ . Networked structure is observed in the BNNTs with tips of the nanotubes appears to be clean. Furthermore, evidence of VLS growth mechanism is also presented in the SEM images.

#### 4.2.2 b. SEM Analysis of Free-standing BNNTs

Morphologies of as-grown BNNTs were analyzed using scanning electron microscope. Free-standing BNNTs can easily be collected from the surface of the alumina boat via simple extraction. Collected BNNTs then was deposited on carbon tape and stuck to SEM stage. Silver paste was used in order to prevent charging on the samples. Both BNNTs after purification and before purification were characterized.

As-synthesized floating BNNTs are clustered with average cluster diameter of  $\sim 3$   $\mu\text{m}$  (Figure 42), lower cluster diameter than floating BNNT cluster observed on the Si wafers (Figure 40 a).

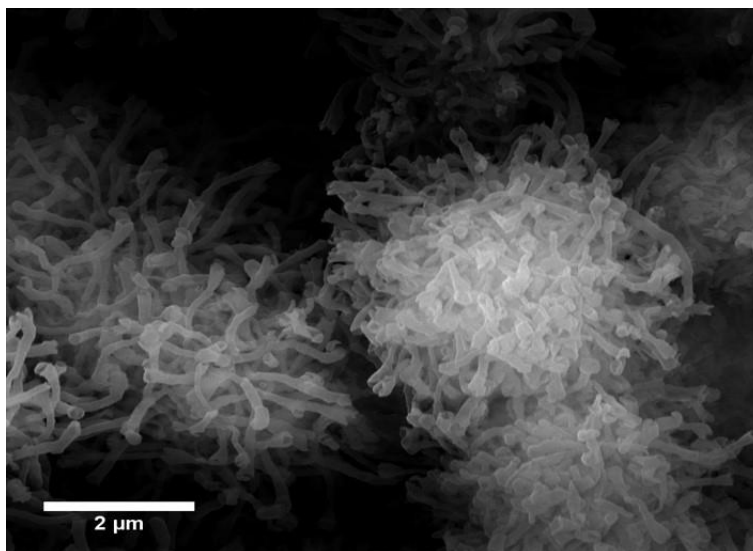


Figure 42 SEM images of floating BNNT clusters.

As-synthesized floating BNNTs have bamboo like, hollow tube morphologies with average diameter of 86 nm and lengths in the order of  $\mu\text{m}$ . (Figure 43). Tips of the floating BNNTs are open just like BNNTs synthesized on Si wafers (Figure 40 b.). High magnification SEM image of floating BNNTs (Figure 43) shows clean tips and walls of nanotubes, in contrast to as-synthesized floating BNNTs before purification (Figure 44 a. and b). Purification process appears to be successful at removing catalyst residues and BN impurities from the floating BNNTs.

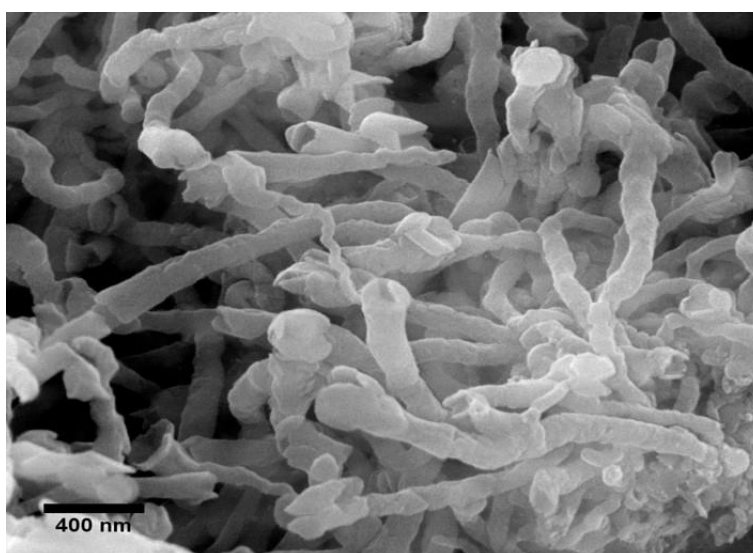


Figure 43 High magnification SEM image of floating BNNTs.

SEM images of floating BNNTs were also taken before the purification process. Higher agglomeration and impurity (catalyst residues and unwanted BN particles) are present on the as-synthesized floating BNNTs before purification (Figure 44. a, b). One interesting result is, nanotube's diameters appears to be 15 nm to 20 nm with very short lengths which is lower compared to BNNT's diameters and lengths after purification process (Figure 43). Although purification process got rid of impurities and network structure, it also increases the cluster size from 1 $\mu$ m to 3 $\mu$ m since BNNT cluster size before purification appears to be 1 $\mu$ m in diameter. Overall, purification process seems to be very effective at getting rid of impurities but increase in agglomeration and loss of small diameter BNNTs on the surfaces are some disadvantages of the purification.

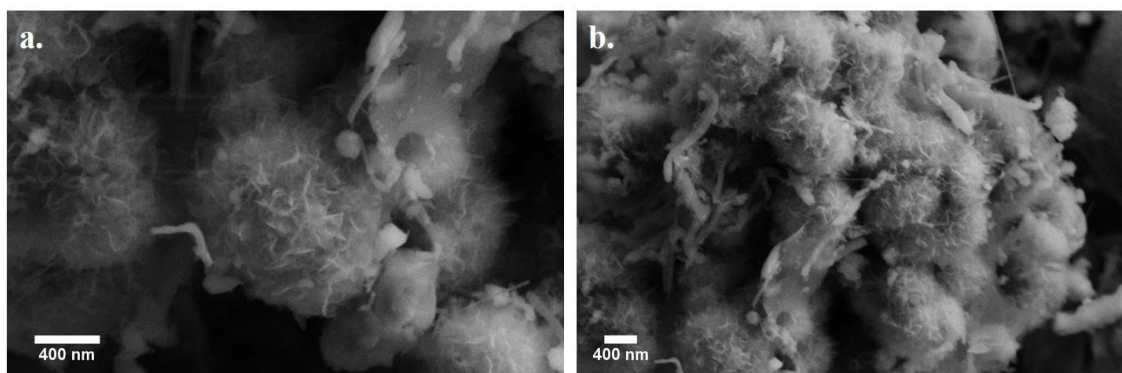


Figure 44 SEM images of floating BNNTs before purification process. a. cluster of floating BNNTs and b. networked structure of floating BNNTs with impurities.

#### 4.2.3 c. SEM analysis of BNNTs synthesized on Fibers

SEM images of BNNFs were taken before and after the BNNT synthesis on them. BNNFs preserves their fiber morphologies after the catalyzation process however, surface roughness can be seen on the fibers (Figure 45). EDX analysis showed, presence of Fe and Mg atoms on the surfaces of nanofibers as result of catalyzation process.



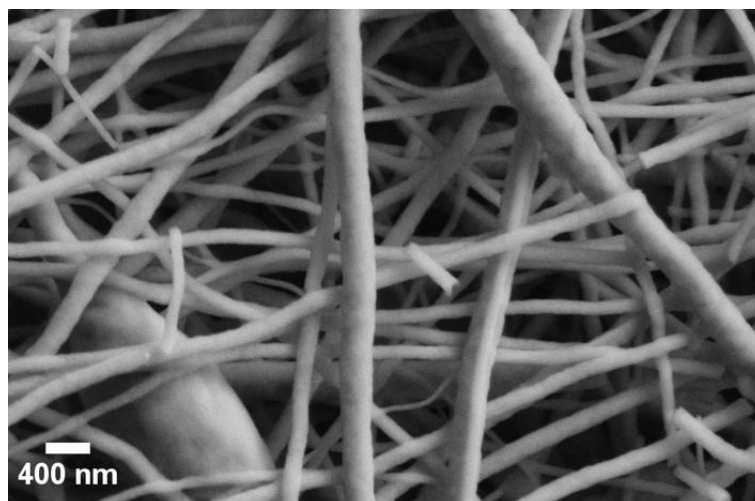


Figure 45 SEM image of BNNFs after catalyzation.

Clusters of BNNTs can be seen on the BNNFs from the SEM images taken after the BNNT synthesis (Figure 46. a). Dense and homogeneous BNNT coating on the BNNF surfaces' which makes spotting BNNF impossible suggest efficient catalyzation process followed by high yield BNNT synthesis for the BNNFs. As-synthesized BNNTs are networked clusters with bamboo like morphologies. Diameter of the BNNTs ranges from 80 nm to 150 nm with lengths in the order of  $\mu\text{m}$  (Figure 46. b).

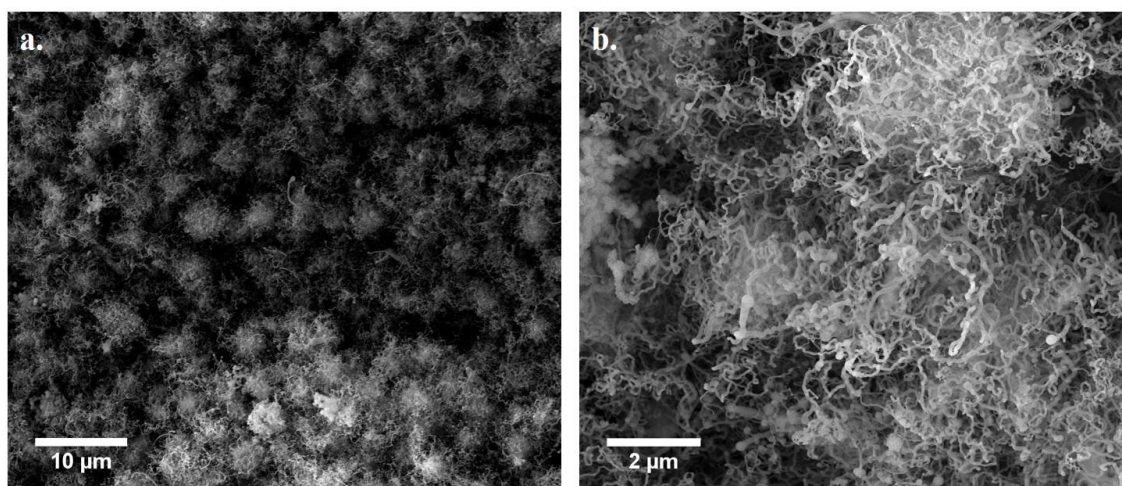


Figure 46 SEM images of BNNFs after BNNT synthesis. a. Surface of the BNNFs where clusters of BNNTs are visible. b. High magnification image of BNNT cluster with networked structure.

SEM images of the BNNFs' surface facing inwards of the alumina boat shows partial coatings of BNNT clusters on the continuous BNNFs (Figure 47). Catalyst particles are visible on the surfaces of BNNFs with no BNNT growth inside of them suggesting low

diffusion depth for the growth vapors. However, SEM images are non-conclusive to determine the interface between the nanotubes and the nanofibers and further characterization is required for the definitive characterization of interface.

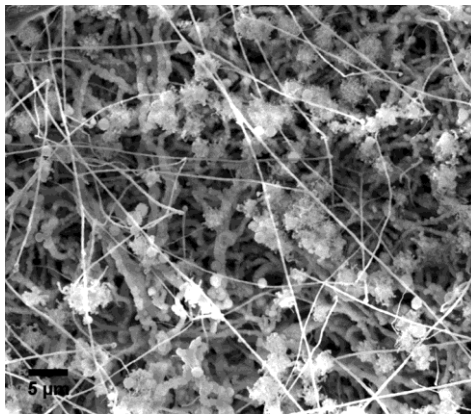


Figure 47 SEM image of BNNFs' surface facing inwards of the alumina boat.

#### 4.2.4 d. SEM analysis of BNNTs synthesized from boron minerals

SEM images of BNNTs synthesized from Ulexite and Etidot-67 boron minerals were taken for the characterization of as-synthesized products. SEM image of white product collected from the walls of the alumina boat after the BNNT synthesis from Ulexite (Image 47. a) shows no BNNT formation. BN-catalyst clusters are observed on the SEM images which are the initial phase for the BNNT synthesis from boron minerals as reported in the literature [149]. BNNTs synthesized from Etidot-67 also shows similar structures on the SEM images where BN-Fe initial phase clusters are present however no BNNT formation is occurring. This images suggest, further optimization of the synthesis is needed to start BNNT formation from the initial BN-Fe phase. Catalyst ratio, temperature and the reaction time effects the BNNT synthesis from boron minerals so optimization of these parameters can result in BNNT synthesis from boron minerals.

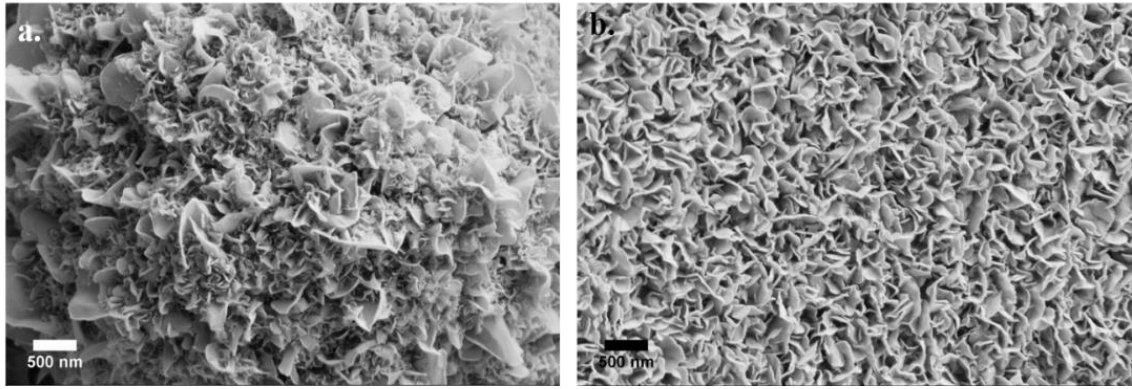


Figure 48 SEM images of BNNTs synthesized from a. Ulexite and b. Etidot-67

### 4.3 TEM and EELS analysis of BNNTs

TEM characterization was performed in order to gather information about the structure and chemical composition of as-synthesized BNNTs. Floating BNNTs were extracted from the surface of the alumina boat and crushed in order to prepare TEM samples. HRTEM images show hollow tube morphology for the as-synthesized BNNTs with ~20 nm diameter (Figure 49. a). Dark fringes on the edge of the nanotubes points out, multi-walled nanotube structure of the BNNTs (Figure 49. b). Moreover, parallel orientation of the walls with respect to tube axes suggests zig-zag nanotube structure [164].

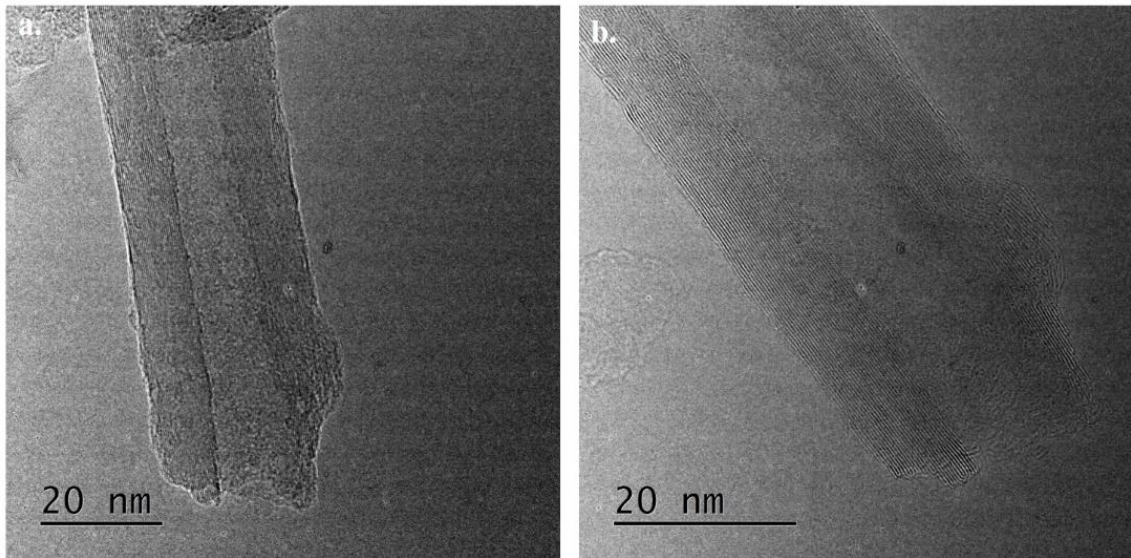


Figure 49 HRTEM images of single BNNTs. a. Bright core and dark edges are the indicators for the hollow tube structure. b. Dark fringes can be seen on the edges of the nanotube.

Profile analysis from the HRTEM image of single BNNTs were performed to calculate the number of walls (Figure 50). Each peak on the graphic represents a wall, giving ~30 number of walls for the as-synthesized BNNTs. Distance between the walls are 0.33 nm which is consistent with the  $d_{002}$  lattice spacing of bulk h-BN [165].

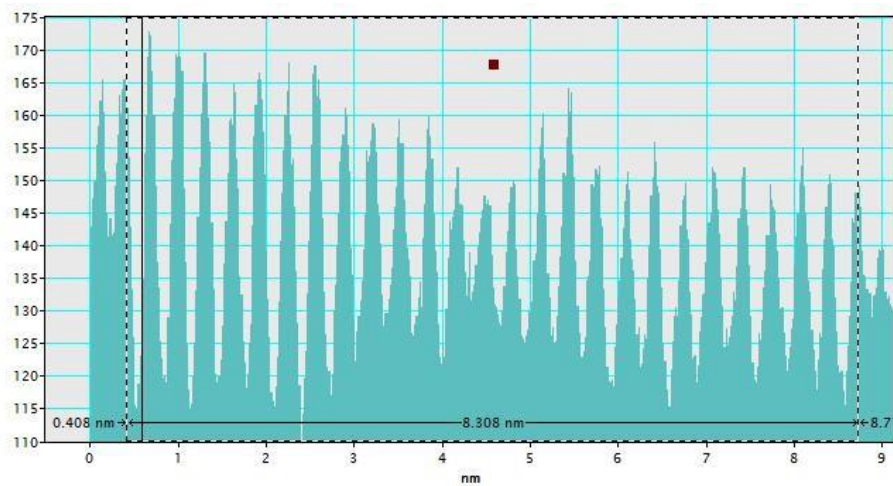


Figure 50 Profile analysis of single BNNT.

Diffraction pattern taken from the single BNNT (Figure 51) shows hexagonal rings which is characteristic for the nanotube structures and orientation of diffraction spots suggest that planes are parallel to tube axes with the inter planar distance of 0.31 nm, a value similar to what have been reported on the literature [45].



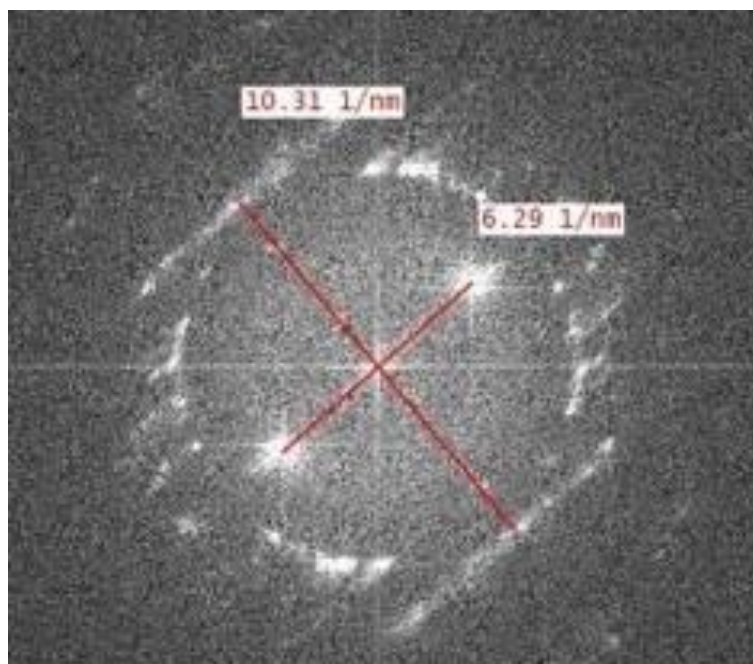


Figure 51 Diffraction pattern from the single BNNT.

As-synthesized nanotubes appear to be open-tip and clean of any catalyst residues (Figure 47). Purification process had been applied to the samples beforehand and no sign of catalyst impurity suggest that, purification process is successful at removing impurities from the nanotubes. EELS analysis were performed in order to analyze chemical composition of the nanotubes. EELS results (Figure 52) shows, strong B k-edges together with strong N k-edges. Additionally,  $sp^2$ -type bonding of h-BN is also clear due to intense  $\pi^*$  peaks of B and N. EELS results are consistent with the previous reports of EELS analysis of BNNTs [153].

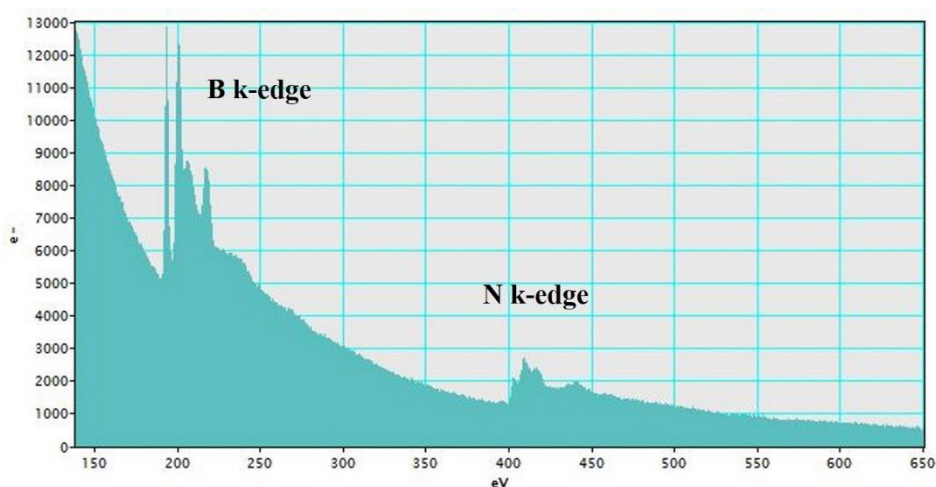


Figure 52 EELS data for the as-synthesized BNNTs.

#### 4.4 Raman and FTIR analysis of BNNTs synthesized on Si wafer

As-synthesized BNNTs were also analyzed by RAMAN spectroscopy (Figure 53). In both spectrums of BNNTs synthesized on Si wafers and floating BNNTs, intense peak at  $1367\text{cm}^{-1}$  is observed and since this peak corresponds to well-defined  $E_{2g}$  in-plane vibrational mode of h-BN structures structure of as-synthesized BNNTs is determined to be h-BN. Single, narrow and intense peak also confirms the high purity of the BNNTs. Slight noise on the RAMAN spectra of floating BNNTs (Figure 53. b) are due to low energy of the exciting laser. When the laser intensity is above 1 percent for the floating BNNTs, detectors detect too much signal coming out of sample thus cannot register the values. BNNT samples was chosen randomly for RAMAN analysis and all of the samples show the same RAMAN peaks. Small bumps present in the RAMAN spectrum of the BNNTs synthesized on Si wafers (Figure 53. a) corresponds to  $520\text{ cm}^{-1}$  adsorption band of Si wafers.

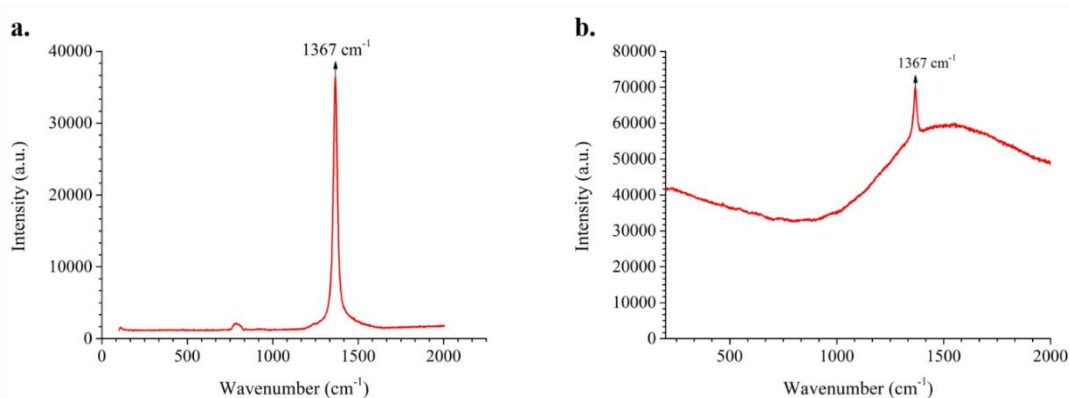


Figure 53 RAMAN data spectrum from a. BNNTs synthesized on Si wafers, b. free – standing BNNTs

RAMAN analysis of BNNTs synthesized from ulexite (Figure 54 a.) and Etidot-67 (Figure 54 b.) minerals were also performed. Like the RAMAN peaks from the BNNTs synthesized on Si wafers and the floating BNNTs, RAMAN spectras slow show intense peak at the  $1367\text{ cm}^{-1}$  which corresponds to high frequency counter phase vibrational mode due to movement of B and N atoms against each other in the h-BN sheet [166].

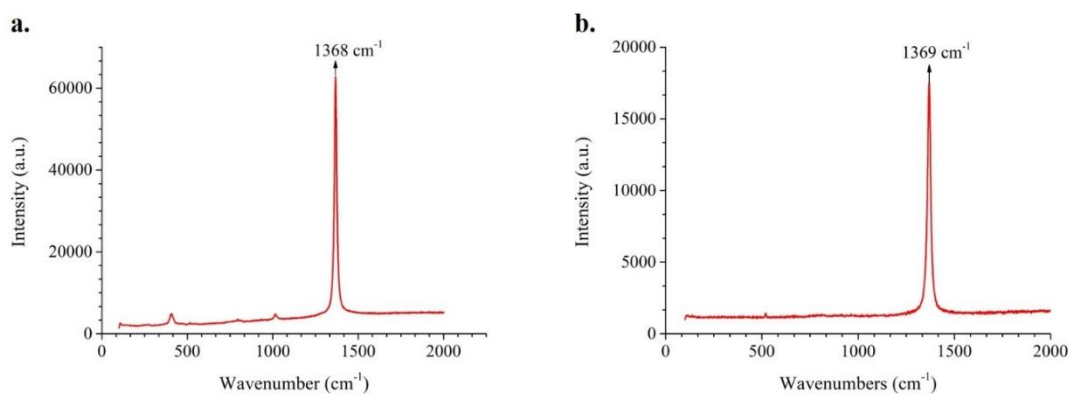


Figure 54 RAMAN spectra of a. ulexit, b. Etidot-67

The FTIR spectra of BNNTs were taken as well to further solidify BNNT structure. Samples from BNNTs synthesized on Si wafers were analyzed without any post-treatment. Floating BNNTs were tested after purification process to investigate the efficiency of purification process. FTIR analysis of the BNNTs were performed in transmission mode of the FTIR.

Theoretical studies [167] done on the BNNTs suggest that three absorption frequency peaks should be observed at  $\sim 806\text{ cm}^{-1}$ ,  $\sim 1369\text{ cm}^{-1}$  and  $\sim 1532\text{ cm}^{-1}$ .  $\sim 1369\text{ cm}^{-1}$  and  $\sim 1532\text{ cm}^{-1}$  absorption bands are characteristics of plane stretching mode of BNNTs and absorption band at  $\sim 806\text{ cm}^{-1}$  corresponds to out-of-plane radial buckling mode (R) of BNNTs. Vibration of h-BN sheets along the tube axis (or longitudinal) creates transverse optical mode (TO) of h-BN which is responsible for strong absorption band at  $\sim 1369\text{ cm}^{-1}$ . Longitudinal optical mode (LO) of h-BN sheets corresponds to stretching of the h-BN sheets along the tangential directions of BNNT which can be observed as an absorption band at  $\sim 1532\text{ cm}^{-1}$ .  $\sim 1532\text{ cm}^{-1}$  absorption band is RAMAN inactive and can only be observed in FTIR analysis. When the curvature of the tube induces strain on the h-BN sheet network LO mode becomes active. This LO mode is non-visible with h-BN bulks or BN thin films. Strain created by the tubular structure can cause small shifts on these absorption bands. Absorption bands introduced above can be described as the fingerprints of the BNNTs however they are indirect indicators of BNNTs as oppose to TEM, SEM or EELS analyses. Vibration modes of the BNNTs can be seen from the Figure 55.

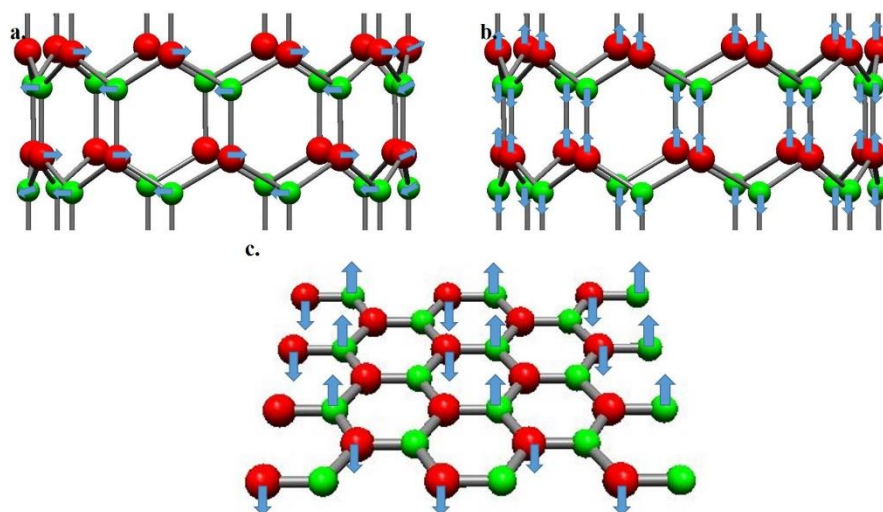


Figure 55 Vibrations modes of BNNTs. a.TO mode, b. LO mode and c. Radical buckling more

During the FTIR analysis of the BNNTs synthesized on Si wafers, FTIR signals coming from the Si wafer is excluded by introducing Si wafer FTIR data as baseline. FTIR analysis shows strong absorption band at  $\sim 1347.24 \text{ cm}^{-1}$  which is attributed to plane stretching mode of h-BN and another absorption band at  $\sim 785.56$  is attributed to out-of-plane radical buckling mode of BNNTs. Both of the absorption bands show small shifts from the h-BN absorption bands. Shoulder at  $\sim 1530 \text{ cm}^{-1}$  coming out of adsorption band at  $\sim 1347.24 \text{ cm}^{-1}$  corresponds to LO mode for BNNT (Figure 56).



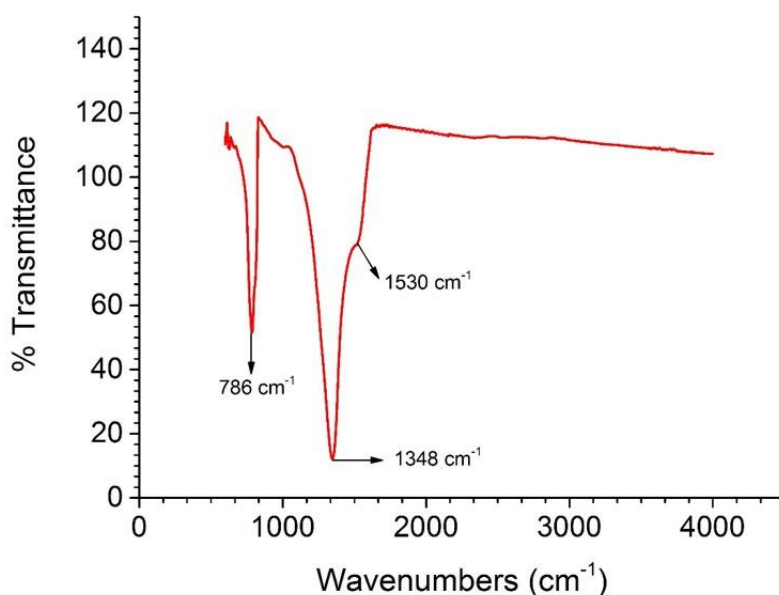


Figure 56 FTIR analysis of BNNTs on Si wafers

Floating BNNTs also show similar absorption bands as BNNTs on Si wafers: strong absorption band shifts to  $\sim 1316 \text{ cm}^{-1}$  (this mode is also RAMAN active) on FTIR analysis however, shift of the band is not present on RAMAN spectroscopy. Out-of-plane buckling mode again shifts to  $\sim 767.99 \text{ cm}^{-1}$ . LO mode of h-BN is very vaguely present on the FTIR spectra of free-standing BNNT. Shoulder at  $\sim 1530 \text{ cm}^{-1}$  coming out of adsorption band at  $\sim 1316$  might be corresponding to LO mode for BNNT (Figure 57). FTIR analysis suggest that samples are indeed h-BN, however there isn't enough data to comment on the morphology of the sample since the  $\sim 1520 \text{ cm}^{-1}$  shoulder which is indicator for tube morphology is not definitive. Due to this, SEM, TEM and EELS analysis of BNNTs were conducted to support our claim.

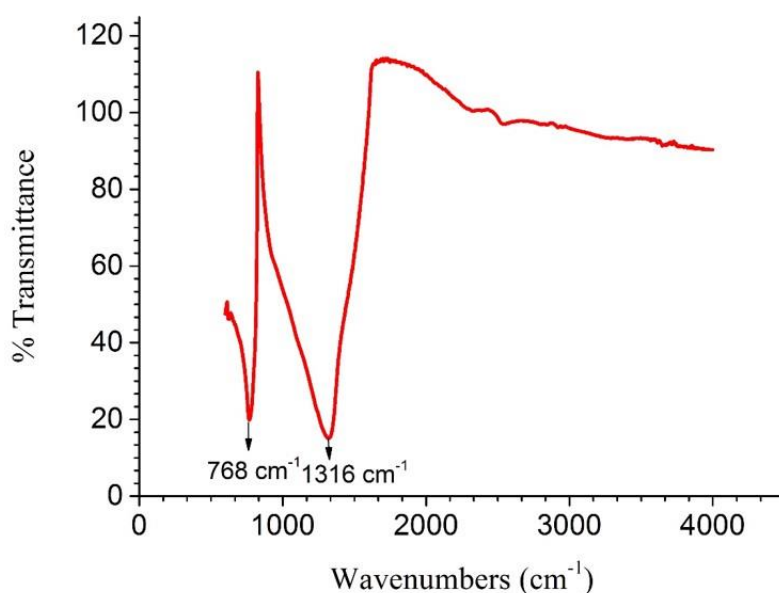


Figure 57 FTIR spectrum of as-synthesized floating BNNTs.

Nearly identical FTIR absorption peaks also suggest that, BNNTs synthesized on Si wafers and floating BNNTs can be accepted as same although some diameter and length differences are present. Both R and TO modes of the h-BN structure is present in the FTIR analysis of the samples and although it is not as clear as others, LO mode due to tubular morphology is also visible in the FTIR analysis. Both samples are h-BN structure with tubular morphology according to FTIR spectrum results.

#### 4.5 Characterization of Functionalized BNNTs.

##### 4.5.5 FTIR Analysis of Covalent Functionalized BNNTs

Covalently functionalized BNNTs were analyzed with FTIR for the detection of the hydroxyl groups on the surface of the nanotubes. Hydroxyl (-OH) group's indicator at FTIR spectrum is the broad band between  $\sim 3000\text{ cm}^{-1}$  and  $\sim 3600\text{ cm}^{-1}$  [136]. FTIR analysis were performed on both ozone treatment of the BNNTs and the HNO<sub>3</sub> treatment of the BNNTs.

Figure 58 shows the FTIR analysis of ozone treated BNNTs. Absorption band at  $\sim 1378.23$   $\text{cm}^{-1}$  corresponds to TO mode of h-BN and absorption band at  $\sim 800.67$  corresponds to radial buckling mode of h-BN structure. This absorption bands is present with a small shift before the ozone treatment as shown in the FTIR spectrum of BNNTs on Si wafers (Figure 55 a). Absorption band corresponding to LO mode of BNNTs are completely disappears after the ozone treatment suggesting deformation of tube morphology during the ozone treatment. Broad absorption band at  $\sim 3393.79$   $\text{cm}^{-1}$  corresponds to the hydroxyl group's vibration on the surfaces of BNNTs, suggesting that ozone treatment is efficient for the hydroxylation of BNNTs.

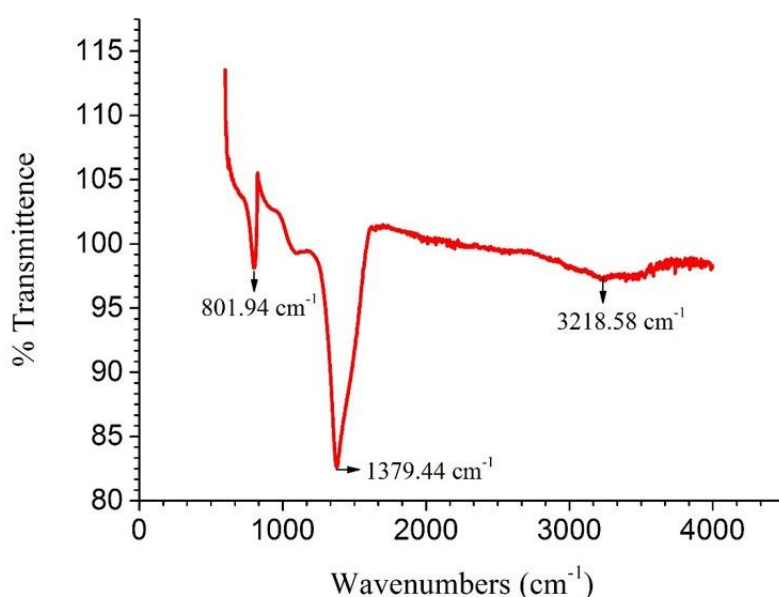


Figure 58 FTIR analysis of BNNTs after ozone treatment

Figure 59 shows the FTIR analysis of nitric acid treated BNNTs. Broad absorption band at  $\sim 3214$   $\text{cm}^{-1}$  again suggests presence of hydroxyl groups on the surfaces of BNNTs. Absorption band at  $\sim 1335.83$   $\text{cm}^{-1}$  corresponds to TO mode of h-BN and absorption band at  $\sim 764.77$   $\text{cm}^{-1}$  corresponds to radial buckling mode of h-BN structure. These absorption bands are also present on the FTIR spectrum of floating BNNTs (Figure 55. b). Absorption band corresponding to LO mode of BNNTs are completely disappears after the nitric acid treatment suggesting deformation of tube morphology during the nitric acid treatment which is expected since nitric acid is very strong corrosion agent.

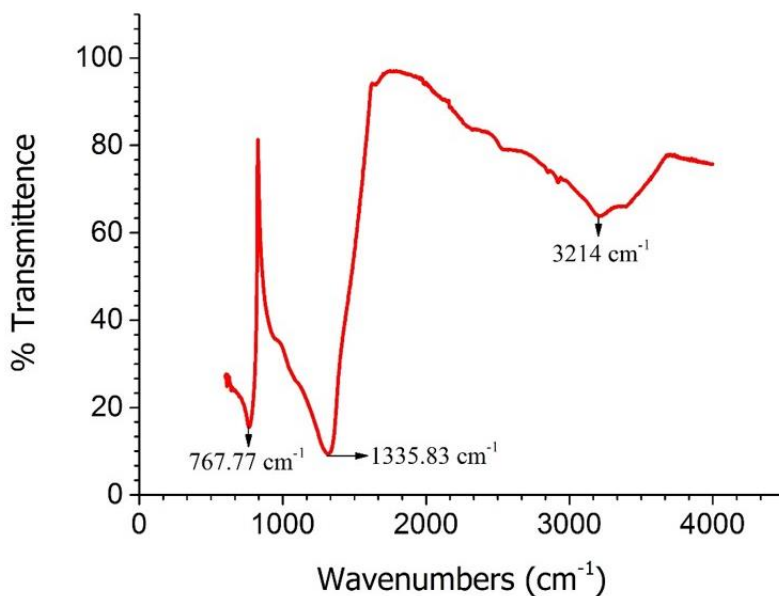


Figure 59 FTIR analysis of BNNTs after nitric acid treatment

Both of the covalent functionalization methods for hydroxylation of BNNTs appears to be successful since the presence of hydroxyl groups can be deduced from the FTIR analysis of the samples. However, ozone treated BNNTs is not suitable for our further applications such as film production via LbL method since extraction of the BNNTs from the Si wafers are very challenging and loss of material is always present. Synthesizing floating BNNTs and hydroxylating them seems to be more logical route. Unfortunately, high flow rate of ozone during the ozone treatment causes high loss of material for floating BNNTs making this hydroxylation route unsuitable for the floating BNNTs. Due to this shortcoming of the ozone treatment system, different functionalization method were selected for the hydroxylation of BNNTs. Nonetheless, our belief is, hydroxylated BNNTs on the Si wafers can be used for number of possible applications in the future.

As shown above (Figure 59), nitric acid treatment of the floating BNNTs resulted in the hydroxylation of the BNNTs. However, hydroxylated BNNTs were not dispersible in aqueous media with high uptake, making them unviable for the LbL method. Due to this shortcoming, non-covalent functionalization methods were explored to disperse BNNTs in aqueous media. In spite the being insoluble in aqueous media, hydroxylated BNNTs can still be used for the further functionalization of BNNTs as we explained in section 1.4. The results show that, their inability to disperse in water is due to low functionalization efficiency of the nitric acid treatment. Hydroxyl groups on the surface

of the as-functionalized BNNTs didn't have enough concentration to prevent agglomeration of the BNNTs in aqueous media resulting in very low uptake of BNNTs on the aqueous dispersions.

#### 4.5.6 Stability of BNNT Aqueous Solutions Prepared via Non-covalent Functionalization

As explained in the chapter 2, aqueous dispersions of BNNTs were prepared using two different non-covalent functionalization methods. (1) BNNT aqueous dispersions with the help of ionic surfactants and (2) polymer wrapping. Zeta potentials of BNNT aqueous dispersions were calculated via dynamic light scattering spectroscopy and 24 h stability test were performed for all of the different aqueous dispersions. 24 h stability test is to simply allow stabilization of the aqueous dispersions for 24 h and observe the changes of the dispersion in a time intervals.

1 mL of as prepared BNNT dispersions were taken as sample to dynamic light scattering spectroscope and the zeta potential values of dispersion was tested at 0 h (right after preparation) and at 24 h (after stabilization of dispersion). Agglomeration of the particles can be decreased by the creating electrical charges on the particles and increases the stability of the dispersion. Zeta analysis of dispersions allows the measurement of the charge on the particles and generally dispersions with zeta values between -20 mV and +20 mV are considered unstable and dispersions with zeta potentials lower than -20 mV and higher than +20 mV is considered stable [21]. Table 11 gives the DLS results.

Table 11 DLS results of the BNNT aqueous dispersions

Dispersion	Zeta Potential	Mobility
Name	mV	$\mu\text{mcm/Vs}$
BNNT-surfactant 0h	-34,7	-2,717
BNNT-surfactant 24h	-35,3	-2,770
BNNT/b-PEI	+20,5	+1.841
BNNT/PAH	0	0

Results suggest that (Table 11), BNNTs in the BNNT-surfactant aqueous dispersion have zeta potential of 34.7 mV at 0 h dispersion which is lower than the -20 mV zeta potential of stable dispersions. Furthermore this zeta potential value is higher than the zeta potential of BNNTs [168]. BNNTs in the BNNT-surfactant dispersion have a zeta potential of 35.3 mV after 24 h. Zeta potential suggest that, agglomerated BNNTs drop to the bottom of the container and only well dispersed BNNTs are left in the aqueous dispersion since the zeta value of the dispersion increases. Additionally, this measurement also suggest that, BNNT-surfactant dispersion is still stable even after 24 h of waiting. All of our findings are in line with the literature on the dispersion of BNNTs with the help of ionic surfactants [103].

Aqueous dispersion of polymer wrapped BNNTs also shows good stability with zeta potential lower than -20 mV (Table 12). However, PAH wrapped BNNTs shows no zeta potential or mobility inside aqueous dispersion (Table 12) but lack of signal is not caused by the bad stability of the dispersion rather caused by the low molecular weight of PAH itself.

All dispersions were left to stabilize for 24 h which allowed large clusters of BNNTs to drop down from the dispersion. Figure 60 shows the BNNT-surfactant dispersion in different time intervals. Light white color of the dispersion is most visible at 0 hour which is right after the preparation of the surfactant. As the time pass by, large BNNT clusters, impurities and BNNT agglomerates begins to precipitate at the bottom of the falcon and the color of the dispersion becomes lighter. After 12 h, dispersion fully stabilizes and preserves its stability further.

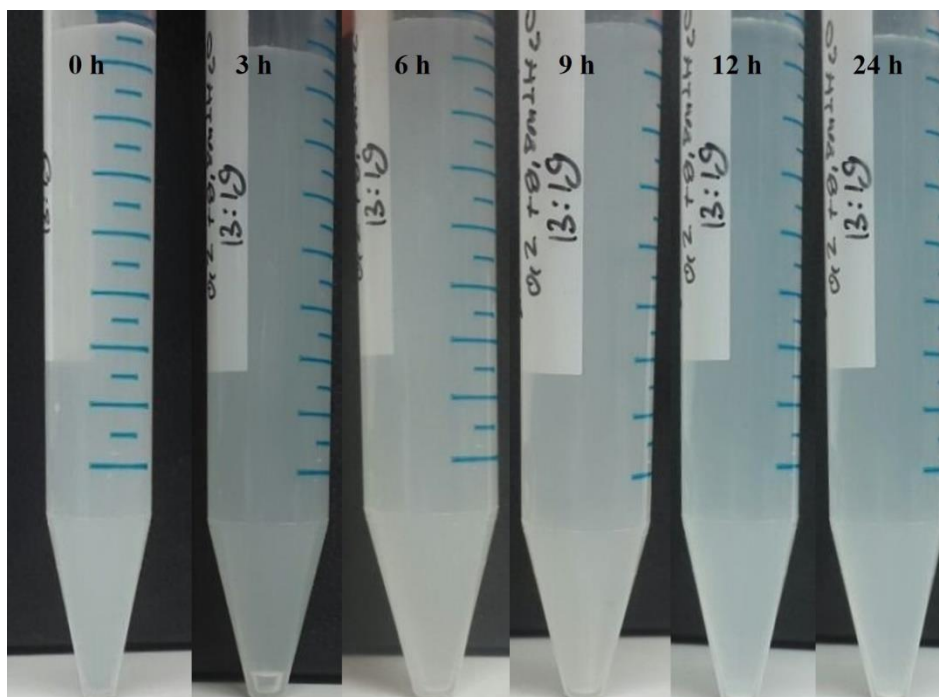


Figure 60 Surfactant assisted dispersion's images from different time intervals

The dispersion of the BNNTs are possible with both ionic surfactant ammonia oleate and polymer wrapping. Ionic surfactant is soluble in the water and the authors of this method suggest that there could be two different ways surfactant might be interacting with the BNNTs [103]. (1) Cylindrical micelles with BNNT core might be forming inside the dispersion or (2) adsorption of surfactant to the surface of the BNNTs with coulombic attraction leads to coating of BNNTs' surfaces with surfactant. Arrangement of the heads and tails of the surfactant leads to long-term stability of dispersion. Final dispersion's pH value was measured to be 6.5.

Below is a collection of images of PEI wrapped BNNT aqueous dispersions taken with 3 hours' time intervals (Figure 61). As can be seen from images precipitation of excess polymer and/or BNNTs are present until 24 h. However, polymer solution is transparent before the addition of BNNTs but loses its transparency when BNNTs are introduced into the solution, suggesting that BNNTs are being wrapped by the polymer and start dispersing in the water. Final pH of the solution was 8.5.

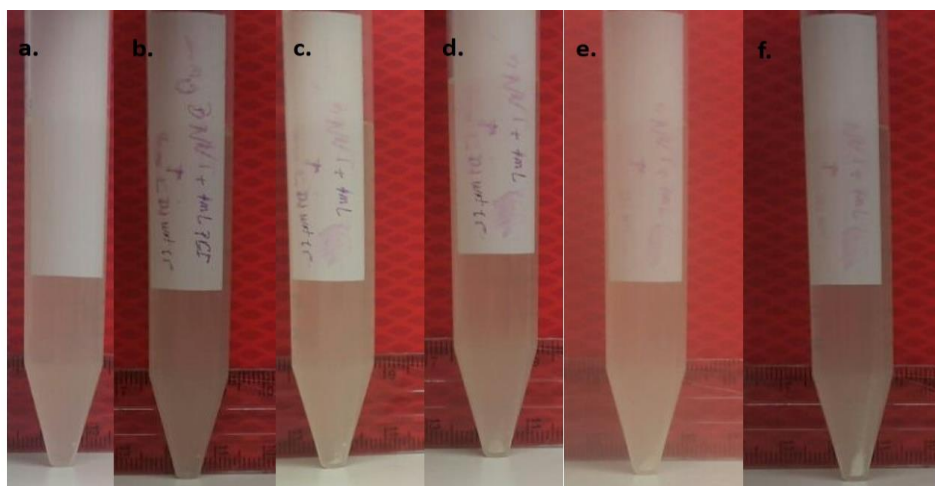


Figure 61 Images of dispersion with different time intervals.

Below is another collection of images polymer-wrapped BNNT aqueous dispersion however this time polymer used is PAH instead of b-PEI (Figure 62). Right after preparation of the dispersion, some big clusters of BNNTs are barely visible to eye and the color of the dispersion is very light white which is expected for the BNNT dispersions [97, 103]. After 3 h of waiting BNNT dispersions appears to be stabilized and no further precipitation or color loss is observed. Final dispersions pH value is 4.11.

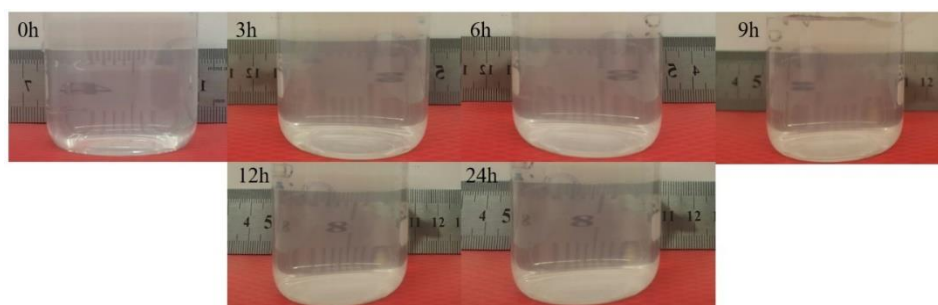


Figure 62 Images of BNNT-PAH dispersion from different time intervals.

Both of the dispersions prepared with the help of the polymer-wrapping appears to be stable and can be used for LbL applications with desired pH adjustments.



## CHAPTER 5 Conclusions and Future Work

In this chapter conclusions of this work will be summarized in terms of synthesis of BNNTs, functionalization of BNNTs, dispersion of BNNTs in aqueous media and BNNT thin film assembly.

### 5.1 Synthesis of BNNTs

Synthesis of BNNTs on Si wafers using growth vapor trapping-BOCVD method were accomplished. SEM images of the as-synthesized BNNTs along with the FTIR and RAMAN spectrums of the as-synthesized BNNTs show the successful synthesis of BNNTs on Si wafers. Synthesis of BNNTs on Si wafers was performed for the understanding of the BNNT synthesis and the success of the synthesis allowed further synthesis of BNNTs in different conditions. As-synthesized BNNTs on Si wafers are 200-300 nm in diameter with lengths in the order of  $\mu\text{m}$ . h-BN structure of the BNNTs were proven by the RAMAN and FTIR analysis where they show fingerprints of the h-BN structure.

After the successful synthesis of BNNTs on Si wafers, floating BNNTs were synthesized using same method. SEM and TEM analyses show tube morphology with diameter ranging from 20nm to 100nm for the as-synthesized BNNTs. BNNTs are exhibited highly agglomerated and clustered structures as presented in the images. FTIR and RAMAN analyses confirms that h-BN structure of the tubes and EELS analysis proves that chemical composition of the as-synthesized BNNTs are indeed consist of B and N atoms. All of the analysis showed no impurities in the as-synthesized BNNTs suggesting efficient purification process.

BNNTs synthesis on BNNFs were also accomplished in this work. SEM images shows synthesis of BNNTs on BNNFs proving efficient catalyzation of BNNFs. However, origin of the nucleation of BNNTs question cannot be answered from the SEM images alone. Further characterization is needed in order to fully understand the mechanisms

behind the BNNT growth on BNNFs and the characteristics of interface between nanofibers and nanotubes.

Synthesis of BNNTs from boron minerals were also accomplished in this thesis work. RAMAN analysis of the as-synthesized products shows h-BN structure is present in the samples however, SEM characterization of BNNTs shows no BNNT formation and only BN-Fe initial phase formation.

Optimization of BNNT synthesis were performed in the terms of temperature, catalyst ratio, catalyst amount, ammonia flow and reaction time. Optimum values for the temperature, catalyst mixture ratio, catalyst mixture amount, reaction time and ammonia flow for the synthesis of BNNTs along with the optimum parameters for the overall system were determined. This experimental optimization allowed efficient synthesis of BNNTs with good quality and yield.

In summary, BNNT synthesis on Si wafers and floating BNNT synthesis were successful in this research. In addition to that, results from the synthesis of BNNTs on BNNFs and synthesis of BNNTs from boron minerals showed promising results. Optimized recipe for the synthesis of BNNTs were also found during this thesis work.

## **5.2 Surface Modifications of BNNTs**

Surface modifications of as-synthesized BNNTs via two different routes: Covalent functionalization and non-covalent functionalization.

Covalent functionalization of the BNNTs were focused on the B site functionalization of the BNNTs. We treated as-synthesized BNNT with ozone and nitric acid in order hydroxylate them. Ozone treatment is a viable option for the hydroxylation of BNNT synthesized on Si wafers and FTIR results shows successful hydroxylation of as-synthesized BNNTs. Nitric acid treatment were used or the hydroxylation of floating BNNTs and FTIR analysis shows successful hydroxylation of BNNTs. However, low uptake of BNNT in aqueous dispersions forced us to find new ways to disperse BNNTs in aqueous media. On the other hand, hydroxylated BNNTs can be used for further functionalization in the future.

Non-covalent functionalization of the BNNTs were achieved by the use of polymer wrapping and ionic surfactant. Surfactant assisted BNNT dispersions gave good results in Zeta potential analysis showing -35 mV charge on the surface of the BNNTs. Furthermore, dispersion prepared by the help of ionic surfactants showed good stability up to weeks. This results suggest that, BNNT dispersion with ionic dispersion is usable in LbL process. Addition to surfactant assisted dispersion of BNNTs, we also performed polymer wrapping of BNNTs with two different polymers. First b-PEI was used for the polymer wrapping of the BNNTs. Polymer wrapped BNNTs are dispersible in aqueous media with stability up to weeks and have zeta potential of +20.5. Due to positive charged nature of the b-PEI, prepared dispersions can be used as positively charged dispersion in LbL process. Secondly, PAH was used for the polymer wrapping of BNNTs. Just like b-PEI wrapped BNNTs, PAH wrapped BNNTs were also dispersible in aqueous media. Dispersion was observed to be stable up to weeks with light-white color. Positively charged nature of the PAH polymer suggest that, dispersion can be used as positively charged dispersion in LbL process.

### **5.3 Thin Film Production via LbL method**

We used as-prepared dispersions in order to produce thin films of BNNTs via LbL method. Three different dispersions were tried for the LbL and none of them were successful. We changed pH of the dispersions in order to achieve thin film on the glass micro-slides however none of our efforts were successful. Insufficient charge density of the as-prepared dispersion and high diameter of as-synthesized BNNT might be preventing assembly of the BNNTs to the surface of glass slides via electrostatic interactions.

### **5.4 Future Work**

Based on the results of this thesis research, future research recommendations and suggestions for the BNNTs were proposed and discussed in the terms of: Synthesis, functionalization and applications.

### 5.4.1 Synthesis

To further investigate potential applications of BNNTs, large-scale synthesis method is required. Although, growth vapor trapping-BOCVD method used in thesis research offers novel and low temperature synthesis of good quality BNNTs, yield of the synthesis is still not enough for the scale up. New high yield synthesis method or modifications to as-used synthesis method is needed for the large-scale synthesis of BNNTs so that more research can be focused on BNNTs and their potential applications or commercialization of the BNNTs like CNTS and CNFs can be achieved.

Another challenge in the synthesis of BNNTs is long time requirement. Lower heating and cooling times are required for the large scale synthesis of BNNTs however, one-end closed quartz test tube used during the BNNT synthesis, limits the heating rate of the furnace to maximum +5 °C/min, which extends BNNT synthesis duration to 12 hours. This limitation results in high synthesis time and increases the cost of the BNNTs. Increase of heating rate can be achieved by replacing quartz test tube with more heat stable tube for example one-end closed alumina test tubes or completely removing it from the system.

Finally, larger tube furnace with bigger sweet spot size can be used for the synthesis of BNNTs which will allow loading of more than one alumina boat as it is the case in this thesis research. 3-zone tube furnaces can allow up to three alumina boats to be loaded into sweet spot of the furnace simultaneously resulting threefold increase in the as-synthesized BNNT amount.

### 5.4.2 Surface Modification

One of the promising applications of BNNTs is polymer/BNNT composites due to BNNTs' extraordinary mechanical, electrical, thermal and optic properties that can be transferred to polymers. However, weak interactions between nanotubes and polymer matrix at the interface and poor dispersibility of nanotubes in polymer matrix are the two main challenges. Surface modifications of BNNTs can increase their compatibility with polymers and overcome above mentioned challenges in polymer/BNNT composites.

Hydroxylated BNNTs prepared in this thesis research are favorable starting materials for such modifications because hydroxyl groups on the surfaces of hydroxylated BNNTs are more chemically active than the inert, pristine BNNTs' surface. In this work, simple and effective hydroxylation of BNNTs was achieved and as-hydroxylated BNNTs can be functionalized with isocyanate, thiol, amino or sulphonyl groups in order to increase their solubility in aqueous or organic solvents in addition to achieving better interface interactions with polymer matrix.

Moreover, non-covalent functionalization methods used in this thesis research suggest that, BNNT have good interactions with certain polymers due to  $\pi$ - $\pi$  interactions. Polymer wrapped BNNTs can be used for the production of polymer/BNNT composites by hot-pressing or solution evaporation methods. Researchers already started investigating such possibilities however, the work is still on the early stages.

### 5.4.3 Applications

Extraordinary properties of BNNTs makes them promising material applications for the polymer matrix composite materials. High mechanical strength and high thermal stability of the BNNTs are highly sought out for the polymer composite materials. Furthermore, their good interactions with the polymers via  $\pi$ - $\pi$  interactions allows good interface interactions between BNNTs and polymer matrix. Dispersions of BNNTs prepared by polymer wrapping have been used for the manufacturing of BNNTs however low BNNT content of the BNNT dispersions prevents transferring of properties of BNNTs to polymer matrix. If this challenge is overcome, strong polymer matrix composites with good

thermal and electrical properties can be manufactured. Especially, stable aqueous dispersions of BNNTs prepared in this thesis research can be used to prepare polymer/BNNT composite thin films with desirable architecture to be used in high technology applications.

Another exciting area for the BNNTs are the radiation shielding applications. Enriched B isotope  $^{10}\text{B}$  can be used for the synthesis of BNNTs by synthesis method used in this research to synthesize  $^{10}\text{BNNT}$  which will have high neutron absorption and scattering cross-section. These BNNTs can be used in aerospace applications to reduce effect of the radiation on the electronic devices as well as humans. Moreover, radiation shielding they provide can prolong the life span of the low orbit satellites to double.

## BIBLIOGRAPHY

1. TAŞÇIOĞLU, S., *Bor ve Silisyum kimyası*. Vol. 1. 1992, Marmara Üniversitesi: Marmara Üniversitesi Teknik Eğitim Fakültesi Döner Sermaye İşletmesi Matbaa Birimi. 181.
2. Kimura, Y., et al., *Boron nitride as a lubricant additive*. *Wear*, 1999. **232**(2): p. 199-206.
3. Farer, A.M., et al., Combination of hollow microspheres of a thermoplastic synthetic material, hexagonal boron nitride and n-acyl lysine as a homogenization agent for cosmetic compacted powders. 1993, Google Patents.
4. Eichler, J. and C. Lesniak, *Boron nitride (BN) and BN composites for high-temperature applications*. *Journal of the European Ceramic Society*, 2008. **28**(5): p. 1105-1109.
5. Cao, G., *Synthesis, properties and applications*. 2004: World Scientific.
6. Iijima, S., *Helical microtubules of graphitic carbon*. *nature*, 1991. **354**(6348): p. 56-58.
7. Smalley, R.E., et al., *Carbon nanotubes: synthesis, structure, properties, and applications*. Vol. 80. 2003: Springer Science & Business Media.
8. Endo, M., S. Iijima, and M.S. Dresselhaus, *Carbon nanotubes*. 2013: Elsevier.
9. Moniruzzaman, M. and K.I. Winey, *Polymer Nanocomposites Containing Carbon Nanotubes*. *Macromolecules*, 2006. **39**(16): p. 5194-5205.
10. Lin, Y., et al., *Advances toward bioapplications of carbon nanotubes*. *Journal of Materials Chemistry*, 2004. **14**(4): p. 527-541.
11. Tans, S.J., A.R.M. Verschueren, and C. Dekker, *Room-temperature transistor based on a single carbon nanotube*. *Nature*, 1998. **393**(6680): p. 49-52.
12. Liu, C., et al., *Hydrogen Storage in Single-Walled Carbon Nanotubes at Room Temperature*. *Science*, 1999. **286**(5442): p. 1127-1129.
13. Rubio, A., J.L. Corkill, and M.L. Cohen, *Theory of graphitic boron nitride nanotubes*. *Physical Review B*, 1994. **49**(7): p. 5081.
14. Blase, X., et al., *Stability and band gap constancy of boron nitride nanotubes*. *EPL (Europhysics Letters)*, 1994. **28**(5): p. 335.
15. Chopra, N.G., et al., *Boron nitride nanotubes*. *Science*, 1995. **269**(5226): p. 966.

16. Wilder, J.W.G., et al., *Electronic structure of atomically resolved carbon nanotubes*. Nature, 1998. **391**(6662): p. 59-62.
17. Xiao, Y., et al., *Specific heat of single-walled boron nitride nanotubes*. Applied Physics Letters, 2004. **84**(23): p. 4626-4628.
18. Chopra, N.G. and A. Zettl, *Measurement of the elastic modulus of a multi-wall boron nitride nanotube*. Solid State Communications, 1998. **105**(5): p. 297-300.
19. Jhi, S.-H., Activated boron nitride nanotubes: a potential material for room-temperature hydrogen storage. Physical Review B, 2006. **74**(15): p. 155424.
20. Tiano, A.L., et al. Boron nitride nanotube: Synthesis and applications. in SPIE Smart Structures and Materials+ Nondestructive Evaluation and Health Monitoring. 2014. International Society for Optics and Photonics.
21. Ferreira, T., et al., Boron nitride nanotubes chemically functionalized with glycol chitosan for gene transfection in eukaryotic cell lines. Journal of Biomedical Materials Research Part A, 2015. **103**(6): p. 2176-2185.
22. Zhi, C., et al., *Boron nitride nanotubes*. Materials Science and Engineering: R: Reports, 2010. **70**(3–6): p. 92-111.
23. Dai, H., E.W. Wong, and C.M. Lieber, Probing Electrical Transport in Nanomaterials: Conductivity of Individual Carbon Nanotubes. Science, 1996. **272**(5261): p. 523-526.
24. Chang, C.W., W.-Q. Han, and A. Zettl, *Thermal conductivity of B–C–N and BN nanotubes*. Applied Physics Letters, 2005. **86**(17): p. 173102.
25. Sauti, G., et al., Boron nitride and boron nitride nanotube materials for radiation shielding. 2011, Google Patents.
26. Kim, P., et al., *Thermal Transport Measurements of Individual Multiwalled Nanotubes*. Physical Review Letters, 2001. **87**(21): p. 215502.
27. Nagasawa, S., et al., *Effect of oxidation on single-wall carbon nanotubes*. Chemical Physics Letters, 2000. **328**(4–6): p. 374-380.
28. Lu, J.P., *Elastic Properties of Carbon Nanotubes and Nanoropes*. Physical Review Letters, 1997. **79**(7): p. 1297-1300.
29. Lee, C.H., et al., Patterned Growth of Boron Nitride Nanotubes by Catalytic Chemical Vapor Deposition. Chemistry of Materials, 2010. **22**(5): p. 1782-1787.
30. Kataura, H., et al., *Optical properties of single-wall carbon nanotubes*. Synthetic Metals, 1999. **103**(1): p. 2555-2558.
31. Thess, A., et al., *Crystalline Ropes of Metallic Carbon Nanotubes*. Science, 1996. **273**(5274): p. 483-487.



32. Guo, T., et al., *Catalytic growth of single-walled nanotubes by laser vaporization*. Chemical Physics Letters, 1995. **243**(1): p. 49-54.
33. Kong, J., A.M. Cassell, and H. Dai, *Chemical vapor deposition of methane for single-walled carbon nanotubes*. Chemical Physics Letters, 1998. **292**(4): p. 567-574.
34. Lee, R.S., et al., Catalyst-free synthesis of boron nitride single-wall nanotubes with a preferred zig-zag configuration. Physical Review B, 2001. **64**(12): p. 121405.
35. Laude, T., et al., *Long ropes of boron nitride nanotubes grown by a continuous laser heating*. Applied Physics Letters, 2000. **76**(22): p. 3239-3241.
36. Lim, S.H., et al., *Synthesis of boron nitride nanotubes and its hydrogen uptake*. Catalysis Today, 2007. **120**(3-4): p. 346-350.
37. Chen, Y., et al., *A solid-state process for formation of boron nitride nanotubes*. Applied Physics Letters, 1999. **74**(20): p. 2960-2962.
38. Terrones, M., et al., *Metal particle catalysed production of nanoscale BN structures*. Chemical Physics Letters, 1996. **259**(5): p. 568-573.
39. Loiseau, A., et al., Boron Nitride Nanotubes with Reduced Numbers of Layers Synthesized by Arc Discharge. Physical Review Letters, 1996. **76**(25): p. 4737-4740.
40. Han, W., et al., Synthesis of boron nitride nanotubes from carbon nanotubes by a substitution reaction. Applied Physics Letters, 1998. **73**(21): p. 3085-3087.
41. Lourie, O.R., et al., *CVD Growth of Boron Nitride Nanotubes*. Chemistry of Materials, 2000. **12**(7): p. 1808-1810.
42. Kim, M.J., et al., Double-walled boron nitride nanotubes grown by floating catalyst chemical vapor deposition. Nano letters, 2008. **8**(10): p. 3298-3302.
43. Chatterjee, S., et al., Syntheses of Boron Nitride Nanotubes from Borazine and Decaborane Molecular Precursors by Catalytic Chemical Vapor Deposition with a Floating Nickel Catalyst. Chemistry of Materials, 2012. **24**(15): p. 2872-2879.
44. Tang, C., et al., *A novel precursor for synthesis of pure boron nitride nanotubes*. Chemical Communications, 2002(12): p. 1290-1291.
45. Zhi, C., et al., *Effective precursor for high yield synthesis of pure BN nanotubes*. Solid State Communications, 2005. **135**(1-2): p. 67-70.
46. Lee, C.H., et al., Effective growth of boron nitride nanotubes by thermal chemical vapor deposition. Nanotechnology, 2008. **19**(45): p. 455605.
47. Fu, J., et al., The synthesis of boron nitride nanotubes by an extended vapour-liquid-solid method. Nanotechnology, 2004. **15**(7): p. 727.
48. Wang, J., et al., Low temperature growth of boron nitride nanotubes on substrates. Nano letters, 2005. **5**(12): p. 2528-2532.

49. Hampden-Smith, M.J. and T.T. Kodas, *Chemical vapor deposition of metals: Part I. An overview of CVD processes*. Chemical Vapor Deposition, 1995. **1**(1): p. 8-23.
50. Zhi, C., et al., *Boron nitride nanotubes/polystyrene composites*. Journal of Materials Research, 2006. **21**(11): p. 2794-2800.
51. Zhi, C., et al., *Purification of Boron Nitride Nanotubes through Polymer Wrapping*. The Journal of Physical Chemistry B, 2006. **110**(4): p. 1525-1528.
52. Zhi, C.Y., et al., Mechanical and Thermal Properties of Polymethyl Methacrylate-BN Nanotube Composites. Journal of Nanomaterials, 2008. **2008**: p. 5.
53. Zhi, C., et al., *Grafting Boron Nitride Nanotubes: From Polymers to Amorphous and Graphitic Carbon*. The Journal of Physical Chemistry C, 2007. **111**(3): p. 1230-1233.
54. Kalay, S., et al., *Synthesis of boron nitride nanotubes and their applications*. Beilstein journal of nanotechnology, 2015. **6**(1): p. 84-102.
55. Zhi, C., et al., *SnO<sub>2</sub> Nanoparticle-Functionalized Boron Nitride Nanotubes*. The Journal of Physical Chemistry B, 2006. **110**(17): p. 8548-8550.
56. Chen, R., et al., *Arsenic (V) adsorption on Fe<sub>3</sub>O<sub>4</sub> nanoparticle-coated boron nitride nanotubes*. Journal of Colloid and Interface Science, 2011. **359**(1): p. 261-268.
57. Ejaz, M., et al., Surface-initiated atom transfer radical polymerization of glycidyl methacrylate and styrene from boron nitride nanotubes. Journal of Materials Chemistry C, 2014. **2**(20): p. 4073-4079.
58. Chee Huei, L., et al., Effective growth of boron nitride nanotubes by thermal chemical vapor deposition. Nanotechnology, 2008. **19**(45): p. 455605.
59. Chen, Y., et al., Synthesis of boron nitride nanotubes at low temperatures using reactive ball milling. Chemical Physics Letters, 1999. **299**(3-4): p. 260-264.
60. Han, W.-Q., et al., *Transformation of B<sub>x</sub>C<sub>y</sub>N<sub>z</sub> nanotubes to pure BN nanotubes*. Applied physics letters, 2002. **81**(6): p. 1110-1112.
61. Wagner, R. and W. Ellis, *Vapor-liquid-solid mechanism of single crystal growth*. Applied Physics Letters, 1964. **4**(5): p. 89-90.
62. Chee Huei, L., Boron Nitride Nanotubes: Synthesis, Characterization, Functionalization, and Potential Applications, in Physics. 2010, Michigan Technological University. p. 183.
63. Sinnott, S.B., et al., *Model of carbon nanotube growth through chemical vapor deposition*. Chemical Physics Letters, 1999. **315**(1-2): p. 25-30.
64. Kong, J., A.M. Cassell, and H. Dai, *Chemical vapor deposition of methane for single-walled carbon nanotubes*. Chemical Physics Letters, 1998. **292**(4-6): p. 567-574.

65. Che, G., et al., Chemical Vapor Deposition Based Synthesis of Carbon Nanotubes and Nanofibers Using a Template Method. *Chemistry of Materials*, 1998. **10**(1): p. 260-267.
66. Xiang, B., et al., Rational synthesis of p-type zinc oxide nanowire arrays using simple chemical vapor deposition. *Nano Letters*, 2007. **7**(2): p. 323-328.
67. Yang, H., et al., Bulk synthesis, growth mechanism and properties of highly pure ultrafine boron nitride nanotubes with diameters of sub-10 nm. *Nanotechnology*, 2011. **22**(14): p. 145602.
68. Lee, C.J., et al., Synthesis of aligned carbon nanotubes using thermal chemical vapor deposition. *Chemical Physics Letters*, 1999. **312**(5-6): p. 461-468.
69. Chang, P.-C., et al., *ZnO Nanowires Synthesized by Vapor Trapping CVD Method*. *Chemistry of Materials*, 2004. **16**(24): p. 5133-5137.
70. Ahmad, P., M.U. Khandaker, and Y.M. Amin, *Synthesis of boron nitride nanotubes by argon supported thermal chemical vapor deposition*. *Physica E: Low-dimensional Systems and Nanostructures*, 2015. **67**: p. 33-37.
71. Hernández, E., et al., *Elastic Properties of C and BxCyNz Composite Nanotubes*. *Physical Review Letters*, 1998. **80**(20): p. 4502-4505.
72. Peng, Y.-J., et al., *Ab initio studies of elastic properties and electronic structures of C and BN nanotubes*. *Physica E: Low-dimensional Systems and Nanostructures*, 2006. **33**(1): p. 155-159.
73. Zhang, L.Y., et al., *Elastic properties of single-wall nanotubes*. *Wuli Xuebao/Acta Physica Sinica*, 2006. **55**(8): p. 4193-4196.
74. Veena, V., V.K. Jindal, and D. Keya, *Elastic moduli of a boron nitride nanotube*. *Nanotechnology*, 2007. **18**(43): p. 435711.
75. Suryavanshi, A.P., et al., *Elastic modulus and resonance behavior of boron nitride nanotubes*. *Applied Physics Letters*, 2004. **84**(14): p. 2527-2529.
76. Golberg, D., et al., Direct Force Measurements and Kinking under Elastic Deformation of Individual Multiwalled Boron Nitride Nanotubes. *Nano Letters*, 2007. **7**(7): p. 2146-2151.
77. Zhang, P. and V.H. Crespi, *Plastic deformations of boron-nitride nanotubes: An unexpected weakness*. *Physical Review B - Condensed Matter and Materials Physics*, 2000. **62**(16): p. 11050-11053.
78. Rubio, A., J.L. Corkill, and M.L. Cohen, *Theory of graphitic boron nitride nanotubes*. *Physical Review B*, 1994. **49**(7): p. 5081-5084.
79. Tang, C., et al., *Fluorination and electrical conductivity of BN nanotubes*. *Journal of the American Chemical Society*, 2005. **127**(18): p. 6552-6553.

80. Golberg, D., et al., Synthesis, analysis, and electrical property measurements of compound nanotubes in the B-C-N ceramic system. *MRS Bulletin*, 2004. **29**(1): p. 38-42.
81. Ishigami, M., et al., *Observation of the giant Stark effect in boron-nitride nanotubes*. *Physical review letters*, 2005. **94**(5): p. 056804.
82. Bai, X., et al., Deformation-Driven Electrical Transport of Individual Boron Nitride Nanotubes. *Nano Letters*, 2007. **7**(3): p. 632-637.
83. Zettl, A., C.W. Chang, and G. Begtrup, *A new look at thermal properties of nanotubes*. *physica status solidi (b)*, 2007. **244**(11): p. 4181-4183.
84. Chang, C.W., et al., *Breakdown of Fourier's Law in Nanotube Thermal Conductors*. *Physical Review Letters*, 2008. **101**(7): p. 075903.
85. Xiao, Y., et al., Specific heat and quantized thermal conductance of single-walled boron nitride nanotubes. *physical Review B*, 2004. **69**(20): p. 205415.
86. Tang, C., et al., *Thermal conductivity of nanostructured boron nitride materials*. *The Journal of Physical Chemistry B*, 2006. **110**(21): p. 10354-10357.
87. Chang, C.W., et al., *Isotope Effect on the Thermal Conductivity of Boron Nitride Nanotubes*. *Physical Review Letters*, 2006. **97**(8): p. 085901.
88. Chen, Y., et al., *Boron nitride nanotubes: Pronounced resistance to oxidation*. *Applied Physics Letters*, 2004. **84**(13): p. 2430-2432.
89. Golberg, D., et al., Synthesis and characterization of ropes made of BN multiwalled nanotubes. *Scripta Materialia*, 2001. **44**(8): p. 1561-1565.
90. Lauret, J.S., et al., *Optical Transitions in Single-Wall Boron Nitride Nanotubes*. *Physical Review Letters*, 2005. **94**(3): p. 037405.
91. Jaffrennou, P., et al., Near-band-edge recombinations in multiwalled boron nitride nanotubes: Cathodoluminescence and photoluminescence spectroscopy measurements. *Physical Review B*, 2008. **77**(23): p. 235422.
92. Zhi, C., et al., *Covalent Functionalization: Towards Soluble Multiwalled Boron Nitride Nanotubes*. *Angewandte Chemie International Edition*, 2005. **44**(48): p. 7932-7935.
93. Zhi, C., et al., Engineering of electronic structure of boron-nitride nanotubes by covalent functionalization. *Physical Review B*, 2006. **74**(15): p. 153413.
94. Sainsbury, T., et al., Self-assembly of gold nanoparticles at the surface of amine- and thiol-functionalized boron nitride nanotubes. *Journal of Physical Chemistry C*, 2007. **111**(35): p. 12992-12999.
95. Ikuno, T., et al., *Amine-functionalized boron nitride nanotubes*. *Solid State Communications*, 2007. **142**(11): p. 643-646.

96. Zhi, C.Y., et al., *Chemically Activated Boron Nitride Nanotubes*. Chemistry – An Asian Journal, 2009. **4**(10): p. 1536-1540.
97. Huang, X., et al., Polyhedral oligosilsesquioxane-modified boron nitride nanotube based epoxy nanocomposites: an ideal dielectric material with high thermal conductivity. *Advanced Functional Materials*, 2013. **23**(14): p. 1824-1831.
98. Ciofani, G., et al., *A simple approach to covalent functionalization of boron nitride nanotubes*. *Journal of colloid and interface science*, 2012. **374**(1): p. 308-314.
99. Zhi, C., et al., *Perfectly dissolved boron nitride nanotubes due to polymer wrapping*. *Journal of the American Chemical Society*, 2005. **127**(46): p. 15996-15997.
100. Ciofani, G., et al., *Assessing cytotoxicity of boron nitride nanotubes: Interference with the MTT assay*. *Biochemical and Biophysical Research Communications*, 2010. **394**(2): p. 405-411.
101. Ciofani, G., et al., Cytocompatibility, interactions and uptake of polyethyleneimine-coated boron nitride nanotubes by living cells: confirmation of their potential for biomedical applications. *Biotechnol. Bioeng*, 2008. **101**.
102. Ciofani, G., et al., Investigation of interactions between poly-L-lysine-coated boron nitride nanotubes and C2C12 cells: up-take, cytocompatibility, and differentiation. *International journal of nanomedicine*, 2010. **5**: p. 285.
103. Yu, J., Y. Chen, and B.-M. Cheng, *Dispersion of boron nitride nanotubes in aqueous solution with the help of ionic surfactants*. *Solid state communications*, 2009. **149**(19): p. 763-766.
104. Koo, J.H., *Polymer nanocomposites*. 2006: McGraw-Hill Professional Pub.
105. Engheta, N., Circuits with light at nanoscales: optical nanocircuits inspired by metamaterials. *Science*, 2007. **317**(5845): p. 1698-1702.
106. Saji, V.S. and J. Thomas, *Nanomaterials for corrosion control*. *Curr Sci*, 2007. **92**(1): p. 51-55.
107. Poizot, P., et al., Nano-sized transition-metal oxides as negative-electrode materials for lithium-ion batteries. *Nature*, 2000. **407**(6803): p. 496-499.
108. Soppimath, K.S., et al., *Biodegradable polymeric nanoparticles as drug delivery devices*. *Journal of controlled release*, 2001. **70**(1): p. 1-20.
109. Zhong, W., et al., *Cosmic radiation shielding tests for UHMWPE fiber/nano-epoxy composites*. *Composites Science and Technology*, 2009. **69**(13): p. 2093-2097.
110. An, J.W., D.H. You, and D.S. Lim, *Tribological properties of hot-pressed alumina–CNT composites*. *Wear*, 2003. **255**(1–6): p. 677-681.
111. Jia, Z., et al., *Study on poly(methyl methacrylate)/carbon nanotube composites*. *Materials Science and Engineering: A*, 1999. **271**(1–2): p. 395-400.

112. Fan, Z., et al., Preparation and characterization of manganese oxide/CNT composites as supercapacitive materials. *Diamond and Related Materials*, 2006. **15**(9): p. 1478-1483.
113. Byrappa, K., et al., Hydrothermal preparation of ZnO:CNT and TiO<sub>2</sub>:CNT composites and their photocatalytic applications. *Journal of Materials Science*, 2008. **43**(7): p. 2348-2355.
114. Xu, C.L., et al., Fabrication of aluminum–carbon nanotube composites and their electrical properties. *Carbon*, 1999. **37**(5): p. 855-858.
115. Pastorin, G., et al., *Double functionalisation of carbon nanotubes for multimodal drug delivery*. *Chemical Communications*, 2006(11): p. 1182-1184.
116. Bianco, A., K. Kostarelos, and M. Prato, *Applications of carbon nanotubes in drug delivery*. *Current Opinion in Chemical Biology*, 2005. **9**(6): p. 674-679.
117. Liu, Z., et al., *Carbon materials for drug delivery & cancer therapy*. *Materials Today*, 2011. **14**(7–8): p. 316-323.
118. Wei, W., et al., *CNT enhanced sulfur composite cathode material for high rate lithium battery*. *Electrochemistry Communications*, 2011. **13**(5): p. 399-402.
119. Lim, H.-D., et al., Enhanced Power and Rechargeability of a Li–O<sub>2</sub> Battery Based on a Hierarchical-Fibril CNT Electrode. *Advanced Materials*, 2013. **25**(9): p. 1348-1352.
120. Emmenegger, C., et al., Investigation of electrochemical double-layer (ECDL) capacitors electrodes based on carbon nanotubes and activated carbon materials. *Journal of Power Sources*, 2003. **124**(1): p. 321-329.
121. Hirsch, A., *Functionalization of single-walled carbon nanotubes*. *Angewandte Chemie International Edition*, 2002. **41**(11): p. 1853-1859.
122. Xie, X.-L., Y.-W. Mai, and X.-P. Zhou, *Dispersion and alignment of carbon nanotubes in polymer matrix: a review*. *Materials Science and Engineering: R: Reports*, 2005. **49**(4): p. 89-112.
123. Lam, C.-w., et al., A review of carbon nanotube toxicity and assessment of potential occupational and environmental health risks. *Critical reviews in toxicology*, 2006. **36**(3): p. 189-217.
124. Ajayan, P.M., et al., Aligned Carbon Nanotube Arrays Formed by Cutting a Polymer Resin—Nanotube Composite. *Science*, 1994. **265**(5176): p. 1212-1214.
125. Zhi, C., et al., *Characteristics of Boron Nitride Nanotube–Polyaniline Composites*. *Angewandte Chemie International Edition*, 2005. **44**(48): p. 7929-7932.
126. Ravichandran, J., et al., A novel polymer nanotube composite for photovoltaic packaging applications. *Nanotechnology*, 2008. **19**(8): p. 085712.

127. Lahiri, D., et al., Boron nitride nanotube reinforced polylactide–polycaprolactone copolymer composite: Mechanical properties and cytocompatibility with osteoblasts and macrophages in vitro. *Acta Biomaterialia*, 2010. **6**(9): p. 3524-3533.
128. Choi, S.R., N.P. Bansal, and A. Garg, Mechanical and microstructural characterization of boron nitride nanotubes-reinforced SOFC seal glass composite. *Materials Science and Engineering: A*, 2007. **460–461**: p. 509-515.
129. Qing, H., et al., Enhancing superplasticity of engineering ceramics by introducing BN nanotubes. *Nanotechnology*, 2007. **18**(48): p. 485706.
130. Lahiri, D., et al., Boron nitride nanotube reinforced hydroxyapatite composite: Mechanical and tribological performance and in-vitro biocompatibility to osteoblasts. *Journal of the Mechanical Behavior of Biomedical Materials*, 2011. **4**(1): p. 44-56.
131. Du, M., et al., Microstructure and properties of SiO<sub>2</sub> matrix reinforced by BN nanotubes and nanoparticles. *Journal of Alloys and Compounds*, 2011. **509**(41): p. 9996-10002.
132. Wang, W.L., et al., Fabrication of alumina ceramic reinforced with boron nitride nanotubes with improved mechanical properties. *Journal of the American Ceramic Society*, 2011. **94**(11): p. 3636-3640.
133. Zhi, C., et al., *DNA-Mediated Assembly of Boron Nitride Nanotubes*. *Chemistry – An Asian Journal*, 2007. **2**(12): p. 1581-1585.
134. Zhi, C., et al., *Immobilization of Proteins on Boron Nitride Nanotubes*. *Journal of the American Chemical Society*, 2005. **127**(49): p. 17144-17145.
135. Chen, X., et al., Boron nitride nanotubes are noncytotoxic and can be functionalized for interaction with proteins and cells. *Journal of the American Chemical Society*, 2009. **131**(3): p. 890-891.
136. Emanet, M., et al., *Interaction of carbohydrate modified boron nitride nanotubes with living cells*. *Colloids and Surfaces B: Biointerfaces*, 2015. **134**: p. 440-446.
137. Barth, R.F., et al., Boron neutron capture therapy for cancer. Realities and prospects. *Cancer*, 1992. **70**(12): p. 2995-3007.
138. Ciofani, G., et al., Folate Functionalized Boron Nitride Nanotubes and their Selective Uptake by Glioblastoma Multiforme Cells: Implications for their Use as Boron Carriers in Clinical Boron Neutron Capture Therapy. *Nanoscale Research Letters*, 2008. **4**(2): p. 113.
139. Yu, J., et al., *Isotopically Enriched 10BN Nanotubes*. *Advanced Materials*, 2006. **18**(16): p. 2157-2160.
140. Thibeault, S.A., et al., *Nanomaterials for radiation shielding*. *MRS Bulletin*, 2015. **40**(10): p. 836-841.

141. Harrison, C., et al., *Polyethylene/boron nitride composites for space radiation shielding*. Journal of applied polymer science, 2008. **109**(4): p. 2529-2538.
142. Jhi, S.-H. and Y.-K. Kwon, Hydrogen adsorption on boron nitride nanotubes: A path to room-temperature hydrogen storage. Physical Review B, 2004. **69**(24): p. 245407.
143. Khan, M.S. and M.S. Khan, Computational study of hydrogen adsorption on potassium-decorated boron nitride nanotubes. International Nano Letters, 2012. **2**(1): p. 1-7.
144. Özdoğan, K. and S. Berber, *Optimizing the hydrogen storage in boron nitride nanotubes by defect engineering*. International Journal of Hydrogen Energy, 2009. **34**(12): p. 5213-5217.
145. Wang, P., et al., Hydrogen in mechanically prepared nanostructured h-BN: a critical comparison with that in nanostructured graphite. Applied Physics Letters, 2002. **80**(2): p. 318-320.
146. Ma, R., et al., *Hydrogen Uptake in Boron Nitride Nanotubes at Room Temperature*. Journal of the American Chemical Society, 2002. **124**(26): p. 7672-7673.
147. Tang, C., et al., *Catalyzed Collapse and Enhanced Hydrogen Storage of BN Nanotubes*. Journal of the American Chemical Society, 2002. **124**(49): p. 14550-14551.
148. Wang, J., C.H. Lee, and Y.K. Yap, *Recent advancements in boron nitride nanotubes*. Nanoscale, 2010. **2**(10): p. 2028-2034.
149. Kalay, S., Z. Yilmaz, and M. Çulha, *Synthesis of boron nitride nanotubes from unprocessed colemanite*. Beilstein journal of nanotechnology, 2013. **4**(1): p. 843-851.
150. Blakely, J. and K. Jackson, *Growth of crystal whiskers*. The Journal of Chemical Physics, 1962. **37**(2): p. 428-430.
151. Mensah, S.L., et al., Formation of single crystalline ZnO nanotubes without catalysts and templates. Applied physics letters, 2007. **90**(11): p. 113108.
152. Tiano, A., et al., Thermodynamic approach to boron nitride nanotube solubility and dispersion. Nanoscale, 2016. **8**(7): p. 4348-4359.
153. Amir, P., et al., A comprehensive analysis of the CVD growth of boron nitride nanotubes. Nanotechnology, 2012. **23**(21): p. 215601.
154. Hussain, F., et al., Review article: polymer-matrix nanocomposites, processing, manufacturing, and application: an overview. Journal of composite materials, 2006. **40**(17): p. 1511-1575.
155. Hou, H. and D.H. Reneker, Carbon Nanotubes on Carbon Nanofibers: A Novel Structure Based on Electrospun Polymer Nanofibers. Advanced Materials, 2004. **16**(1): p. 69-73.



156. Chen, H., et al., *Purification of boron nitride nanotubes*. Chemical Physics Letters, 2006. **425**(4–6): p. 315-319.
157. Xie, S.-Y., et al., *Solubilization of boron nitride nanotubes*. Chemical Communications, 2005(29): p. 3670-3672.
158. Decher, G. and J.D. Hong. Buildup of ultrathin multilayer films by a self-assembly process, 1 consecutive adsorption of anionic and cationic bipolar amphiphiles on charged surfaces. in *Makromolekulare Chemie. Macromolecular Symposia*. 1991. Wiley Online Library.
159. Decher, G. and J. Hong, Buildup of ultrathin multilayer films by a self-assembly process: II. Consecutive adsorption of anionic and cationic bipolar amphiphiles and polyelectrolytes on charged surfaces. *Berichte der Bunsengesellschaft für physikalische Chemie*, 1991. **95**(11): p. 1430-1434.
160. Srivastava, S. and N.A. Kotov, *Composite layer-by-layer (LBL) assembly with inorganic nanoparticles and nanowires*. Accounts of chemical research, 2008. **41**(12): p. 1831-1841.
161. Lee, S.W., et al., Layer-by-layer assembly of all carbon nanotube ultrathin films for electrochemical applications. *Journal of the American Chemical Society*, 2008. **131**(2): p. 671-679.
162. Zhang, M., et al., Layer-by-layer assembled carbon nanotubes for selective determination of dopamine in the presence of ascorbic acid. *Biosensors and Bioelectronics*, 2005. **20**(7): p. 1270-1276.
163. Zhao, H. and H. Ju, Multilayer membranes for glucose biosensing via layer-by-layer assembly of multiwall carbon nanotubes and glucose oxidase. *Analytical biochemistry*, 2006. **350**(1): p. 138-144.
164. Golberg, D., et al., Fine structure of boron nitride nanotubes produced from carbon nanotubes by a substitution reaction. *Journal of Applied Physics*, 1999. **86**(4): p. 2364-2366.
165. Golberg, D., et al., *Insights into the structure of BN nanotubes*. Applied Physics Letters, 2000. **77**(13): p. 1979-1981.
166. Yu, J., et al., Vertically Aligned Boron Nitride Nanosheets: Chemical Vapor Synthesis, Ultraviolet Light Emission, and Superhydrophobicity. *ACS Nano*, 2010. **4**(1): p. 414-422.
167. Wirtz, L., et al., *Ab initio* calculations of the lattice dynamics of boron nitride nanotubes. *Physical Review B*, 2003. **68**(4): p. 045425.
168. Li, X., et al., Boron nitride nanotubes functionalized with mesoporous silica for intracellular delivery of chemotherapy drugs. *Chemical Communications*, 2013. **49**(66): p. 7337-7339.

## Curriculum Vitae

### Deniz Köken

December 28, 2016

Orta Mah. Üniversite Cd.  
No:27, 34956  
Orhanli/Tuzla/İstanbul  
Cell: 0532 201 42 70  
[denizkoken@gmail.com](mailto:denizkoken@gmail.com)

#### Education

- ❖ 2014 – Present Sabanci University, Msc. Materials Science and Engineering
- ❖ 2010 – 2014 Yıldız Technical University, BS Metallurgy and Materials Engineering

#### Internship and Work Experience

- ❖ 01/2015 – 12/2016 Sabanci University, Master Teaching Assistant (Nature of Science 102)
- ❖ 09/2014 – 12/2014 Sabanci University, Teaching Assistant (Nature of Science 102)
- ❖ 07/2014 – 08/2014 Sabanci University, SUNUM, Research internship
- ❖ 06/2012 – 08/2012 Eti Elektrometalurji A.Ş, Casting internship

#### Research Projects

- ❖ 09/2014 – 12/2016 Sabanci University, Master Thesis Project (Synthesis and Optimization of Boron Nitride Nanotubes for Stable Aqueous Dispersions)
- ❖ 09/2014 – 01/2015 Sabanci University, Battery design (Synthesis of Cathode Materials for Li-ion Batteries)
- ❖ 02/2014 – 06/2014 Yıldız Technical University, Bachelor Thesis Project (Design of Solar Cell Electrodes Containing Nanotubes)
- ❖ 09/2013 – 01/2014 Yıldız Technical University, Design of antimicrobial face-masks (Synthesis of CuO and Cu nanoparticles, Synthesis of Ag nanoparticles)

#### Certificates

- ❖ Toefl: Reading: 29, Listening: 30, Speaking: 24, Writing: 24, Total: 107/120
- ❖ Ales: 75.35/100
- ❖ YDS:96.25/100

#### Skills

- ❖ Computer Programs: MsOffice, Origin, Matlab
- ❖ Equipment: SEM, RAMAN, FTIR, CVD, Electrospinnig, PVD, EPD systems, Induction furnaces, Arc furnaces
- ❖ Language: English (Upper-advanced)
- ❖ Drivers License